CHARACTERIZING α-SYNUCLEIN MEMBRANE BOUND STRUCTURE

Thesis by

Bert Tsunyin Lai

In Partial Fulfillment of the Requirement

for the Degree of

Doctor of Philosophy

California Institute of Technology

Pasadena, California

2008

(Defended April 29, 2008)

ACKNOWLEDGEMENTS

As I am writing my thesis, I am just very grateful to so many people for this experience. I have learned so much from various people. First of all, I would like to thank Prof. Harry Gray for granting me this wonderful opportunity. I am constantly inspired by his enthusiasm towards science. To Dr. Jay Winkler, I am deeply grateful to have a chance to learn from him, his vast amount of knowledge, his attitude towards science, and his quest for perfection.

To Prof. Judy Kim, thank you for inspiring me to be the best graduate student I can be. But, my project would not have gone this far without the guidance of Dr. Jennifer Lee. I have also had a great opportunity to work with some brilliant undergraduate students, namely Dustin Hawker, Stephanie Schulze, and Matthew Robinson. My learning process has also become much more enjoyable with my three wonderful colleagues, Crystal Shih, Melanie Pribisko, and Dr. Gitrada Arjara.

For my personal life, I would like to thank my family for being supportive for everything I do and letting me be who I am. To the Agnews, thank you for making me feel so welcomed. To my seven closest friends from LSC (Benne Chan, Marcus Chan, William Fung, Ivan Lai, Arthur Mok, Joey Siu, and Caran Wong), thank you for making high school so memorable. To Silvia Li and Carole Agelopas, thank you for being there for me during my journey to find the real me. To Ariele Hanek, Heather Wiencko, and Katie Brennen, thank you for everything during the past 5 years. Finally, to Kitty Lai-Agnew, thank you for your unconditional love. But my life will never be completed without Heather Agnew, who appreciates me for my virtues, but loves me for my flaws.

ABSTRACT

A feature of Parkinson's disease is the presence of fibrillar protein deposits composed mostly of α-synuclein and calcium ions in the brain's *substantia nigra* region. Although α-synuclein is natively unfolded, the N-terminal region of the protein is highly helical in the presence of membrane mimics, such as acidic phospholipid vesicles and SDS micelles. The C-terminal region of α-synuclein is known to bind to calcium ions and modulates aggregation. In this thesis, the structure of α-synuclein variants, incorporated with tryptophan and 3-nitrotyrosine as donor and energy acceptor pairs, have been characterized in the presence of SDS micelles, small unilammelar vesicles, and calcium ions by various techniques. Distance distributions extracted from time-resolved fluorescence energy-transfer measurements provide site-specific information on the protein conformations. In addition, similar studies using mutants linked to early onset Parkinson's disease were also performed to investigate the structural effect caused by these mutations. Furthermore, single tryptophan mutants have been designed as fluorescent reporters. The locations of these different tryptophan residues in the bilayer were probed by lipids labeled with bromine and dinitrophenol quenchers. Finally, preliminary studies of the intramolecular structure of α-synuclein aggregates have been carried out, while elucidation of intermolecular α-synuclein aggregate structures was made possible by the synthesis of new dyes that allow for long-range fluorescent energy transfer.

TABLE OF CONTENTS

LIST OF TABLES, FIGURES, AND SCHEMES

CHAPTER 1: α-Synuclein: Background, Methods, and Initial Studies

CHAPTER 2: Phospholipid Interaction Sites of α-Synuclein Determined by Tryptophan

CHAPTER 3: α-Synuclein Membrane Bound Structures Characterized by Fluorescence Energy-transfer Kinetics

CHAPTER 4: Calcium Binding Behavior of α-Synuclein's C-terminal Tail

Chapter 1

α-Synuclein: Background, Methods, and Initial Studies

1.1 INTRODUCTION

α-Synuclein.

Parkinson's disease develops from the loss of dopaminergic neurons in the *substania nigra* region located in the brain stem. It also can be characterized by the presence of intracellular inclusions, namely Lewy bodies,[1] which are mostly comprised of α-synuclein (α-syn).[2,3] Although the detailed role of α-syn in the pathogenic mechanism is unclear, the protein is commonly found in the cytosol and presynaptic nerve terminals of a neuron.[4-6] The localization mechanism of α-syn is not well understood. Unlike other presynaptic proteins, α-syn does not tightly associate with the synaptic plasma membrane or the synaptic vesicle.[7,8]

Though the protein is characterized to be unstructured *in vitro,*[9] numerous experimental data now indicate that α-syn is not a random coil, but contains regions of structural preferences.[10-15] In the presence of acidic phospholipid vesicles, the protein will adopt α-helical structures. Notably, α-syn does not appear to interact with neutral phospholipid vesicles.[16] These structures have been characterized by circular dichroism (CD),[17] nuclear magnetic resonance (NMR),[18-20] and electron paramagnetic resonance (EPR) spectroscopies.[21,22] These conformers are particularly important because α-helical dimers and multimers have been observed in lipid environments.[23,24] Furthermore, there is evidence suggesting that these oligomers may participate in membrane permeabilization, one of the proposed molecular pathways of disease.[25,26]

The primary amino acid sequence of human α-syn has been illustrated in **Figure 1.1**. The N-terminal region of α-syn includes seven imperfect repeats (consensus XKTKEGVXXXX) containing eleven amino acids each.[4] This repeating pattern is commonly found in exchangeable apolipoproteins, implying that α-syn has the capability of binding to lipid surfaces reversibly.[17,27-29] The C-terminal tail is rich in glutamate, whose acidic properties prevent tail association with the negatively-charged phospholipid membrane. Another particularly interesting region is the non-amyloid β component (NAC) domain located between residues 61 and 95. This peptide fragment is highly hydrophobic and has been identified in senile plaques characteristic of Alzheimer's disease.[30]

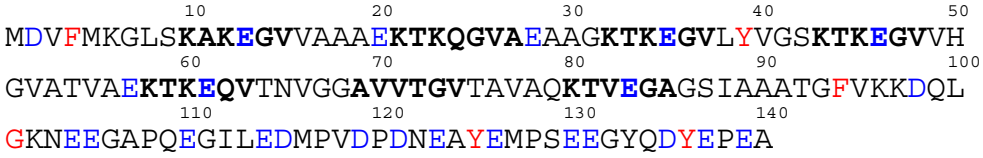

Figure 1.1. Amino acid sequence for α-syn. The acidic residues (blue) and Trp mutation sites (red) are highlighted. The seven imperfect repeats are bolded.

1.2 MATERIALS AND METHODS

Materials.

Lipids were purchased in chloroform from Avanti Polar Lipids (Alabaster, AL). N-acetyl-tryptophanamide (NATA), sodium dodecyl sulfate (SDS), and tetranitromethane (TNM) were used as received from Sigma. BL21(DE3)pLysS was obtained from Stratagene.

Protein Preparation, Modification, and Characterization.

M. Goedert (Medical Council Research Laboratory of Molecular Biology, Cambridge, U.K.) provided the wild-type human α-syn expression vector.[8] Mutations were introduced in three various positions by site-directed mutagenesis. All the sequences were confirmed by DNA sequencing.

Expression and purification of mutants were achieved following previously published protocols with minor modifications.[31] The mutant plasmids were transformed into *E. coli* BL21(DE3)pLysS and plated onto LB agar plates containing 34 μg/mL of chloramphenicol and 100 μg/mL of ampicillin. Single colonies were chosen and grown in 25 mL of LB medium with the same antibiotic concentrations for 15 hours. Cells harvested from this starter culture were used to inoculate large LB medium with the same antibiotic concentrations. Cells were grown in 4 L flasks containing 1 L of medium at 30 °C until $Abs_{600} \sim 0.6$. IPTG was then added and the cells were harvested 6 hours after induction. The harvested cells were stored at -80 °C.

α-Syn was extracted from the frozen cells by boiling and acid precipitation. The crude protein solution was then purified by Q-Sepharose Fast Flow 16/10 column (Amersham Biosciences) by fast protein liquid chromatography (FPLC) equilibrated with 20 mM Tris buffer (pH 8.0). The protein was eluted with a gradient from 0 to 0.5 M NaCl. The semi-pure protein fractions were combined and further purified on a Mono-Q 10/10 column (Amersham Biosciences).

Proteins were nitrated following published protocol with minor modification.[32] Purified and concentrated (~100 μM) α-syn in 20 mM Tris buffer with 200-300 mM NaCl at pH 8.0 was stirred under Ar for 20 min in the dark. To the stirring protein solution (850 μL), TNM in ethanol [1% (vol/vol), 75 μL] was added dropwise. A second aliquot of TNM solution was added after 10 min. After another 10 min, the reaction was desalted by gel filtration chromatography (HiPrep Desalting 26/10, Amersham Biosciences) using FPLC. The desalted protein was then purified on a Mono-Q 10/10 column.

The concentration of non-nitrated protein was determined using a molar extinction coefficient estimated by amino acid content: ε_{280} = 6 970 $M^{-1} \cdot cm^{-1}$, while nitrated protein concentration was determined by literature molar extinction coefficient: ε_{381} = 2 200 $M^{-1} \cdot cm^{-1}$.[33] Absorption measurements were carried out by a Hewlett-Packard 8452 diode array spectrophotometer. Purities of all protein samples were evaluated by SDS-PAGE on a Pharmacia PhastSystem (Amersham Biosciences). Molecular weights of all protein samples were determined by electrospray mass spectrometry (California Institute of Technology Protein/Peptide Microanalytical

Laboratory). All protein stock solutions were concentrated using Amicon YM-3 (molecular weight cutoff 3 kD; Millipore) and stored in -80 °C.

Preparation of Membrane Mimics.

Small Unilammelar Vesicles (SUVs) were made from published protocols.[34] Chloroform from the lipid solutions was removed under a stream of Ar and then dried under vacuum. 20 mM sodium phosphate (NaP_i) buffer (pH 7.4) was used to resuspend the dried lipid into a concentration of 5 mg/mL. The lipid solution was then sonicated by a Branson ultrasonicator microtip (Plainview, NJ) for 30 min at 50% duty cycle (200 W). The sonicated SUVs were then diluted to a final concentration of 2 mg/mL with NaP_i buffer and equilibrated overnight at room temperature. Titanium dust and particulates were removed by centrifuging the SUV solution at 10,000 × *g* for 10 min. Freshly prepared SUVs were used for all experiments. SDS micelles were made by preparing a 40 mM solution of SDS. The micelle solution was then filtered by 0.22 μm filter before use.

Steady-State Measurements.

Tryptophan (Trp) luminscence spectra were obtained by exciting the sample at 295 nm (1 nm band-pass) and recording between 300 and 500 nm (1 nm band-pass, 0.25 s integration) on a Fluorolog2 spectrofluorimeter (Jobin Yvon, Longjumeau, France) in a 1 cm cuvette. For kinetics studies, the sample was excited at 290 nm (1 nm band pass) and the fluorescence emission was monitored at 350 nm (4 nm band-pass, 0.5 s integration). Circular dichroism spectra were measured by Aviv 62ADS

spectropolarimeter (Aviv Associates, Lakewood, NJ) in a 1 mm cuvette at 25 °C. Measurements of 5 μM α-synuclein were recorded between 200 nm and 260 nm with a band-pass of 1.5 nm.

Time-Resolved Fluorescence Measurements.

Trp fluorescence-decay kinetics were measured as described in literature.[35] The experimental samples were prepared as described above and deoxygenated by 30 cycles of evacuation/Ar-fill on a Schlenk line. The Trp was excited by a 292 nm polarized pulse (35° from vertical) from a regeneratively amplified femtosecond Ti:sapphire laser (Spectra-Physics). Interference filters were used to select Trp emissions between 325 and 400 nm. The Trp fluorescence decay kinetics were recorded in single photon counting mode by a picosecond streak camera (Hamamatsu Photonics C5680, Hamamatsu City, Japan). Control experiments were performed using the Trp model complex, NATA.

Data Analysis.

Trp fluorescence decay kinetics were modeled with **Equation 1**, where $I_0(t)$ is the Trp fluorescent decay without the presence of quencher, $P(r)$ is the probability of observing the donor-acceptor distance r, and $k_{et}(r)$ is the energy transfer rate at distance r.

$$I(t) = I_0(t)\int P(r)\exp(-k_{et}(r)t)dr \quad (1)$$

The decay kinetics were fitted to extract the distance distributions by numerical inversion of the Laplace transform describing $I(t)$. This inversion was

constrained by the requirement of $P(r) \geq 0$. The narrowest $P(k)$ distributions were projected by a linear least-squares (LLS) MATLAB (Mathworks, Natick, MA) algorithm with a non-negative constraint (LSQNONNEG). The $P(k)$ distribution obtained from the above fitting routine was recasted into a distribution of r using the Förster equation (**Equation 2**), where k_R is the measured radiative decay rate constant of excited NATA.

$$r = R_0(\Phi_D k_R / k_{et})^{1/6} \quad (2)$$

1.3 RESULTS AND DISCUSSION

Different SUVs studies.

Five types of lipids have been utilized in this thesis (**Figure 1.2**). Previous work has suggested that α-syn will only form a helical structure when acidic SUVs are present. Therefore, most of the SUVs were made of a 1:1 molar mixture of 1-palmitoyl-2-oleoyl-*sn*-glycero-3-phosphocholine (POPC) and 1-palmitoyl-2-oleoyl-*sn*-glycero-3-phosphate (POPA). The other three types of lipids used were 1-palmitoyl-2-stearoyl(6,7-dibromo)-*sn*-glycero-3-phosphocholine (6,7-DiBr), 1-palmitoyl-2-stearoyl(11,12-dibromo)-*sn*-glycero-3-phosphocholine (11,12-DiBr), and N-dinitrophenyl phosphatidylethanolamine (DNP).

We have prepared some SUVs with only POPC lipids, which are not charged. **Figure 1.3** shows the CD spectrum of wild type α-syn in solution (red), SDS micelles (blue) , 1:1 POPC:POPA SUVs (black), and POPC (green) SUVs. The α-helical signature peaks were demonstrated when wild type α-syn was mixed with 1:1

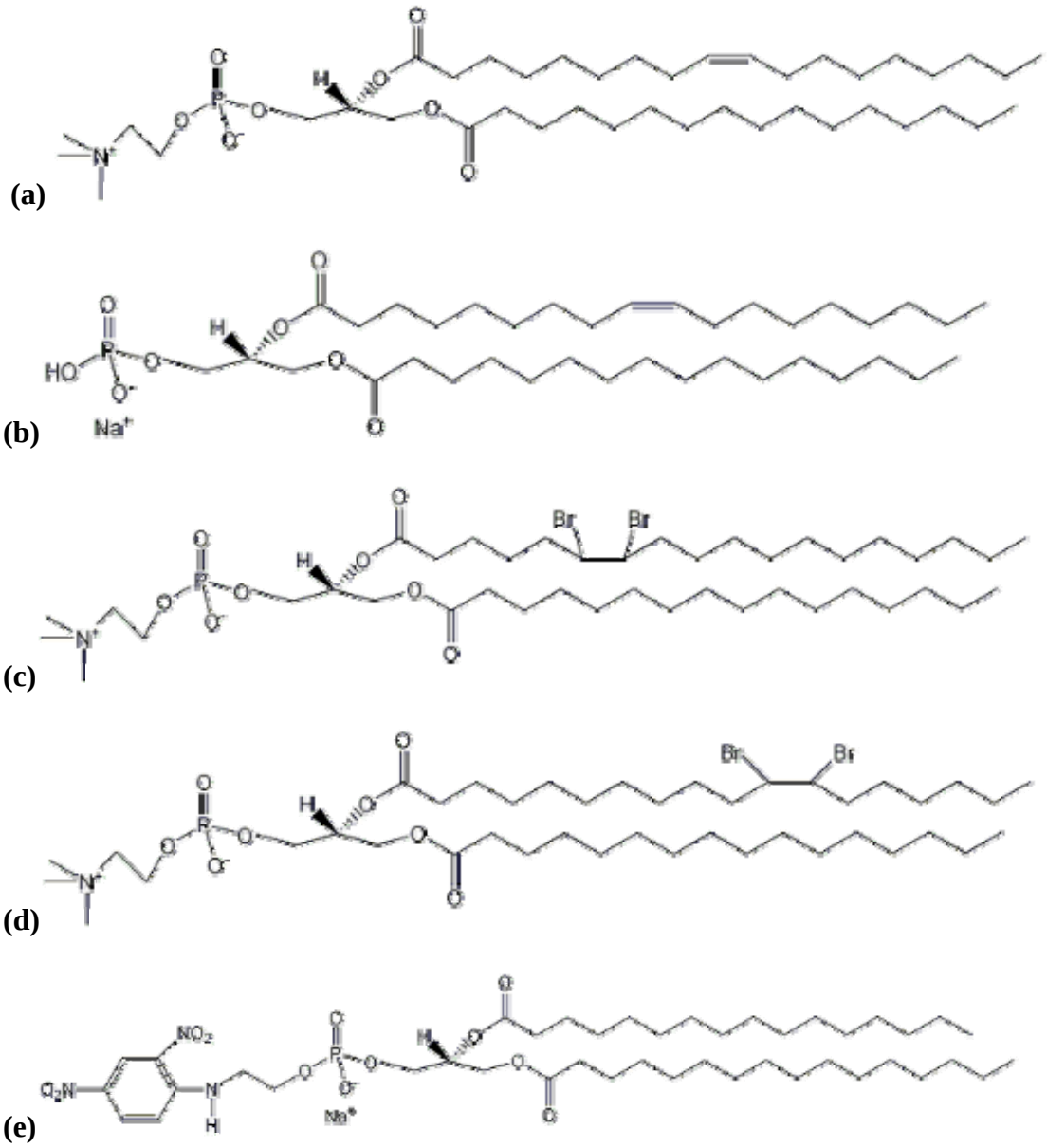

Figure 1.2. Structure of **(a)** 1-palmitoyl-2-oleoyl-*sn*-glycero-3-phosphocholine (POPC), **(b)** 1-palmitoyl-2-oleoyl-*sn*-glycero-3-phosphate (POPA), **(c)** 1-palmitoyl-2-stearoyl(6,7-dibromo)-*sn*-glycero-3-phosphocholine (6,7-DiBr), **(d)** 1-palmitoyl-2-stearoyl(11,12-dibromo)-*sn*-glycero-3-phosphocholine (11,12-DiBr), and **(e)**N-dinitrophenyl phosphatidylethanolamine (DNP)

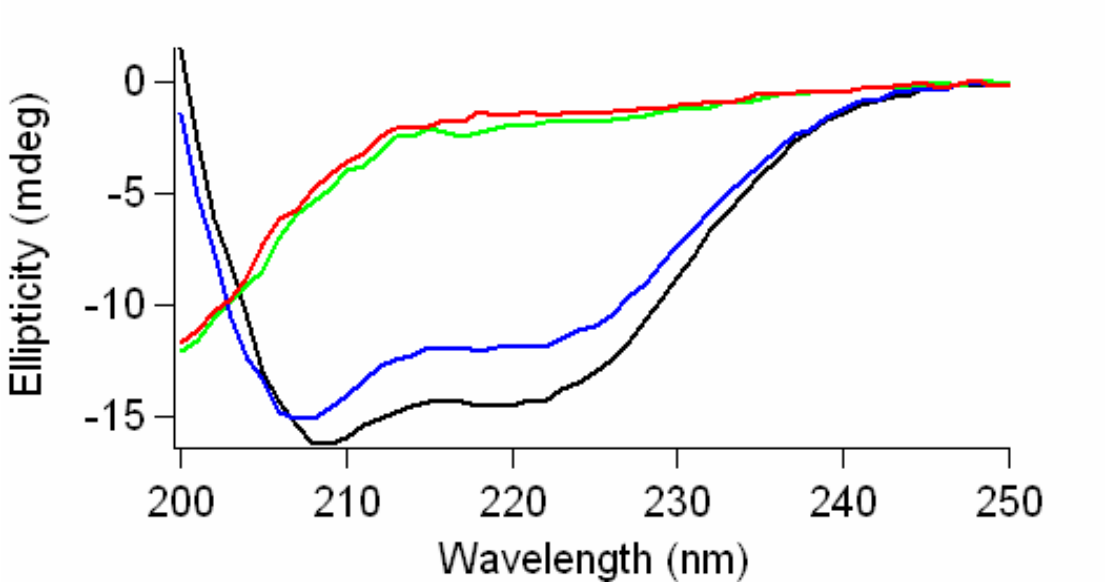

Figure 1.3. The CD signal for wild-type α-syn in 20 mM NaP_i buffer (red), 31 mM SDS micelles (blue), POPC SUVs (green), and 1:1 POPC:POPA SUVs (black)

POPC:POPA SUVs and SDS micelles. However, the CD spectra are comparable in solution and POPC SUVs, implying that minimal structures were induced when neutral vesicles are utilized.

This phenomenon was further proven by submitting a Trp-containing α-syn mutant (W39/Y55) to steady-state fluorescence spectroscopy in the aforementioned environments (**Figure 1.4**). Protein local environments can often be elucidated from Trp emissions.[36-39] The data suggests the λ_{max} of Trp emission for this α-syn mutant in solution is 347 nm. This emission maxima is similar when the mutant was placed in POPC SUVs (λ_{max} = 348 nm).

On the contrary, blue-shifted emission was observed when the α-syn mutant was placed in 31 mM SDS micelles (λ_{max} = 336 nm). This blue-shifted emission implies that the Trp is in a more hydroprobic environment, namely the micelles. In addition, an even more pronounced blue-shifted emission was observed when the mutant was placed in 1:1 POPC:POPA SUVs (λ_{max} = 332 nm). These CD and steady-state fluorescence studies show that the acidic lipids must be incorporated into the SUVs in order to induce structural formation of α-syn.

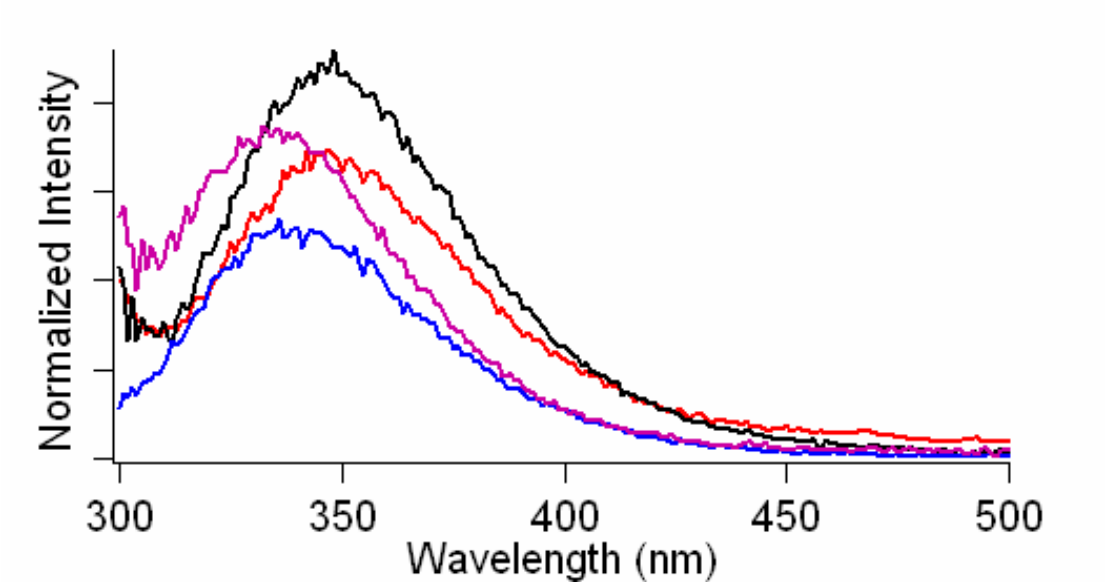

Figure 1.4. The steady-state fluorescence spectra of W39/Y55 α-syn mutants in the presence of 20 mM NaPi buffer (red), 31 mM SDS micelles (blue), POPC SUVs (black), and 1:1 POPC:POPA (purple)

α-Syn Insertion Studies.

It is important to determine the timescale for α-syn insertion into the bilayer to ensure that spectroscopic studies will be carried out after the samples have been fully equilibrated. As mentioned above, the quantum yield of Trp increases when it is placed in a more hydrophobic environment. We took advantage of this phenomenon to study the insertion kinetics of α-syn. The emission was monitored in 350 nm. Therefore, when the Trp is inserted into the bilayer, the fluorescence will increase significantly.

Figure 1.5 shows the fluorescence spectra when W4 was mixed with 1:1 POPC:POPA SUVs. A concentrated W4 solution was injected into a cuvette of SUVs when time = 62 s. Therefore, a significant increase of emission was observed at that point. After the sharp increase, there was a step of an appreciable decrease of fluorescence that lasts approximately another 150 s (inset). This implies that the insertion of α-syn into the lipid bilayer is almost instantaneous, followed by an equilibration step that lasts for minutes.

Trp's emission was further monitored for another 1.5 h, during which a very slow decrease of fluorescence intensity was observed. This event can be attributed to photodamage caused by long irradiation of the Trp.

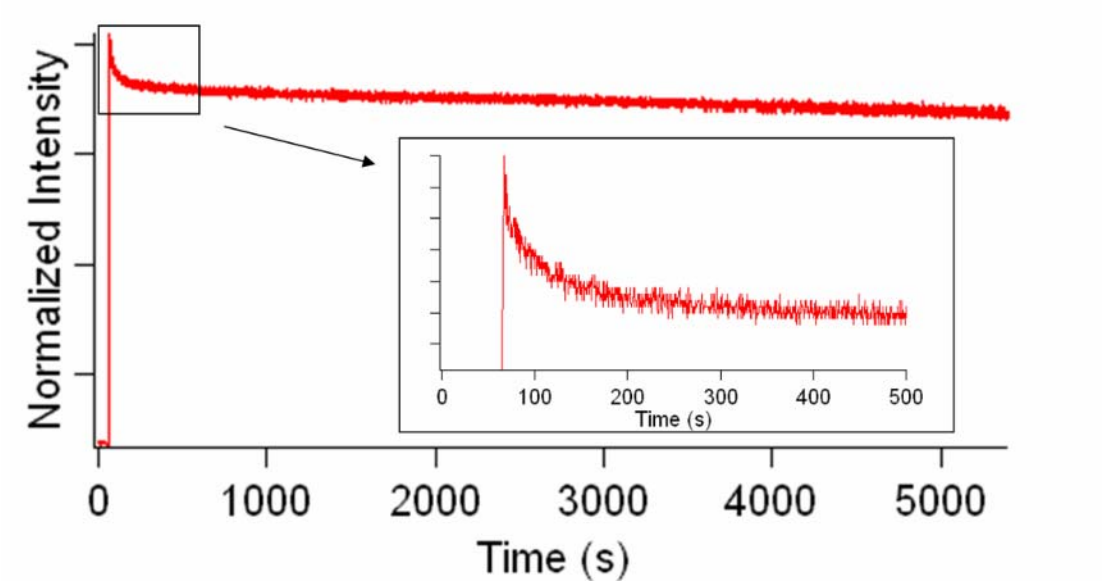

Figure 1.5. Steady-state fluorescence of Trp4 inserting into 1:1 POPC:POPA SUVs monitored at 350 nm

1.4 ACKNOWLEDGEMENT

This work is completed in collaboration with Dr. Jennifer C. Lee.

1.5 REFERENCE

(1) Galvin, J. E.; Lee, V. M.; Schmidt, M. L.; Tu, P. H.; Iwatsubo, T.; Trojanowski, J. Q..*Adv. Neurol.* **1999**, *808*, 313–324.
(2) Spillantini, M. G.; Crowther, R. A.; Jakes, R.; Hasegawa, M.; Goedert, M. *Proc. Natl. Acad. Sci. U. S. A.* **1998**, *95*, 6469–6473.
(3) Spillantini, M. G.; Schmidt, M. L.; Lee, V. M. Y.; Trojanowski, J. Q.; Jakes, R.; Goedert, M. *Nature* **1997**, *388*, 839–840.
(4) George, J. M.; Jin, H.; Woods, W. S.; Clayton, D. F. *Neuron* **1995**, *15*, 361–372.
(5) Iwai, A.; Masliah, E.; Yoshimoto, M.; Ge, N. F.; Flanagan, L.; Desilva, H. A. R.; Kittel, A.; Saitoh, T. *Neuron* **1995**, *14*, 467–475.
(6) Irizarry, M. C.; Growdon, W.; Gomez-Isla, T.; Newell, K.; George, J. M.; Clayton, D. F.; Hyman, B. T. *J. Neuropath. Exp. Neur.* **1998**, *57*, 334–337.
(7) Maroteaux, L.; Scheller, R. H. *Mol. Brain Res.* **1991**, *11*, 335–343.
(8) Jakes, R.; Spillantini, M. G.; Goedert, M. *Febs. Lett.* **1994**, *345*, 27–32.
(9) Weinreb, P. H.; Zhen, W. G.; Poon, A. W.; Conway, K. A.; Lansbury, P. T. *Biochemistry* **1996**, *35*, 13709–13715.
(10) Bertoncini, C. W.; Jung, Y. S.; Fernandez, C. O.; Hoyer, W.; Griesinger, C.; Jovin, T. M.; Zweckstetter, M. *Proc. Natl. Acad. Sci. U. S. A.* **2005**, *102*, 1430–1435.
(11) Lee, J. C.; Gray, H. B.; Winkler, J. R. *J. Am. Chem. Soc.* **2005**, *127*, 16388–16389.
(12) Lee, J. C.; Langen, R.; Hummel, P. A.; Gray, H. B.; Winkler, J. R. *Proc. Natl. Acad. Sci. U. S. A.* **2004**, *101*, 16466–16471.
(13) Lee, J. C.; Lai, B. T.; Kozak, J. J.; Gray, H. B.; Winkler, J. R. *J. Phys. Chem. B* **2007**, *111*, 2107–2112.
(14) Dedmon, M. M.; Lindorff-Larsen, K.; Christodoulou, J.; Vendruscolo, M.; Dobson, C. M. *J. Am. Chem. Soc.* **2005**, *127*, 476–477.
(15) Bernado, P.; Bertoncini, C. W.; Griesinger, C.; Zweckstetter, M.; Blackledge, M. *J. Am. Chem. Soc.* **2005**, *127*, 17968–17969.
(16) Conway, K. A.; Harper, J. D.; Lansbury, P. T. *Biochemistry* **2000**, *39*, 2552–2563.
(17) Davidson, W. S.; Jonas, A.; Clayton, D. F.; George, J. M. *J. Biol. Chem.* **1998**, *273*, 9443–9449.
(18) Eliezer, D.; Kutluay, E.; Bussell, R.; Browne, G. *J. Mol. Biol.* **2001**, *307*, 1061–1073.
(19) Bussell, R.; Eliezer, D. *J. Mol. Biol.* **2003**, *329*, 763–778.
(20) Chandra, S.; Chen, X. C.; Rizo, J.; Jahn, R.; Sudhof, T. C. *J. Biol. Chem.* **2003**, *278*, 15313–15318.

(21) Ramakrishnan, M.; Jensen, P. H.; Marsh, D. *Biochemistry* **2003**, *42*, 12919–12926.
(22) Jao, C. C.; Der-Sarkissian, A.; Chen, J.; Langen, R. *Proc. Natl. Acad. Sci. U. S. A.* **2004**, *101*, 8331–8336.
(23) Narayanan, V.; Scarlata, S. *Biochemistry* **2001**, *40*, 9927–9934.
(24) Lee, H. J.; Choi, C.; Lee, S. J. *J. Biol. Chem.* **2002**, *277*, 671–678.
(25) Volles, M. J.; Lansbury, P. T. *Biochemistry* **2002**, *41*, 4595–4602.
(26) Zhu, M.; Li, J.; Fink, A. L. *J. Biol. Chem.* **2003**, *278*, 40186–40197.
(27) Perrin, R. J.; Woods, W. S.; Clayton, D. F.; George, J. M. *J. Biol. Chem.* **2000**, *275*, 34393–34398.
(28) McLean, P. J.; Kawamata, H.; Ribich, S.; Hyman, B. T. *J. Biol. Chem.* **2000**, *275*, 8812–8816.
(29) Jo, E. J.; McLaurin, J.; Yip, C. M.; St George-Hyslop, P.; Fraser, P. E. *J. Biol. Chem.* **2000**, *275*, 34328–34334.
(30) Ueda, K.; Fukushima, H.; Masliah, E.; Xia, Y.; Iwai, A.; Yoshimoto, M.; Otero, D. A. C.; Kondo, J.; Ihara, Y.; Saitoh, T. *Proc. Natl. Acad. Sci. U. S. A.* **1993**, *90*, 11282–11286.
(31) Winkler, G. R.; Harkins, S. B.; Lee, J. C.; Gray, H. B. *J. Phys. Chem. B* **2006**, *110*, 7058–7061.
(32) Rischel, C. *J. Mol. Biol.* **1996**, *257*, 877–885.
(33) Riordan, J. F.; Vallee, B. L. *Meth. Enzymol.* **1972**, *25*, 515–521.
(34) Kim, J. E.; Arjara, G.; Richards, J. H.; Gray, H. B.; Winkler, J. R. *J. Phys. Chem. B* **2006**, *110*, 17656–17662.
(35) Wu, P. G.; Brand, L. *Anal. Biochem.* **1994**, *218*, 1–13.
(36) Reshetnyak, Y. K.; Koshevnik, Y.; Burstein, E. A. *Biophys. J.* **2001**, *81*, 1735–1758.
(37) Kleinschmidt, J. H.; den Blaauwen, T.; Driessen, A. J. M.; Tamm, L. K. *Biochemistry* **1999**, *38*, 5006–5016.
(38) Doring, K.; Konermann, L.; Surrey, T.; Jahnig, F. *Eur. Biophys. J.* **1995**, *23*, 423–432.
(39) Surrey, T.; Jahnig, F. *Proc. Natl. Acad. Sci. U. S. A.* **1992**, *89*, 7457–7461.

Chapter 2

Phospholipid Interaction Sites of α-Synuclein Determined by Tryptophan

2.1 ABSTRACT

A hallmark of Parkinson's disease is the presence of fibrillar α-synuclein deposits in the brain. Although its function is ill defined, α-synuclein is found to associate with synaptic vesicles. Interestingly, α-synuclein appears to be natively unfolded *in vitro*. However, in the presence of membrane mimics (e.g., SDS micelles and acidic phospholipid vesicles), the protein adopts a highly helical conformation. We have prepared six single tryptophan-containing variants (W4, W39, W94, W101, W125, and W136). Their interactions with phospholipid vesicles by steady-state and time-resolved fluorescence measurements were probed. Using energy-transfer (dinitrophenol) and heavy-atom (bromine) labeled phospholipids, the relative location of the different Trp residues in the bilayer was determined to be on the order of W4>>W94>W39>W101>W136≥W125, from buried to water exposed.

2.2 INTRODUCTION

Though α-syn is characterized to be unstructured *in vitro*,[1] numerous experimental data now indicate that α-syn is not a random coil, but contains regions of structural preferences.[2-7] In the presence of acidic phospholipid vesicles, the protein will adopt α-helical structures. Notably, α-syn does not appear to interact with neutral phospholipid vesicles.[8] These structures have been characterized by circular dichroism (CD),[9] nuclear magnetic resonance (NMR),[10-12] and electron paramagnetic resonance (EPR) spectroscopies.[13,14]

Previously, Ulmer et al.[15] have investigated the structure of α-syn in association with SDS micelles using NMR. Their results show that two α-helices are formed within the N-terminal region (residues 3-37 and 45-92) in an antiparallel arrangement, joined by a short linker (residues 38-44). The C-terminal tail remains unstructured. In a separate study, Langen and coworkers[14] have characterized the location of residues 8-89 when associated with small unilammelar vesicles (SUVs) using site-directed spin labeling. In contrast to the micellar bound conformer, each eleven-residue repeat folds into three α-helical turns. This arrangement can be attributed to the charge distribution of the amino acids within the repeats: the negatively charged residues are solvent exposed, alanine and valine residues are lipid exposed, and lysine residues are localized near the polar head group. Although a short linker also is observed when α-syn is associated with the vesicles, it does not arrange the helices in an antiparallel fashion.

In this study, measurements of steady-state and time-resolved fluorescence were employed to characterize the interactions of SUVs with α-syn. A single tryptophan mutation was incorporated into six different sites (W4, W39, W94, W101, W125, and W136) to serve as a fluorescent probe for distinct regions of the protein: W4 on the N-terminus, W39 in the linker region, W94 on the C-terminal end of the NAC sequence, W101, W125, and W136 in the highly acidic C-terminus. In addition, we utilized commercially available phospholipids containing heavy-atom (Br) and energy-transfer (dinitrophenol) quenchers to elucidate the specific location of the individual Trp residues with respect to the lipid bilayer.

2.3 METHODS

Preparation of Small Unilamellar Vesicles (SUVs).

SUVs were prepared from a 1:1 molar mixture of lipids, 1-palmitoyl-2-oleoyl-*sn*-glycero-3-phosphocholine (POPC), and 1-palmitoyl-2-oleoyl-*sn*-glycero-3-phosphate (POPA) following published protocols and was described in Chapter 1.[16] Brominated lipids chosen for this experiment were 1-palmitoyl-2-stearoyl(6,7-dibromo)-*sn*-glycero-3-phosphocholine (6,7-DiBr) and 1-palmitoyl-2-stearoyl(11,12-dibromo)-*sn*-glycero-3-phosphocholine (11,12-DiBr); mixed vesicles were made in a 1:2:1 molar ratio of POPC:POPA:Di-Br. The distances between the headgroup/hydrocarbon boundary and the bromine atoms were 3.5 Å and 8.0 Å, respectively.[17] The lipid labeled with an energy-transfer quencher, N-dinitrophenyl

phosphatidylethanolamine (DNP), located at the head group, were used in a molar ratio of 4:5:1 POPC:POPA:DNP.

Protein Preparation, Modification, and Characterization.

The protein preparation, modification, and characterization processes were described in Chapter 1. Site-directed mutagenesis was performed to introduce tryptophan at six different sites (W4, W39, W94, W101, W125, and W136). All mutated sequences were confirmed by DNA sequencing (California Institute of Technology DNA Sequencing Core Facility).

Steady-state Absorption and Fluorescence Spectroscopy.

Using gel filtration chromatography (PD-10 desalting columns, GE Healthcare), all purified protein samples were exchanged into 20 mM NaP_i (pH 7.4) for the N-terminal tail mutants or 10 mM HEPES (pH 7.4) for the C-terminal tail mutants. Buffer solutions were filtered through a 0.22-μm filter to remove any particulates, while stock protein solutions were filtered through Microcon YM-100 (MWCO 100 kD) (Millipore) spin filter units to ensure removal of oligomeric species before diluting into prepared SUVs. All samples contained 5 μM of protein with 1.4 mg/mL of SUVs. For the N-terminal tail mutants, measurements were made with proteins in buffer, POPC:POPA, and SUVs with the three types of different quenchers. Since it has been suggested not to insert the C-terminal tail into the membrane, the SUVs with Br(11,12)-POPC incorporated were not utilized.

To evaluate the amount of quenching for α-syn mutants in 25% 6,7-DiBr and 25% 11,12-DiBr SUVs, the ratios of quenched-to-unquenched emission (F/F_0) were calculated. Emissions were integrated between 300 nm and 500 nm after background substrations. The ratio was then obtained by comparing the integrated emissions of α-syn mutants between brominated SUVs and quencher-free SUVs.

Time-resolved Fluorescence Measurements.

Time-resolved fluorescence decay experiments were carried out as previously described in Chapter 1. For anisotropy decay kinetics measurements, samples were excited by a vertically polarized laser pulse and both polarizations (I_{VV} and I_{VH}) were collected simultaneously for each sample.

Data Analysis.

The measured fluorescence decay kinetics were fitted by previously described procedures.[5] Kinetics traces were logarithmically compressed (100 points per time decade) and modeled with NNLS fitting protocol to project the narrowest *P(k)* distributions from the fluorescence kinetics.[4] To provide more information on the amount of quenching for α-syn mutants in SUVs containing brominated lipids, quenched-to-unquenched lifetime ratio (τ/τ_0) was also determined by comparing their weighed fluorescent decay rate.

To calculate time-resolved anisotropy decay kinetics, the ratio of sensitivities (G) for the vertically and horizontally polarized light in the system is assumed to be one. However, all luminescence spectra were adjusted according to the I_{VV} and I_{VH}

luminescence spectra obtained from NATA. Then, the anisotropy value (r) could be obtained by applying this equation,

$$r = \frac{I_{VV} - GI_{VH}}{I_{VV} + 2GI_{VH}}.$$

The anisotropy decay curve was then fitted against single exponential decay to determine the rotational correlation time of each mutant in POPC:POPA SUVs.

2.4 RESULTS AND DISCUSSIONS

Steady-state Fluorescence.

Tryptophan emission is an extremely sensitive probe of protein local environments.[20-23] Shown in **Figure 2.1** and **Table 2.1** are the fluorescence properties of Trp mutants in NaP_i buffer and when bound to SUVs (1:1 POPC:POPA). For the model complex, NATA, and the C-terminal mutants, the Stokes shifts (59 nm) are similar for both buffer and vesicle solutions. These shifts are characteristic of a completely water-exposed indole (**Figure 2.1**). In contrast, the three N-terminal α-syn variants exhibit smaller Stokes shifts upon the addition of vesicles, revealing that the three Trp residues are located in more hydrophobic environments, while the C-terminal mutants remain in hydrophilic environments.

Among the three N-terminal mutants, W4 has the most pronounced blue-shifted emission (λ_{max} = 326 nm), suggesting that it is protected from water and embedded in the lipid bilayer. On the other hand, a lower quantum yield and a less blue-shifted peak for W94 demonstrates that this indole side chain is located in a less hydrophobic environment, likely closer to the polar phospholipid headgroups. The

	λ_{max} (nm)	
	20 mM NaP_i	1:1 POPC:POPA
NATA	354	353
W4	348	326
W39	348	340
W94	351	335
W101	348	352
W125	349	353
W136	346	352

Table 2.1. Fluorescence maxima of NATA and α-syn mutants in the presence of NaP_i and 1:1 POPC:POPA vesicles

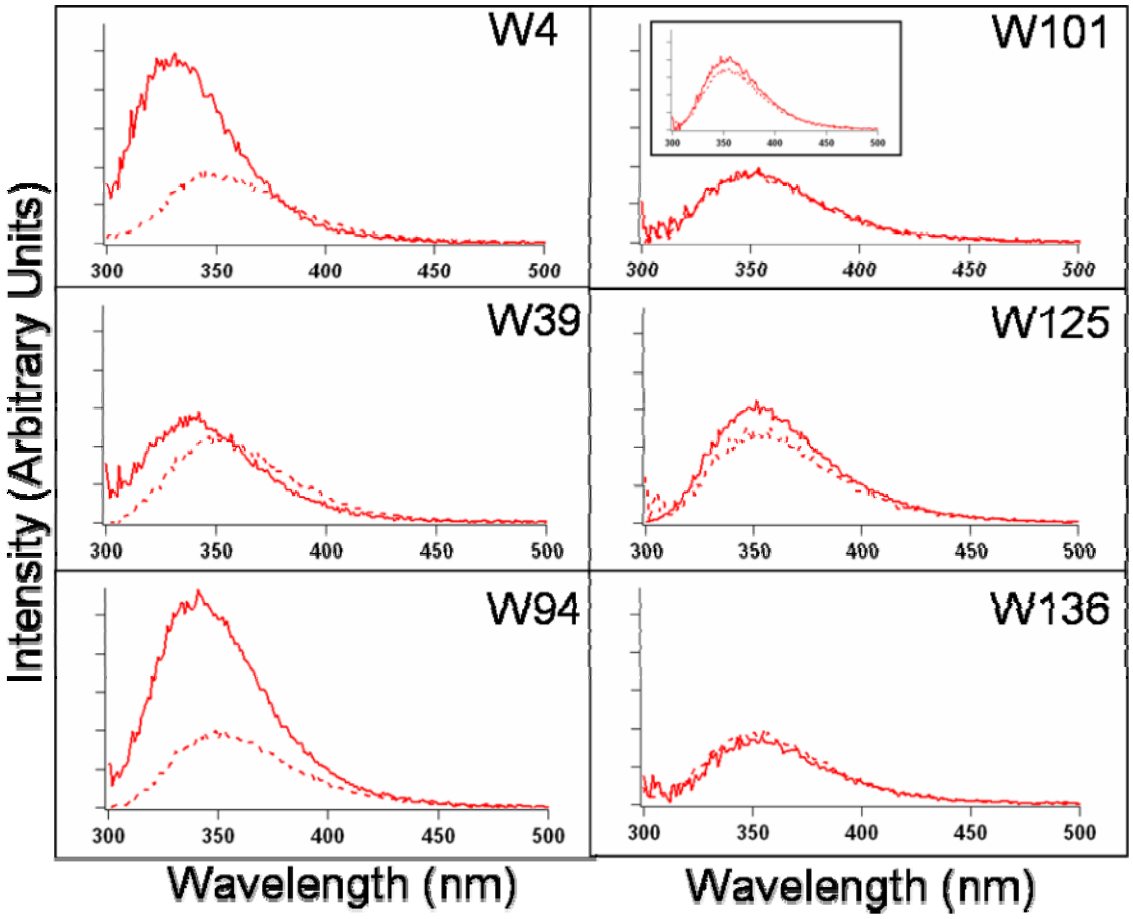

Figure 2.1. Steady-state fluorescence spectra of NATA (inset), W4 (top-left panel), W39 (middle-left panel), W94 (bottom-left panel), W101 (top-right panel), W125 (middle-right panel), and W136 (bottom-right panel) α-syn mutants in the presence of NaP_i (dotted) and 1:1 POPC:POPA vesicles (solid)

W39 protein exhibits the smallest quantum yield, suggesting that this residue is located closest to the surface of the SUV.

Using SUVs containing brominated lipids, distances between Trp and bromine quencher can be extrapolated empirically according to the degree of quenching by the bromine atoms.[24] W39 shows modest amount of quenching (< 10%) in the presence of the heavy atoms (**Table 2.2**), indicating that the tryptophan residue is at least > 14 Å away from both sites (6,7- and 11,12-DiBr, structures are shown in **Figure 1.2**). In contrast, nearly complete quenching (> 90% with 6,7- and ~ 40% with 11,12-Di-Br) is observed for the N-terminal W4, indicating that this indole is the most deeply inserted side-chain amongst the fluorophores.

For the C-terminal mutants, only 6,7-DiBr SUVs were examined because W101 and W136 showed minor quenching (< 10%) in the presence of the brominated lipids, while W125 fluorescence is unaffected. This agrees closely to previously published data that suggest that the C-terminal fragment is not involved in membrane binding.[11-14,25,26] However, our results reveal that W101 and W136 may be located closer to the membrane than W125.

To further map out the Trp locations with respect to the polar headgroup, we utilized a phospholipid labeled with an energy acceptor moiety, dinitrophenol (λ_{abs} = 350 nm) in the headgroup. For all the mutants studied (W4, W39, W94, W101, W125, and W136), a high degree of tryptophan quenching was observed in the presence of the dinitrophenol group, attributable to inner filter effect of the energy-transfer quencher (data not shown). To eliminate the inner filter effects ($\varepsilon_{350\ nm}$ (DNP) = 13,353 $M^{-1}cm^{-1}$; OD > 2 at 10% DNP), time-resolved fluorescence decay kinetics

		F/F_0	Trp-Br Distance (Å)	τ/τ_0
W4	25 % 6,7-DiBr	0.1	6	0.1
	25 % 11,12-DiBr	0.6	11	0.2
W39	25 % 6,7-DiBr	0.8	> 14	0.9
	25 % 11,12-DiBr	0.9	> 14	1.0
W94	25 % 6,7-DiBr	0.6	11	0.2
	25 % 11,12-DiBr	0.7	14	0.4
W101	25 % 6,7-DiBr	0.9	> 14	0.8
W125	25 % 6,7-DiBr	1.0	> 14	0.9
W136	25 % 6,7-DiBr	0.9	> 14	0.9

Table 2.2. Ratios of quenched-to-unquenched emission (F/F_0), and quenched-to-unquenched lifetime (τ/τ_0) for α-syn mutants in 25% 6,7-DiBr and 25% 11,12-DiBr SUVs, and estimated distance between tryptophan and bromine atoms

measurements were required to assess the Trp→DNP quenching.

Time-resolved Fluorescence Kinetics.

To probe for phospholipid-protein interactions, Trp fluorescence decay kinetics were examined in the presence of 1:1 POPC:POPA vesicles (**Figure 2.2**). The fits extracted from non-negative linear least-squares (NNLS) analysis show that there are two dominant components, 3 x 10^{-9} s^{-1} (60%) and 1 x 10^{-9} s^{-1} (40%), for NATA in buffer. Indeed, all the α-syn mutants investigated show similar biexponential decays in the presence or absence of 1:1 POPC:POPA (**Figure 2.3 and Figure 2.4**).

Again, SUVs containing brominated lipids were used to determine the position of Trps when folded into the vesicles. The FET kinetics data were collected and fitted using the NNLS method (**Figure 2.5 and 2.6**). The degree of quenching (**Table 2.1**) can be evaluated by the quenched-to-unquenched ratio (τ/τ_0) of the Trp lifetimes. Conclusions on the relative location of Trps when inserted into the SUVs are similar to the predictions drawn from the steady state fluorescence studies.

Fitting the FET kinetics data in the presence of 10% DNP SUVs using the NNLS method can reveal the locations of tryptophan residues with respect to the surface of the vesicle. The appearance of ultra-fast lifetimes (< 0.1 ns) corresponds to energy transfer to the dinitrophenol group. The Förster distance between Trp-DNP is calculated to be 27.5 Å. The data indicate that W39 contains the highest subpopulation (~ 25%) of fast decay constants, while the N-terminal W4 has the least amount (~ 12%) (**Figure 2.7**). This result is consistent with our di-Br studies where

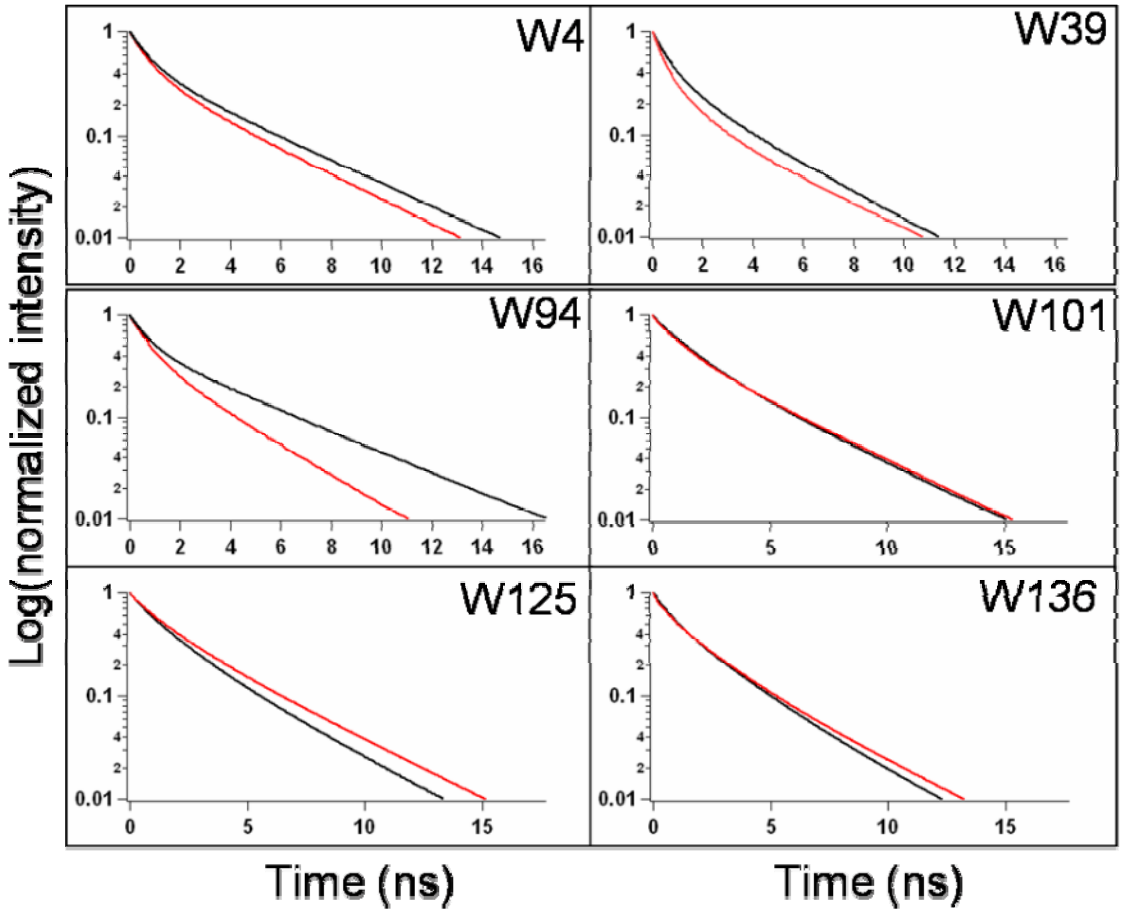

Figure 2.2. Time-resolved fluorescent kinetics of W4 (top left), W39 (top right), W94 (middle left), W101 (middle right), W125 (bottom left), and W136 (bottom right) α-syn mutants in 20 mM NaP_i buffer (red) and 1:1 POPC:POPA SUVs (black)

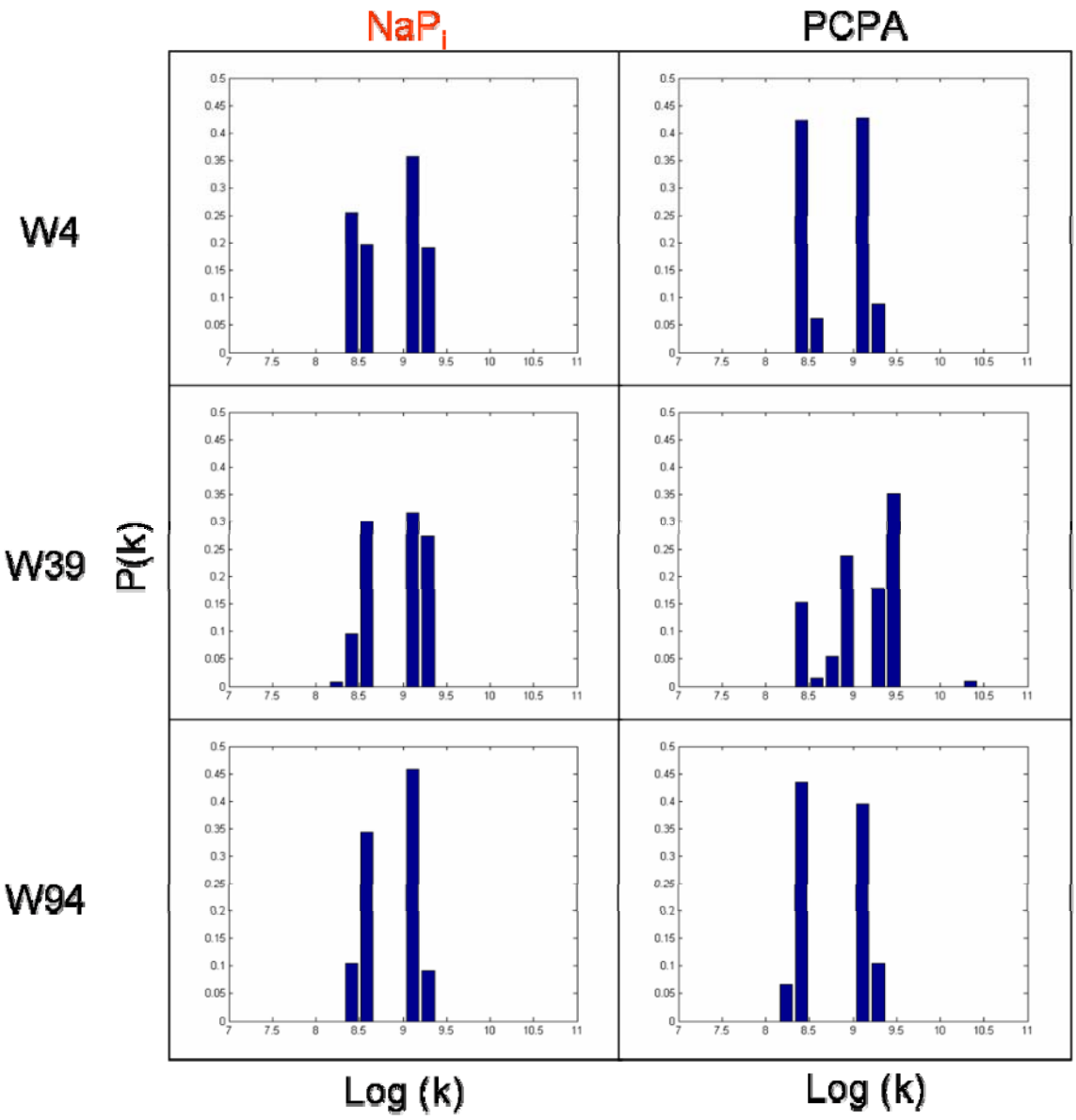

Figure 2.3. Distributions of tryptophan decay rate constants (k) for W4 (top), W39 (middle), and W94 (bottom) α-syn mutants in 20 mM NaP_i buffer (left) and 1:1 POPC:POPA SUVs (right)

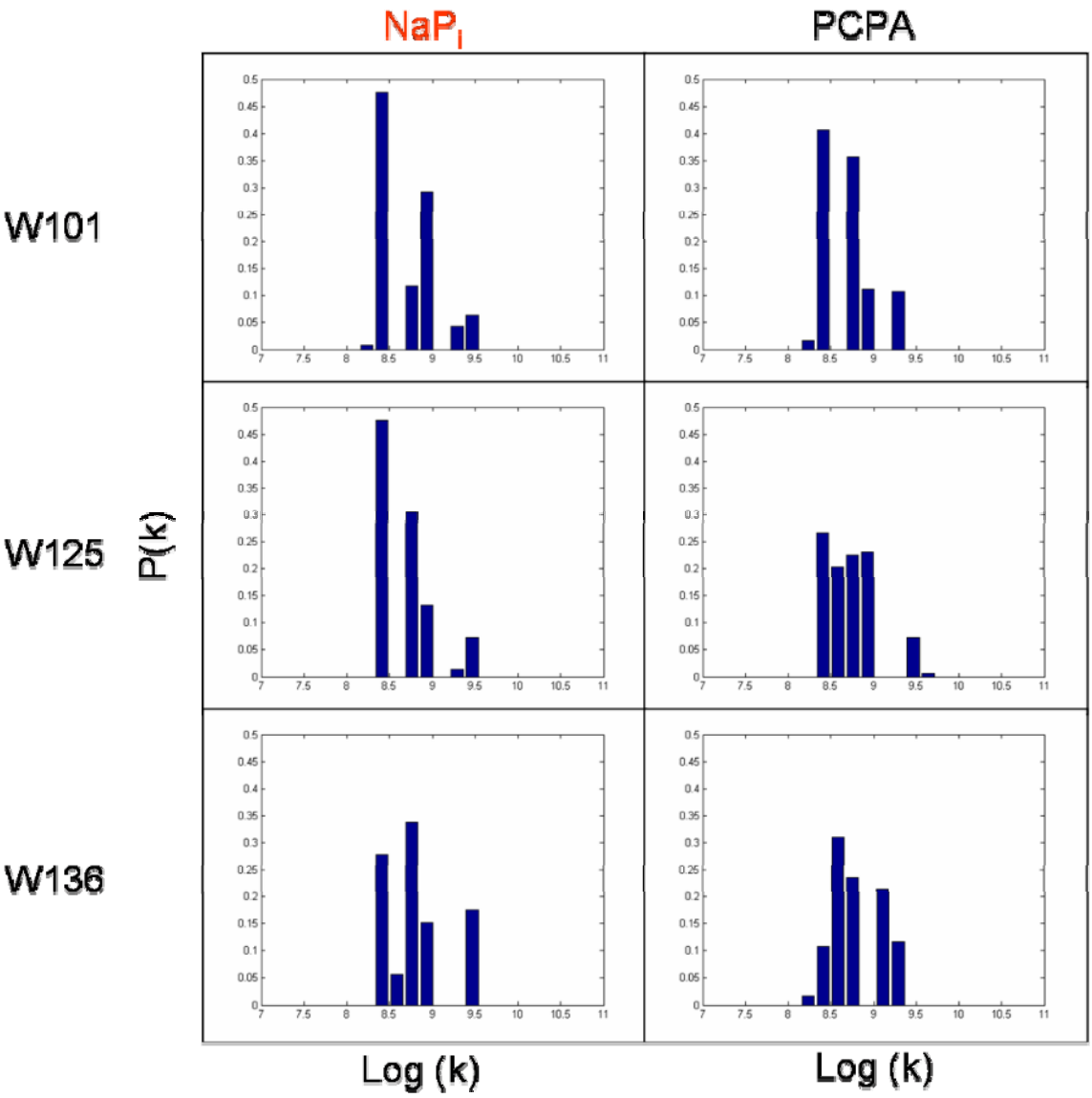

Figure 2.4. Distributions of tryptophan decay rate constants (k) for W101 (top), W125 (middle), and W136 (bottom) α-syn mutants in 20 mM NaP_i buffer (left) and 1:1 POPC:POPA SUVs (right)

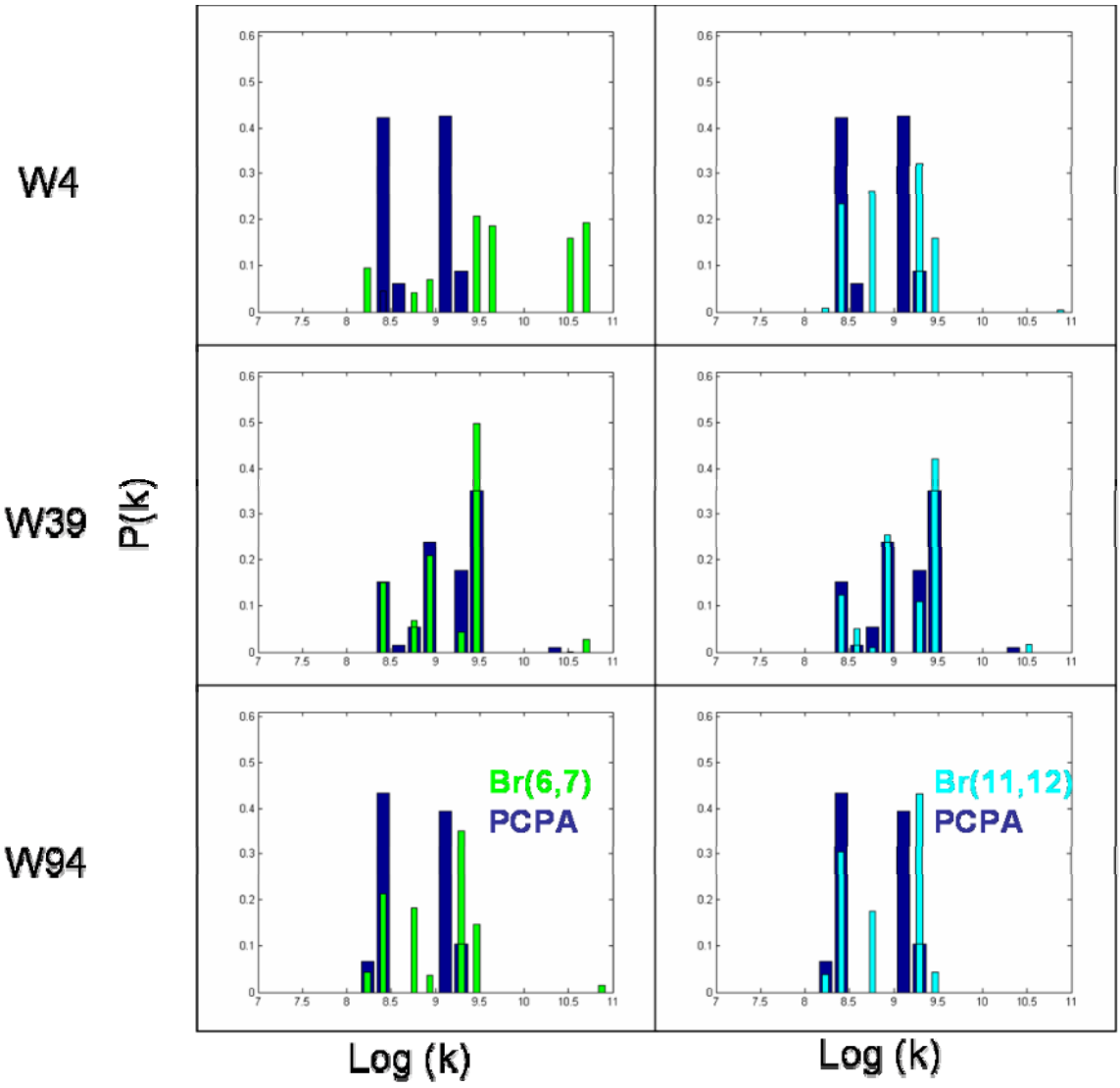

Figure 2.5. Distributions of tryptophan decay rate constants (k) for W4 (top), W39 (middle), and W94 (bottom) α-syn mutants in 1:1 POPC:POPA SUVs (dark blue), 6,7-DiBr SUVs (green), and 11,12-DiBr SUVs (aqua)

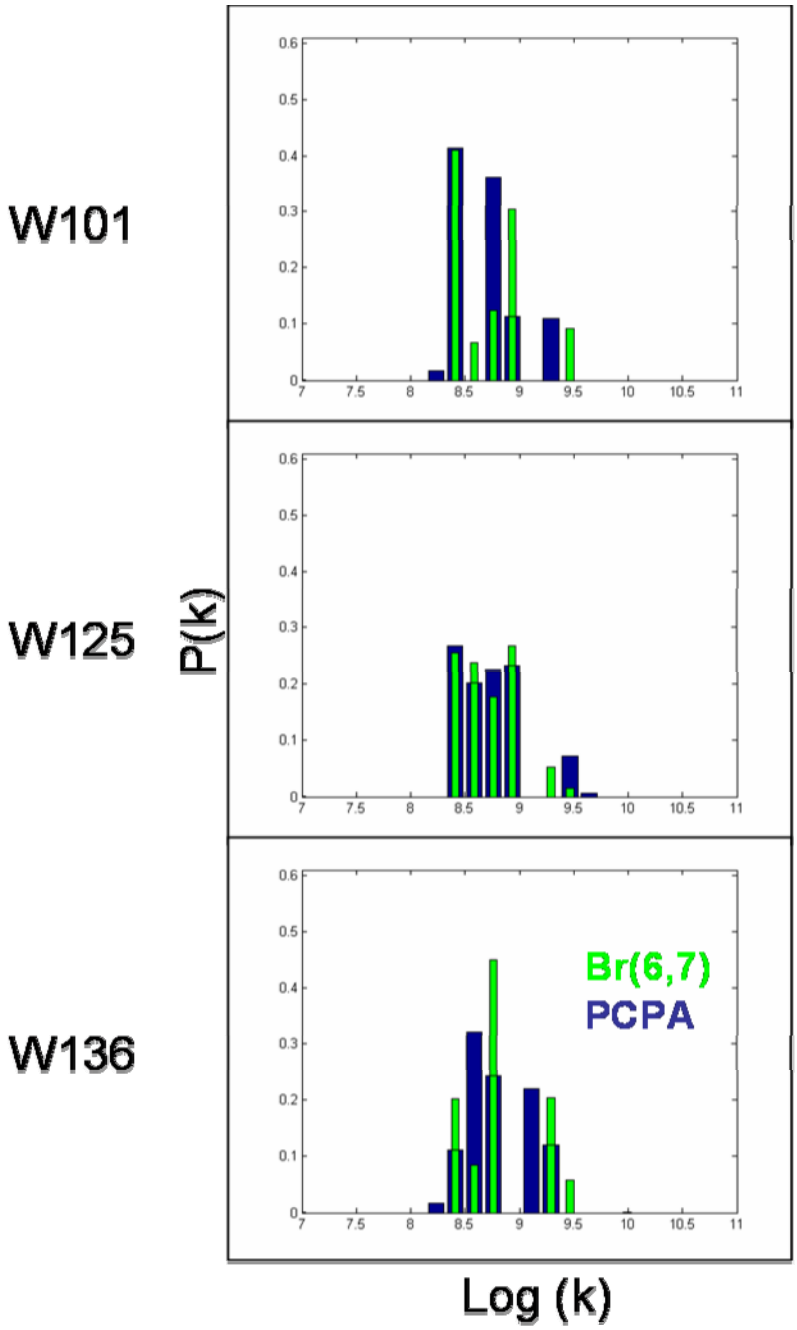

Figure 2.6. Distributions of tryptophan decay rate constants (k) for W101(top), W125 (middle), and W136 (bottom) α-syn mutants in 1:1 POPC:POPA SUVs (dark blue) and 6,7-DiBr SUVs (green)

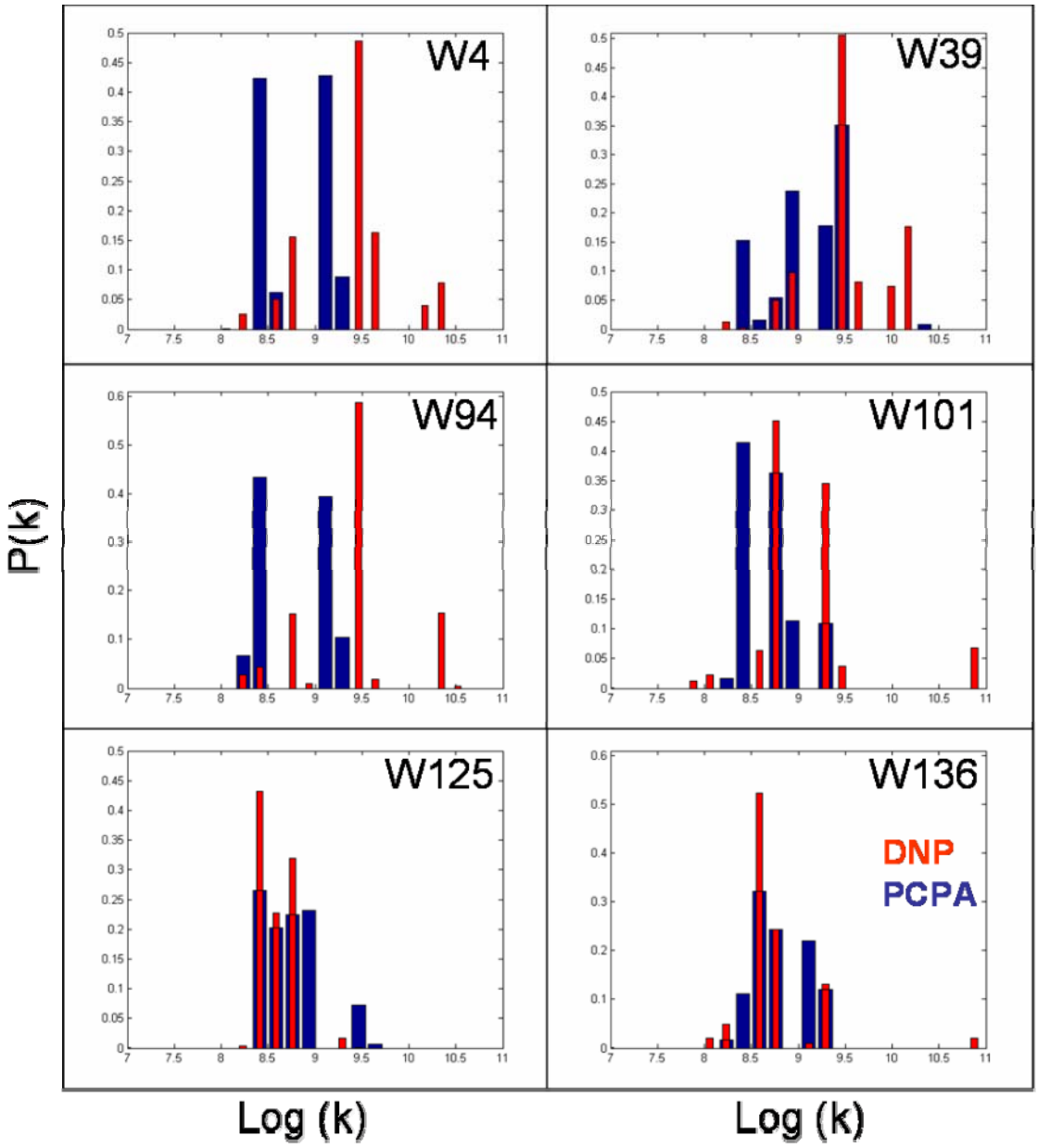

Figure 2.7. Distributions of tryptophan decay rate constants (k) for W4 (top left), W39 (top right), W94 (middle left), W101 (middle right), W125 (bottom left), and W136 (bottom right) α-syn mutants in the presence of 10 % DNP SUVs (red) and 1:1 POPC:POPA SUVs (dark blue)

W39 is located closest to the surface of the SUV. Notably, W4 is also the farthest away from the surface of the membrane when the protein associated with the phospholipid bilayer. Similarly, time-resolved fluorescence data obtained with brominated lipids gave the same order of proximity (W39 > W94 > W4) to the hydrocarbon core of the bilayer.

Similar experiments were performed on the C-terminal tail mutants, and the results were compared to the N-terminal tail mutants (**Figure 2.7**). The ultra-fast lifetimes observed for the N-terminal tail mutants were not present in the C-terminal tail positions, suggesting that these residues are not inserted in the interfacial region. However, the population of fast decay component (~ 1 x 10^{-9} s^{-1}) does increase, where W101 exhibits a sizable amplitude (41%) when it is associated with 10% DNP SUVs, suggesting that although it is not directly associated in the polar headgroup region, it is in close proximity to the surface (d ~ 30 Å). On the contrary, W136 shows considerably much less quenching in the ultra-fast population (14%), while W125 shows a negligible amount of quenching (2%). Along with the steady-state fluorescence results, we can deduce that W101 is located closest to the membrane surface, followed by W136 and W125.

Fluorescence Anisotropy Decay Kinetics.

Fluorescence anisotropy decay measurements were employed to characterize the Trp microenvironments and gain better understanding on the structural fluctuations during the excited-state decay.[16] **Figure 2.8** shows the fluorescence anisotropy decays and their exponential fits for the α-syn variants studied in the

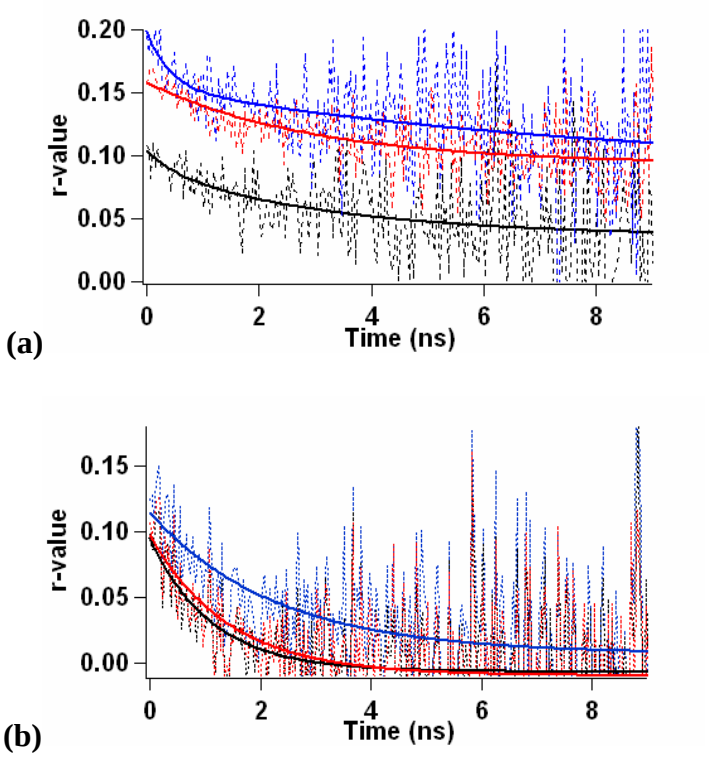

Figure 2.8. **(a)** Anisotropy decay for W4 (blue), W39 (black), and W94 (red) in 1:1 POPC:POPA SUVs. **(b)** Anisotropy decay for W101 (blue), W125 (black), and W136 (red) 1:1 POPC:POPA SUVs

presence of 1:1 POPC:POPA SUVs. Rotation correlation times (θ) were extracted from the anisotropy decays. Since rotation correlation times are related to the size and flexibility of the molecule, it is possible to draw conclusions regarding how embedded the Trp residues are in the membrane.

When α-syn is in solution, all Trp mutants demonstrate small rotation correlation times (θ ~ 1–2.5 ns). In association of SUVs, W4 has the highest rotation correlation time (θ ~ 8.3 ns). On the other hand, W39 and W94 are nearly identical θs (3.4 ns for W39 and 3.2 ns for W94). Among the C-terminal tail tryptophans, W101 has the slowest correlation time (θ ~ 2.3 ns), followed by W136 (θ ~ 1.4 ns) and W125 (θ ~ 1.1 ns). The rotation correlation times for these three mutants in solution and in vesicles show minimal increases, implying minimal insertion into the bilayer. The longest θ from W4 suggests that it is the most inserted into the membrane among the six mutants studied, followed by W94 and W39.

Other than comparing θs, anisotropy at time zero (r_0) can also be utilized to illustrate the degree of insertion of a Trp. In previous studies, it has been demonstrated that θ and r_0 increase when the rotational freedom of Trp is restricted. Kim et al. have shown that when outer membrane protein A is inserted into SUVs, the Trp's r_0 increased by approximately 50%.[16] Significant increases in θs were also demonstrated. Other studies have also shown the increase of Trp's θ when bound, such as when micelles were introduced to human apoliprotein C-I.[27] In **Figure 2.8**, it shows that W4 has the highest r_0, followed by W94 and W39. All the C-terminal tail mutants have a lower r_0 than the N-terminal mutants, with W101 showing the highest r_0 value among the three, while W125 and W136 show comparable r_0 values.

Clearly, the C-terminal Trp residues are much more flexible than the ones near the N-terminal sites. Unexpectedly, not all the C-terminal Trp data are equivalent. Our data suggest that the whole C-terminal tail is not free from influence from the membrane; in particular, in the vicinity of W101, likely through the anchoring at position 94, there is a measurable increase in local environment viscosity and polypeptide rigidity. The overall conclusions drawn from the fluorescence anisotropy measurements agree with the data collected from the other studies we performed, but differences were revealed amongst the C-terminal sites, especially in W101.

α-Syn Structure in Association with SUVs.

In summary, we can propose the following phospholipid-protein interactions illustrated in **Figure 2.9**. W39 is positioned near the surface of the SUVs, while W4 is the most inserted into the lipid bilayer among the six α-syn mutants investigated. W94 is shown to be inserted into the lipid bilayer, implying that the whole NAC region and the N-terminus participate in the α-helical structure when the protein is associated with acidic SUVs.

Since tyrosine and tryptophan both possess highly hydrophobic and hydrophilic character,[28] they are commonly found in the membrane-water interface. This phenomenon has been confirmed by this study. In fact, it has been proposed that

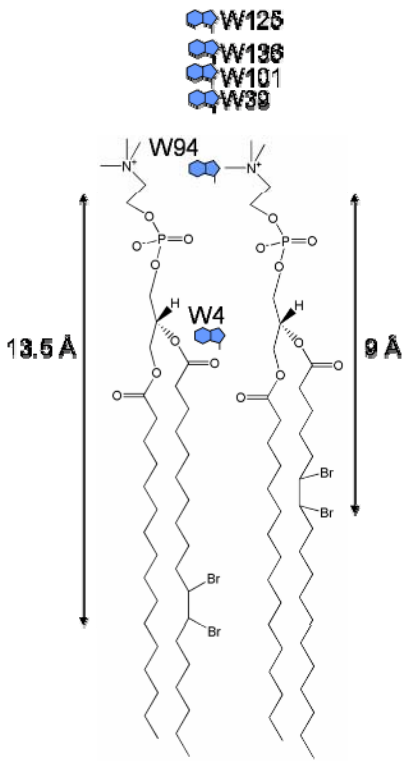

Figure 2.9. Approximate location of tryptophan residues in α-syn when associated with SUVs, drawn with respect to 11,12-DiBr (left) and 6,7-DiBr (right)

Y39 is the cause for the presence of the short linker when α-syn is associated with the membrane mimics.[11]

While the N-terminus forms a helical structure across the surface of the membrane, the C-terminal tail has been suggested to remain unstructured in the presence of acidic SUVs. Although we do agree that the C-terminal tail is not inserted in nor tightly associated to the lipid bilayer, our data suggest the possibility that W101 is in close proximity to the membrane surface and exhibits limited mobility compared to the rest of the C-terminus. This observation can be attributed to the residue being in proximity to the highly helical region.

Interestingly, we also have demonstrated that W136 has a closer interaction with the lipid bilayer than W125. It has been suggested by previous work that α-syn may possess nonrandom structure in solution.[2,3,5-7,29] Therefore, it is highly likely that the far end of the C-terminus of α-syn also has some propensity to interact closer to the membrane in the presence of acidic SUVs.

We have demonstrated that the SUVs made from lipids labeled with bromines and dinitrophenol can be used as a sensitive probe to characterize the structure of a membrane protein. Using these SUVs, we are able to assign the locations of the tryptophan residues in a phospholipid vesicle. In general, our work is in agreement with other studies conducted with NMR and EPR,[11-14] showing that the N-terminal tail of α-syn associates strongly with acidic SUVs, but does not penetrate through the membrane. On the other hand, our C-terminal tail results suggest that there could be some preferential behavior formed in that region in the presence of SUVs.

Positions for W4 and W94 when α-syn is associated with SUVs were not characterized by Langen et al. in their EPR study. They have concluded that α-syn forms three helical turns for every eleven amino acids in the region where there are seven imperfect repeats. Continuing this trend, we can postulate that W4 should be lipid exposed and W94 should be solvent exposed. Although our experimental results show that W4 is embedded into the SUV, W94 is not solvent exposed. This demonstrates that the helical property of α-syn may be contained outside of the 11-residue repeat region. On the other hand, the discrepancy observed for W94 can be attributed to the fact that the binding pattern of α-syn with membranes after residue 89 is not as structured as the repeat region.

These studies have provided additional structural insights on the folded membrane bound α-syn and serve as a foundation for future investigations. More spectroscopic studies, such as fluorescence energy transfer and dynamic contact quenching, will be employed to provide information on heterogeneous distance distributions and tertiary contacts formed in the protein, respectively.

2.5 ACKNOWLEDGEMENTS

This work was completed with Dr. Jennifer Lee's guidance.

2.6 REFERENCES

(1) Weinreb, P. H.; Zhen, W. G.; Poon, A. W.; Conway, K. A.; Lansbury, P. T. *Biochemistry* **1996**, *35*, 13709–13715.

(2) Bertoncini, C. W.; Jung, Y. S.; Fernandez, C. O.; Hoyer, W.; Griesinger, C.; Jovin, T. M.; Zweckstetter, M. *Proc. Natl. Acad. Sci. U. S. A.* **2005**, *102*, 1430–1435.

(3) Lee, J. C.; Gray, H. B.; Winkler, J. R. *J. Am. Chem. Soc.* **2005**, *127*, 16388–16389.
(4) Lee, J. C.; Langen, R.; Hummel, P. A.; Gray, H. B.; Winkler, J. R. *Proc. Natl. Acad. Sci. U. S. A.* **2004**, *101*, 16466–16471.
(5) Lee, J. C.; Lai, B. T.; Kozak, J. J.; Gray, H. B.; Winkler, J. R. *J. Phys. Chem. B* **2007**, *111*, 2107–2112.
(6) Dedmon, M. M.; Lindorff-Larsen, K.; Christodoulou, J.; Vendruscolo, M.; Dobson, C. M. *J. Am. Chem. Soc.* **2005**, *127*, 476–477.
(7) Bernado, P.; Bertoncini, C. W.; Griesinger, C.; Zweckstetter, M.; Blackledge, M. *J. Am. Chem. Soc.* **2005**, *127*, 17968–17969.
(8) Conway, K. A.; Harper, J. D.; Lansbury, P. T. *Biochemistry* **2000**, *39*, 2552–2563.
(9) Davidson, W. S.; Jonas, A.; Clayton, D. F.; George, J. M. *J. Biol. Chem.* **1998**, *273*, 9443–9449.
(10) Eliezer, D.; Kutluay, E.; Bussell, R.; Browne, G. *J. Mol. Biol.* **2001**, *307*, 1061–1073.
(11) Bussell, R.; Eliezer, D. *J. Mol. Biol.* **2003**, *329*, 763–778.
(12) Chandra, S.; Chen, X. C.; Rizo, J.; Jahn, R.; Sudhof, T. C. *J. Biol. Chem.* **2003**, *278*, 15313–15318.
(13) Ramakrishnan, M.; Jensen, P. H.; Marsh, D. *Biochemistry* **2003**, *42*, 12919–12926.
(14) Jao, C. C.; Der-Sarkissian, A.; Chen, J.; Langen, R. *Proc. Natl. Acad. Sci. U. S. A.* **2004**, *101*, 8331–8336.
(15) Ulmer, T. S.; Bax, A.; Cole, N. B.; Nussbaum, R. L. *J. Biol. Chem.* **2005**, *280*, 9595–9603.
(16) Kim, J. E.; Arjara, G.; Richards, J. H.; Gray, H. B.; Winkler, J. R. *J. Phys. Chem. B* **2006**, *110*, 17656–17662.
(17) McIntosh, T. J.; Holloway, P. W. *Biochemistry* **1987**, *26*, 1783–1788.
(18) Jakes, R.; Spillantini, M. G.; Goedert, M. *FEBS Letters* **1994**, *345*, 27–32.
(19) Winkler, G. R.; Harkins, S. B.; Lee, J. C.; Gray, H. B. *J. Phys. Chem. B* **2006**, *110*, 7058–7061.
(20) Reshetnyak, Y. K.; Koshevnik, Y.; Burstein, E. A. *Biophys. J.* **2001**, *81*, 1735–1758.
(21) Kleinschmidt, J. H.; den Blaauwen, T.; Driessen, A. J. M.; Tamm, L. K. *Biochemistry* **1999**, *38*, 5006–5016.
(22) Doring, K.; Konermann, L.; Surrey, T.; Jahnig, F. *Eur. Biophys. J.* **1995**, *23*, 423–432.
(23) Surrey, T.; Jahnig, F. *Proc. Natl. Acad. Sci. U. S. A.* **1992**, *89*, 7457–7461.
(24) Bolen, E. J.; Holloway, P. W. *Biochemistry* **1990**, *29*, 9638–9643.
(25) Narayanan, V.; Scarlata, S. *Biochemistry* **2001**, *40*, 9927–9934.
(26) Lee, H. J.; Choi, C.; Lee, S. J. *J. Biol. Chem.* **2002**, *277*, 671–678.
(27) Jonas, A.; Privat, J. P.; Wahl, P.; Osborne, J. C. *Biochemistry* **1982**, *21*, 6205–6211.
(28) Killian, J. A.; von Heijne, G. *Trends Biochem. Sci.* **2000**, *25*, 429–434.
(29) Lee, J. C.; Gray, H. B.; Langen, R.; Winkler, J. R. *Biophys. J.* **2004**, *86*, 268A-268A.

Chapter 3

α-Synuclein Membrane-bound Structures Characterized by Fluorescence Energy-transfer Kinetics

3.1 ABSTRACT

A hallmark of Parkinson's disease is the presence of fibrillar protein deposits in the brain, composed mostly of α-synuclein. Although its function is unknown, α-synuclein is found to associate with synaptic vesicles. Interestingly, α-synuclein appears to be natively unfolded *in vitro*. However, in the presence of membrane mimics, such as SDS micelles and acidic phospholipid vesicles, α-synuclein adopts a highly helical conformation. We have characterized the structures of α-synuclein variants, incorporated with tryptophan and 3-nitrotyrosine as donor and energy acceptor pairs, in the presence of SDS micelles and small unilammelar vesicles by time-resolved fluorescence energy-transfer measurements. Distance distributions extracted from these data provide site-specific information on the protein conformations.

3.2 INTRODUCTION

Previously, Ulmer et al. have employed NMR to characterize the structure of α-syn in the presence of SDS micelles.[1] The 20 lowest conformations of the structure (PDB file: 1XQ8) demonstrated that α-syn forms two helices, residues 3-37 (referred to as the N-terminal helix) and residues 45-92 (referred to as the C-terminal helix). These two helices are arranged in an antiparallel fashion and joined by a linker consisting of residues 38 through 44. The highly acidic C-terminal tail remains unstructured.

On the other hand, Langen et al. have investigated the structure of α-syn in the presence of acidic small unilammelar vesicles (SUVs) using EPR.[2] They concluded that residues 8 to 89 arrange themselves into three helices every 11 amino acids (α11/3 helices). They have also observed the formation of the motif of two helices and a linker. However, the helices do not arrange themselves in an antiparallel fashion.

SDS micelles have been typically estimated to have a circumference of 15 nm,[3] while the SUVs used for this study are approximately ten times larger in surface area. Since micelles are much smaller in size compared to SUVs, it was suggested by Bussell et al. that α-syn must adopt a more compact structure when it is associated with micelles.[4] They also reported that α-syn forms α11/3 helices in the presence of micelles and SUVs.

Time-resolved fluorescence energy-transfer (FET) has been employed to determine the structure and dynamics of α-syn in solution, SDS micelles, and acidic SUVs. Since FET rate is inversely proportional to the sixth power of fluorescent

donor-acceptor (D-A) distances,[5] it is possible to extract probability distributions of D-A distances from the fluorescence decay kinetics.[6-9] Fluorescent donor and energy acceptor chosen for this study were the fluorescent amino acid tryptophan (Trp) and a chemically modified tyrosine (Tyr), 3-nitrotyrosine [Y(NO_2)], respectively. This D-A pair has a Förster distance of 26 Å,[10] with a maximum extractable distance of 40 Å.

Six D-A pairs have been placed in strategic positions to probe the behavior of α-syn in sodium phosphate (NaP_i) buffer, SDS micelles, and acidic SUVs. The positions of the mutations have been highlighted in **Figure 3.1.**[11] W4/Y19(NO_2) and Y19(NO_2)/W39 were engineered to examine the N-terminal helix, while Y39(NO_2)/W94 and Y74(NO_2)/W94 were for C-terminal helix. W39/Y55(NO_2) was used to probe the linker region. W4/Y94(NO_2) was designed to investigate whether the two helices were brought into close proximity in the presence of different membranes by antiparallel arrangement.

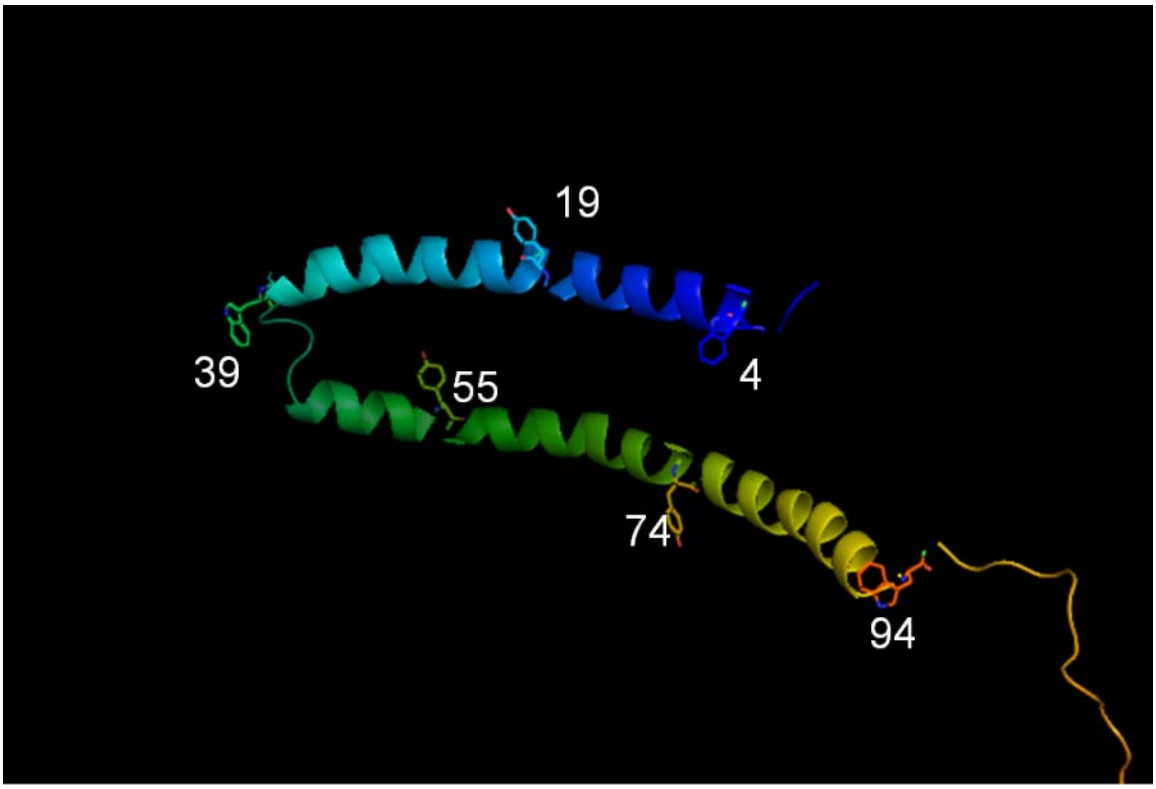

Figure 3.1. The structure of α-syn bound to SDS micelles elucidated by Ulmer et al.[1] Mutations constructed for this study are numbered.

3.3 METHODS

Protein Preparation, Modification, and Characterization.

A single Trp mutation was introduced in three various positions to replace an aromatic amino acid (F4, Y39, and F94) by site-directed mutagenesis. Except for Y39/W94, where three of the four native tyrosines were mutated into phenylalanines, all four tyrosines were mutated to phenylalanines, and an additional tyrosine residue was introduced in four various positions (A19, V55, V74, and F94). All the sequences were confirmed by DNA sequencing (California Institute of Technology DNA Sequencing Core Facility). Expression and purification of mutants were achieved by following protocols outlined in Chapter 1.

Preparation of Membrane Mimics.

SDS micelles and SUVs were fabricated according to procedures located in Chapter 1. SUVs were made from a 1:1 molar mixture of lipids, 1-palmitoyl-2-oleoyl-*sn*-glycero-3-phosphocholine (POPC), and 1-palmitoyl-2-oleoyl-*sn*-glycero-3-phosphate (POPA), following published protocols.[12] The SUVs were characterized by dynamic light scattering.

Dynamic Light Scattering.

The SUVs made from 1:1 POPC:POPA phospholipids were characterized using dynamic light scattering. DLS measurements were made with a 0.1 mg/mL vesicles solution in NaP_i buffer at 25 °C on a PD4043 detector (Precision Detectors,

Inc., Bellingham, MA). The DLS sample was illuminated with a diode laser operating at 658 nm at a scattering angle of 90°. The radii populations were extrapolated from the collected correlation functions by Precision Deconvolve[32] software.

Spectroscopic Measurements.

Prior to preparing samples for measurements, oligomeric materials in the concentrated protein stock were removed by filtration through Microcon YM-100 spin filter units (molecular weight cutoff 100 kD; Millipore). The protein samples were also exchanged into 20 mM NaP_i buffer (pH 7.4). Protein samples (5 μM) were measured at 25 °C. For samples containing SDS micelles and 1:1 POPC:POPA SUVs, a final concentration of 31 mM micelles and 1.4 mg/mL of vesicles were achieved, respectively. Luminscence spectra and time-resolved fluorescence measurements were obtained by methods outlined in Chapter 1. The time-resolved fluorescent energy transfer kinetics were fitted using the NNLS practice.

3.4 RESULTS AND DISCUSSIONS

Dynamic Light Scattering.

Figure 3.2 shows the distance distribution extracted from the DLS correlation functions. The data suggests that the vesicles were uniform in size, with a measured radius of 7.57 nm. Assuming that both SDS micelles and 1:1 POPC:POPA

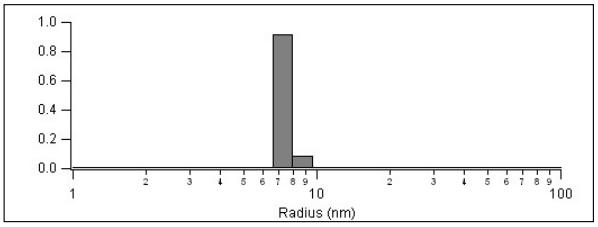

Figure 3.2. The fitted spectra for DLS correlation function of 0.1 mg/mL of 1:1 POPC:POPA SUVs in 20 mM NaP_i buffer (pH 7.4). The average radius for the SUVs is 7.57 nm.

vesicles are perfect spheres, the surface area of the vesicles is more than ten times larger than that of the micelles.

Trp fluorescence.

Trp was incorporated into all the mutants at three different sites (W4, W39, and W94). Trp emission is a useful probe to determine the local environment of Trp.[13-16] **Table 3.1** shows the fluorescence maxima of the Trp mutants and NATA, in NaP_i buffer, SDS micelles, and 1:1 POPC:POPA vesicles. The results shown are similar to the fluorescence maxima reported in previously published work.[17,18] It is shown that the fluorescence maxima in NaP_i buffer are similar between NATA and all Trp mutants.

In the presence of SDS micelles, it is shown all three Trp emissions exhibit a prominent blue shift. This blue shift is indicative that the Trp residues are located in a more hydrophobic environment. Further blue shifts of the fluorescence maxima are only observed when W4 and W94 are introduced into SUVs. On the contrary, there is a slight red-shift in emission for W39 inserted into SUVs vs. micelles. The difference of Trp behavior between micelles and SUVs implies that different structures can be formed when α-syn is associated with the two different membranes.

	λ_{max} (nm)		
	20 mM NaP_i	SDS micelles	1:1 POPC:POPA
NATA	354	352	353
F4W	348	328	326
Y39W	348	338	340
F94W	351	338	335

Table 3.1. Fluorescence maxima of NATA and α-syn mutants in the presence of NaP_i, SDS micelles, and 1:1 POPC:POPA vesicles

Time-resolved fluorescence kinetics.

Since α-syn is unstructured in solution, most of the mutants are expected to have distances longer than 40 Å. **Figure 3.3** to **Figure 3.5** shows the D-A distance populations extrapolated from the time-resolved fluorescence energy-transfer kinetics when the α-syn mutants were in solution (top panel), 1:1 POPC:POPA SUVs (middle panel), and SDS micelles (bottom panel).

W4/Y19(NO_2) and Y19(NO_2)/W39 were mutants used to investigate the behavior of the N-terminal helix when α-syn was present in solution, SUVs, and micelles. **Figure 3.3a** and **3.3b** displays the distances extracted from the experiments. These figures suggest that the size of the N-terminal helix formed when α-syn is associated with 1:1 POPC:POPA and with SDS micelles are comparable. W4/Y19(NO_2) has a population of intermediate polypeptides with distance of 24 Å (~ 50%) in SUVs, compared to 23 Å (~ 50%) in micelles. Similar conclusions can be drawn for Y19(NO_2)/W39 (23 Å, 32% in SUVs vs. 21 Å, 44% in micelles).

The structure of the C-terminal helix was probed by introducing Y39(NO_2)/W94 and Y74(NO_2)/W94. The D-A distances extracted (**Figure 3.4a** and **3.4b**) show distance distributions of these mutants when they were in association with micelles and SUVs. Y39(NO_2)/W94 D-A pair gives ~ 90% of its distance population at > 40 Å (NaP_i and 1:1 POPC:POPA) and ~ 37 Å (SDS micelles). The results imply that the more compact helix is formed when micelles are introduced, rather than SUVs. A similar trend was observed for the Y74(NO_2)/W94 D-A pair. The majority of the polypeptide distance populations when α-syn is associated with SUVs is 28 Å (~ 80%), while with SDS micelles it is 23 Å (~ 60%).

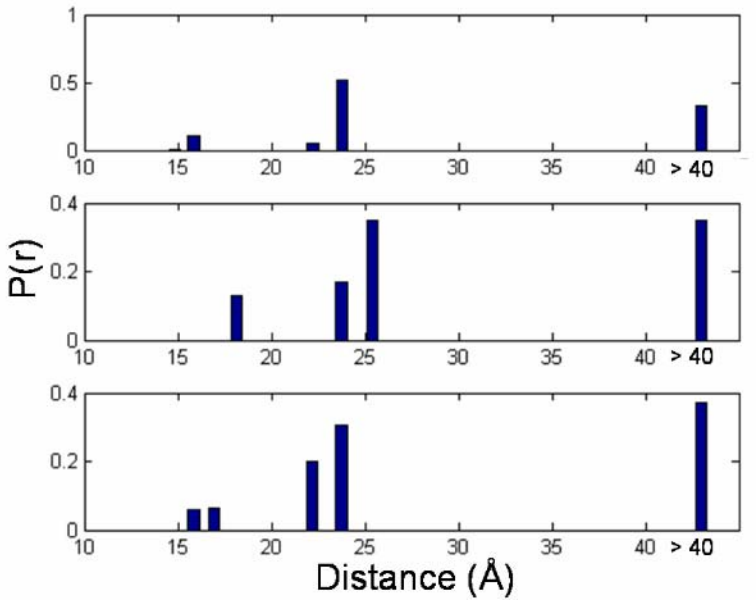

(a)

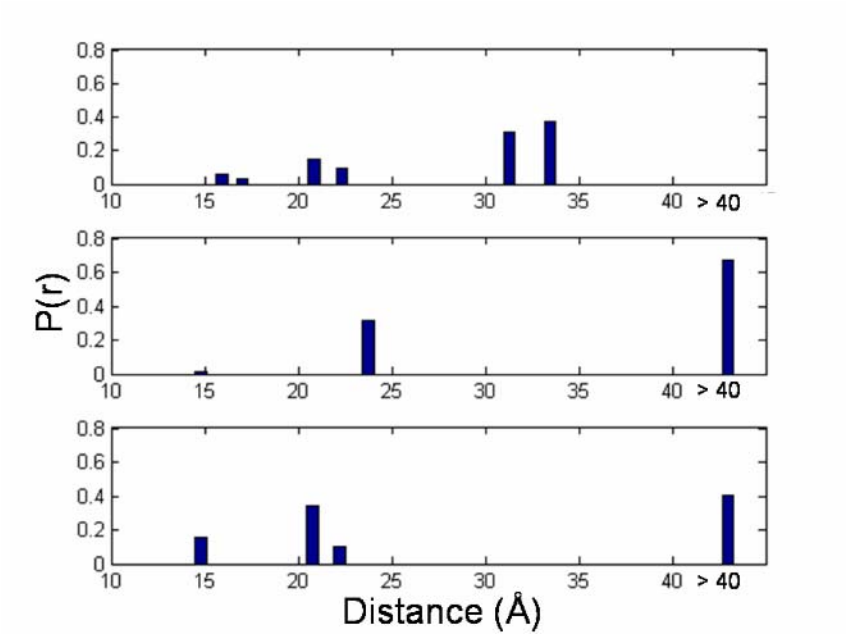

(b)

Figure 3.3. D-A distance distributions extrapolated from FET kinetics for **(a)** W4/Y19(NO_2) and **(b)** Y19(NO_2)/W39 in 20 mM NaP_i buffer (top panel), 1:1 POPC:POPA (middle panel), and 40 mM SDS (bottom panel)

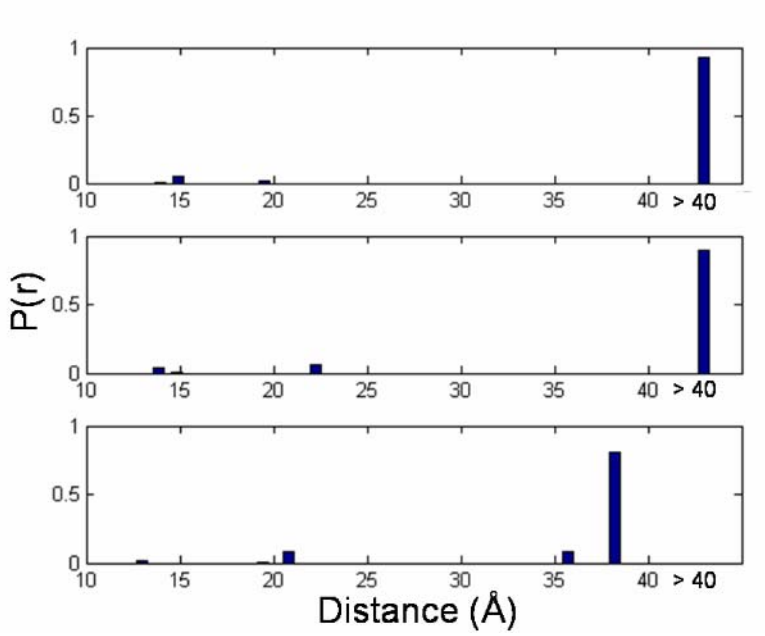

(c)

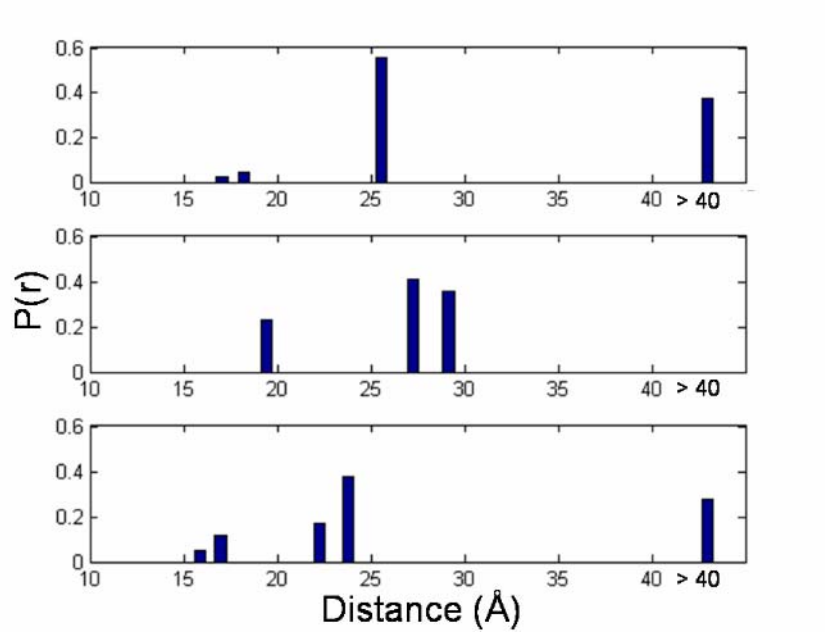

(d)

Figure 3.4. D-A distance distributions extrapolated from FET kinetics for **(c)** Y39(NO_2)/W94 and **(d)** Y74(NO_2)/W94 in 20 mM NaP_i buffer (top panel), 1:1 POPC:POPA (middle panel), and 40 mM SDS (bottom panel)

When comparing the previously published structures of α-syn as associated with SUVs and micelles, the most prominent difference is the arrangement of the two helices. A turn region between residues 38 and 45 brings the two helices in antiparallel arrangement when α-syn is associated with SDS micelles. However, while the linker between the two helices was observed, the helices of α-syn were not brought closer together in the presence of SUVs. Therefore, W4/Y94(NO_2) and W39/Y55(NO_2) were introduced to investigate whether the two helices were brought together in antiparallel fashion.

The W4/Y94(NO_2) mutant is expected to have long D-A distances in NaP_i buffer and SUVs, while the antiparallel motif of the helices should provide a much shorter D-A distance when this α-syn mutant is present in SDS micelles. For W39/Y55(NO_2), W39 is located at the end of the N-terminal helix while Y55(NO_2) is located ten residues from the beginning of the C-terminal helix. Therefore, the D-A distances should be the shortest when the mutant is associated with SDS micelles, followed by SUVs and solution.

Figure 3.5a shows that the extracted distance ensembles confirm this hypothesis. For the W4/Y94(NO_2) mutant, a majority of the distance populations in NaP_i (~ 90%) and SUVs (~ 90%) are longer than 40 Å. However, in the presence of SDS micelles, a significant distance population at ~ 19 Å (~ 30%) and ~ 24 Å (~ 30%) can be observed. In fact, these distances agree with the information provided by Ulmer et al. This implies that the two helices do indeed come into close proximity in the presence of the small SDS micelles. On the other hand, possibly due to the larger size of the SUV, W4 and Y94 are not brought together in such fashion.

For the W39/Y55(NO_2) mutant (**Figure 3.5b**), the ensemble of D-A distances for the micelle-associated structure consists of short (15 Å, 18%), intermediate (21 Å, 44%) and extended (> 40 Å, 38%) polypeptides. The majority of the extracted distances belong to the intermediate polypeptides, agreeing with the proposed distances by NMR micellear structure. On the other hand, the SUV associated structure has a population of short (18 Å, ~ 11%), intermediate (28 Å, ~57%) and extended (> 40 Å, 32%) polypeptides. This above implies that a more compact structure at the turn region is formed when α-syn is associated with micelles than with SUVs, hence matching our prediction. Interestingly, the longest polypeptide observed when the mutant is in NaP_i buffer alone (34 Å, 38%) is much shorter than the ones formed in association with SUVs and micelles. This could be evidence that this turn region has some structural preference in solution and is predisposed to form this turn motif once it is associated with a membrane mimic.

(e)

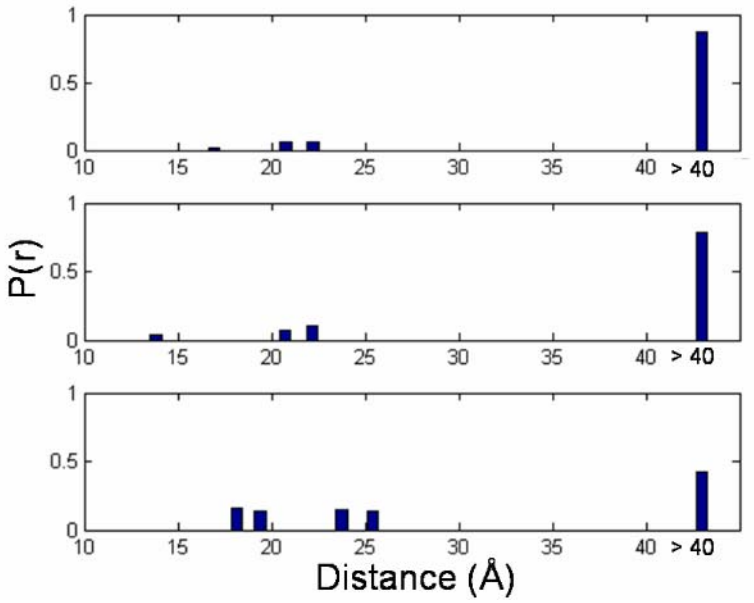

(f)

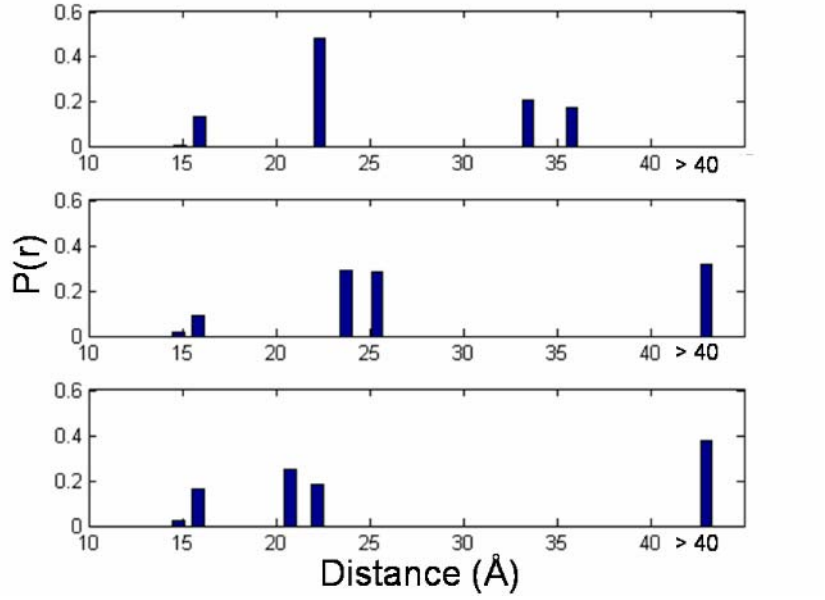

Figure 3.5. D-A distance distributions extrapolated from FET kinetics for **(e)** W4/Y94(NO_2) and **(f)** W39/Y55(NO_2) in 20 mM NaP_i buffer (top panel), 1:1 POPC:POPA (middle panel), and 40 mM SDS (bottom panel)

In conclusion, our results suggest that the linker brings the helices into close proximity when α-syn is in association with SDS micelles. When 1:1 POPC:POPA SUVs were introduced, this phenomenon was not observed. It is also noted that the C-terminal helix is tighter than the N-terminal helix when SDS micelles are present. The opposite phenomenon was observed when SUVs were added. A plausible explanation is that the C-terminal helix has more amino acids (48 residues) to fit into limited spaces than the N-terminal helix (35 residues). Therefore, in small membrane mimics, like SDS micelles, α-syn must create a tighter C-terminal helix for steric purposes. While in association with larger membrane mimics, namely 1:1 POPC:POPA, sterics are no longer an issue and therefore, the C-terminal helix can be relatively relaxed.

3.5 ACKNOWLEDGEMENTS

This work was completed in collaboration with Dr. Jennifer C. Lee.

3.6 REFERENCES

(1) Ulmer, T. S.; Bax, A.; Cole, N. B.; Nussbaum, R. L. *J. Biol. Chem.* **2005**, *280*, 9595–9603.
(2) Jao, C. C.; Der-Sarkissian, A.; Chen, J.; Langen, R. *Proc. Natl. Acad. Sci. U. S. A.* **2004**, *101*, 8331–8336.
(3) Gennis, R. B. *Biomembranes: Molecular Structure and Function*; Springer: New York, 1989.
(4) Bussell, R.; Eliezer, D. *J. Mol. Biol.* **2003**, *329*, 763–778.
(5) Forster, T. *Ann. Phys.-Berlin* **1948**, *2*, 55–75.
(6) Beechem, J. M.; Haas, E. *Biophys. J.* **1989**, *55*, 1225–1236.
(7) Navon, A.; Ittah, V.; Landsman, P.; Scheraga, H. A.; Haas, E. *Biochemistry* **2001**, *40*, 105–118.

(8) Lyubovitsky, J. G.; Gray, H. B.; Winkler, J. R. *J. Am. Chem. Soc.* **2002**, *124*, 14840–14841.
(9) Lee, J. C.; Engman, K. C.; Tezcan, F. A.; Gray, H. B.; Winkler, J. R. *Proc. Natl. Acad. Sci. U. S. A.* **2002**, *99*, 14778–14782.
(10) Wu, P. G.; Brand, L. *Anal. Biochem.* **1994**, *218*, 1–13.
(11) DeLano, W. L. *The PyMOL User's Manual;* Palo Alto, CA. 2002.
(12) Kim, J. E.; Arjara, G.; Richards, J. H.; Gray, H. B.; Winkler, J. R. *J. Phys. Chem. B* **2006**, *110*, 17656–17662.
(13) Reshetnyak, Y. K.; Koshevnik, Y.; Burstein, E. A. *Biophys. J.* **2001**, *81*, 1735–1758.
(14) Kleinschmidt, J. H.; den Blaauwen, T.; Driessen, A. J. M.; Tamm, L. K. *Biochemistry* **1999**, *38*, 5006–5016.
(15) Doring, K.; Konermann, L.; Surrey, T.; Jahnig, F. *Eur. Biophys. J.* **1995**, *23*, 423–432.
(16) Surrey, T.; Jahnig, F. *Proc. Natl. Acad. Sci. U. S. A.* **1992**, *89*, 7457–7461.
(17) Lee, J. C.; Lai, B. T.; Kozak, J. J.; Gray, H. B.; Winkler, J. R. *J. Phys. Chem. B* **2007**, *111*, 2107–2112.
(18) Lee, J. C.; Langen, R.; Hummel, P. A.; Gray, H. B.; Winkler, J. R. *Proc. Natl. Acad. Sci. U. S. A.* **2004**, *101*, 16466–16471.

Chapter 4

Calcium Binding Behavior of α-Synuclein's C-terminal Tail

4.1 ABSTRACT

A feature of Parkinson's disease is the presence of fibrillar protein deposits composed mostly of α-synuclein and calcium ions in the *substantia nigra* region of the brain. Although α-synuclein is natively unfolded, the N-terminal region of the protein is highly helical in the presence of membrane mimics, such as acidic phospholipid vesicles. It has been postulated that calcium ions bind to the acidic C-terminal tail of α-synuclein. We have incorporated three tryptophan variants (W101, W125, and W136) in that region and investigated the interactions between the phospholipid vesicles and calcium ions by steady-state and time-resolved fluorescence spectroscopy. We have also prepared seven mutants (W94/Y113(NO_2), W94/Y125(NO_2), W94/Y136(NO_2), W101/Y74(NO_2), W101/Y125(NO_2), W101/Y136(NO_2), and W125/Y136(NO_2)), and probed the change of distance distributions in the presence of calcium ions by fluorescent energy transfer and electron transfer using tryptophan as the donor and 3-nitrotyrosine as the acceptor. The results suggest that the C-terminal tail is capable of binding to two calcium ions in solution, while one of the calcium binding regions weakens when the α-synuclein mutants are placed in phospholipid vesicles.

4.2 INTRODUCTION

α-Syn is a 140-residue protein with unknown function.[1] The protein is commonly classified into three regions. The C-terminal domain consists of residues 96–140. This region has been noted by the large number of acidic residues (10 Glus and 5 Asps) and its ability to bind to calcium ions,[2,3] copper ions,[4] microtubule-associated proteins 1B,[5] and polyamines.[6]

The C-terminal domain has been demonstrated to be multi-functional and is strongly related to the aggregation properties of α-syn. It is responsible for the protein's stability at high temperature,[7] acts as a solubilizing domain for chaperone function,[8-11] and prevents aggregation. It has been previously shown that α-syn with a truncated C-terminal tail has a tendency to aggregate at a faster rate.[12-14] Post-translational modifications of some C-terminal tail residues can also change the susceptibility for α-syn to aggregate.[15,16] Although the C-terminal tail is responsible for mediating aggregation, it is structurally found on the surface of the fibrils, rather than being incorporated into the core.[17-19]

A high concentration of calcium ions and α-syn are two important factors for the initiation of PD.[20] In addition, aging is an important risk factor for PD. The aging process, such as the neurodegeneration observed in PD, has been associated with oxidative stress.[21] This oxidative stress has been linked to calcium dysregulation, which can possibly affect cellular processes through an influx of calcium ions, thus increasing the internal calcium ion concentration.[22-25]

In the presence of membrane mimics, such as SDS micelles and acidic SUVs, the N-terminal portion of α-syn becomes highly helical, while the C-terminal tail has been shown to remain largely unstructured. De Laureto et al. have previously studied the influence of calcium ions on the structure of the C-terminal tail α-syn by proteolysis.[26] They have observed that, in the presence of calcium ions, thermolysin, proteinase K, and Glu-specific V8-protease can degrade α-syn into various small fragments in solution. However, in the presence of 10 mM SDS micelles, fragmentation sites were only identified at the C-terminal end of residues 111, 113, and 123. This result illustrates that the C-terminal tail can be made rigid by the presence of membrane mimics.

Separately, Tamamizu-Kato et al. introduced a pyrene fluorophore onto residue 125 of α-syn.[20] They have observed an increase in the band III fluorescence emission upon addition of calcium ions, thus suggesting that there is increased interaction between residue 125 and the membrane. It has been proposed that the N-terminal domain and lipids first interact with each other, then the C-terminal tail is associated with the lipid bilayer triggered by the addition of calcium ions.

In this study, we first investigated whether the C-terminal tail of α-syn binds to the surface of SUVs in the presence of calcium ions by steady-state and time-resolved fluorescence spectroscopy. Single Trp mutants (W101, W125, and W136) were employed as a fluorescent probe and represent different regions of the C-terminal tail. Phospholipids containing heavy-atom (Br) and energy-transfer (dinitrophenol) quenchers were incorporated into SUVs to determine the position of the Trp mutants in the presence of calcium ions.[27]

Time-resolved fluorescent energy-transfer (FET) was then used to probe the structural changes in the C-terminal tail of α-syn in solution and acidic SUVs upon the addition of calcium ions. Since fluorescent donor-acceptor (D-A) distance is inversely proportional to the FET rate,[28] probability distribution of D-A distances can be extracted.[27,29-33] Seven α-syn mutants have been expressed with D-A placed along various parts of the C-terminal tail to further probe behavior in the presence of SUVs and calcium ions.

The fluorescent amino acid tryptophan (Trp) has been chosen as the fluorescent donor for this study. A chemically modified tyrosine, 3-nitrotyrosine [Tyr(NO_2)], was utilized as an energy acceptor. The Förster distance for this D-A pair is 26 Å.[34] The N-terminal and C-terminal interface was probed by Y74(NO_2)/W101, W94/Y113(NO_2). The whole C-terminal tail was characterized by W94/Y125(NO_2), W94/Y136(NO_2), W101/Y125(NO_2), W101/Y136(NO_2). The extreme C-terminal end of the protein was studied by W125/Y136(NO_2).

It is also our interest to study the effect of calcium ions on the tertiary contact formation of the C-terminal tail of α-syn. Photoinduced electron transfer (ET) from the triplet excited state of tryptophan to 3-nitrotyrosine can be measured to determine the contact formation in various environments.[35,36] Time-resolved absorption experiments were employed to study the mutants listed above. Tryptophan is excited by a laser pulse to generate a singlet excited state ($^1W^*$). This singlet excited state can proceed through intersystem crossing to create a Trp triplet excited state ($^3W^*$). This triplet excited state can then be quenched by 3-nitrotyrosine if it is in proximity of the $^3W^*$.

4.3 METHODS

Protein Expression, Modification, and Purification.

The plasmid of wild-type α-syn was provided by M. Goedert [37]. For the single Trp studies, site-directed mutagenesis was employed to introduce Trp in five different sites (W4, W94, W101, W125, and W136). For studies involving Trp as a donor and Tyr as an acceptor, a single Trp was mutated into the sequence (W101, W125, and W136). Extra Tyrs were also mutated away into Phes. One Tyr was introduced or remained in the sequence as the nitration site.

Expression, modification, purification, and nitration protocols have been adopted from Chapter 1. The purity of protein samples were evaluated by SDS-PAGE on a Pharmacia Phastsystem (Amersham Biosciences) and mass spectrometry (California Institute of Technology Protein/Peptide Microanalytical Laboratory).

SUVs Fabrication.

Quencher-free SUVs were made with 1:1 molar mixture of two lipids, namely 1-palmitoyl-2-oleoyl-*sn*-glycero-3-phosphocholine (POPC) and 1-palmitoyl-2-oleoyl-*sn*-glycero-3-phosphate (POPA). For SUVs containing brominated lipids, 1-palmitoyl-2-stearoyl(6,7-dibromo)-*sn*-glycero-3-phosphocholine (DiBr) was chosen, with a 1:2:1 molar ratio of POPC:POPA:DiBr. The distance between the polar end of the lipid and the bromine atoms is 9 Å. On the other hand, the lipid labeled with an energy-transfer quencher, N-dinitrophenyl phosphatidylethanolamine (DNP), was

used to fabricate SUVs with a quencher installed at the head group. A molar ratio of 4:5:1 POPC:POPA:DNP was achieved in these SUVs.

SUVs were fabricated following protocol in Chapter 1. Lipid solutions were dried under a stream of Ar for 5 min and under vacuum for 30 min. Dried lipids were suspended in 10 mM HEPES (pH 7.4) at a concentration of 5 mg/mL. The lipid solution was then sonicated by a Branson ultrasonicator microtip (Plainview, NJ) for 30 min at 50% duty cycle (200 W). The sonicated SUVs were then diluted with HEPES to yield a final concentration of 2 mg/mL and equilibrated at room temperature overnight. However, for ET experiments, lipid solutions were sonicated and equilibrated at 10 mg/mL. The SUV solution was then centrifuged at 10,000 × *g* for 10 min to remove titanium dust and particulates. Freshly prepared SUVs were used for all experiments.

Sample Preparation and Steady-state Fluorescence Experiments.

Sample preparation and data processing procedures for fluorescence studies have been described in Chapter 1, except all protein samples were exchanged into 10 mM HEPES (pH 7.4). All experimental samples contained 5 μM protein with 1.4 mg/mL SUVs. However, for ET experiments, 15 μM protein with 4.2 mg/mL SUVs was used. Calcium ions were supplied by $CaCl_2$.

Time-resolved Absorption Experiment.

Experimental samples were deoxygenated using the same protocol as described above.[36] N_2O, a solvated-electron scavenger, was equilibrated with the

sample. ^{3}W* was generated by exciting the sample with the second harmonic (290 nm) of a nanosecond Nd:YAG pumped optical parametric oscillator laser (Spectra-Physics). An Ar-ion laser (457.9 nm) was used as a source of probe light. The sensitivity of our measurements was improved by passing the probe light through the sample multiple times, thus increasing the path length from 1 to 7 cm. Transient absorption kinetics were detected by a photodiode and recorded using an 8-bit, 500-MHz digital oscilloscope (LeCroy 9354A).

For data analysis, the traces were transformed to absorbance changes [$-\log_{10}(I_{sample}/I_{reference})$]. They were then logarithmically compressed (100 points per decade) and normalized [$OD(t) - OD(t_\infty)/OD(t_0) - OD(t_\infty)$]. The adjusted traces were then fitted with NNLS.

4.4 DISCUSSIONS AND CONCLUSIONS.

Calcium Ion Titration Curve.

To determine the amount of calcium ions needed to induce structural formation, steady-state fluorescence spectra of single Trp mutants at different concentrations of calcium ions were taken. Acquired Trp fluorescence is an excellent probe in determining Trp microenvironment [38-41]. It has been demonstrated that a smaller Stokes shift and a higher quantum yield can be observed when the Trp is inserted into the lipid bilayer. Therefore, the integrated intensities between 325 and 500 nm can reveal whether the Trps are inserted into the lipid bilayer at various calcium ion concentrations.

Figure 4.1a shows the integrated intensities of the three Trps (Trp101, Trp125, and Trp136) and the tryptophan analog, NATA, in the presence of various calcium ion concentrations and SUVs. It is demonstrated that the integrated intensities remain relatively unchanged for W125, W136, and NATA between 0 - 1 mM of calcium ions. On the other hand, a steady increase of fluorescence intensity was observed as more calcium ions were added to the W101 sample, with the intensity reaching a steady maximum around 1 mM. This experiment implies that only Trp101 became more closely associated with the lipid bilayer when 1 mM calcium ions were added in the presence of SUVs. Adding more calcium ions yielded no changes to all three mutants studied, along with NATA (data not shown).

Similar calcium ion titration experiments were performed in the presence of SUVs. **Figure 4.1b** shows that the integrated fluorescence intensities for all three Trps and NATA remained largely unchanged when 1 mM calcium ions were added. Although this experiment shows that the Trps will remain in similar environments when calcium ions are added in the presence of SUVs, it is unclear whether the C-terminal tail binds to any calcium ions.

Time-resolved Fluorescent Lifetime Studies.

We have previously employed DiBr-containing SUVs to characterize Trp positions when the protein is folded into the lipid bilayer [37,39,42,43]. **Figure 4.2** shows the NNLS-fitted time-resolved fluorescent decay of the three Trps studied. Similar lifetimes of NATA have been observed in solution (blue traces), 1:1 POPC:POPA SUVs (red traces), and DiBr SUVs (green traces) in the presence (dotted traces) or

(a)

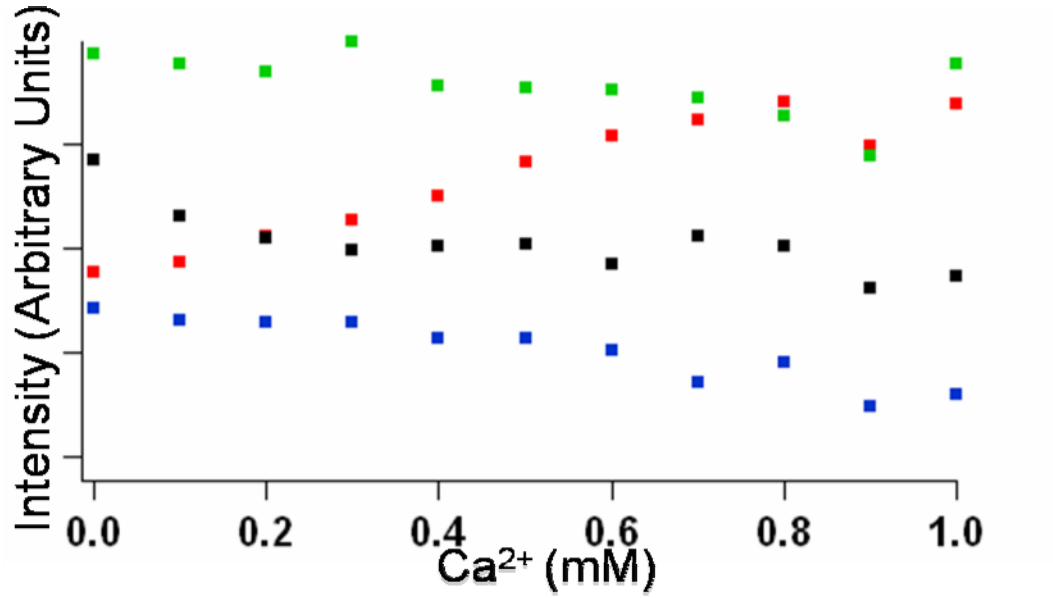

(b)

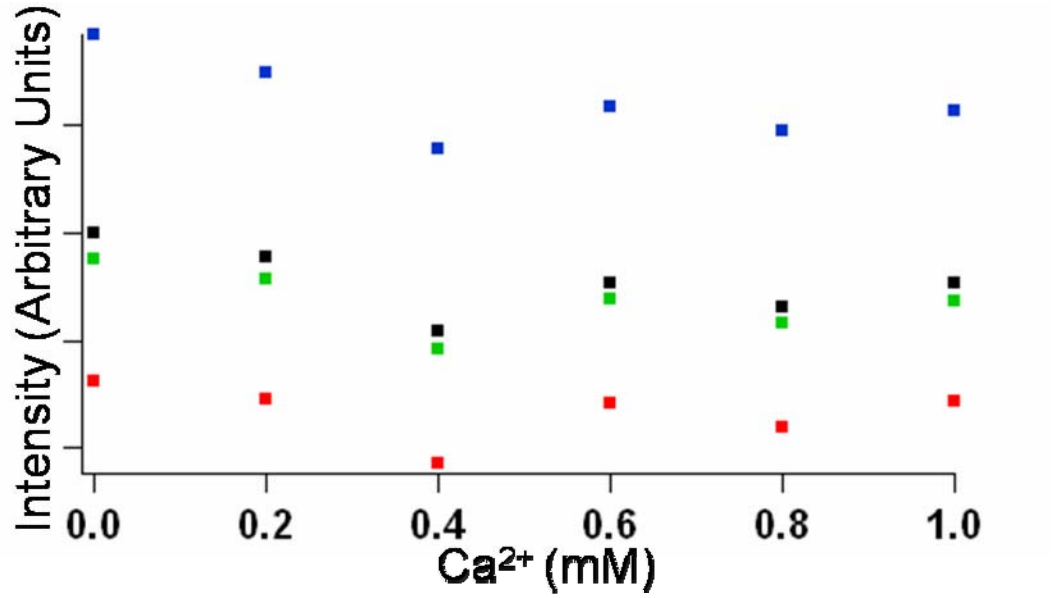

Figure 4.1. Integrated fluorescence intensity between 325 nm and 500 nm of W101 (red), W125 (green), W136 (blue), and NATA (black) in various concentrations of Ca^{2+} and in the **(a)** absence or **(b)** presence of SUVs

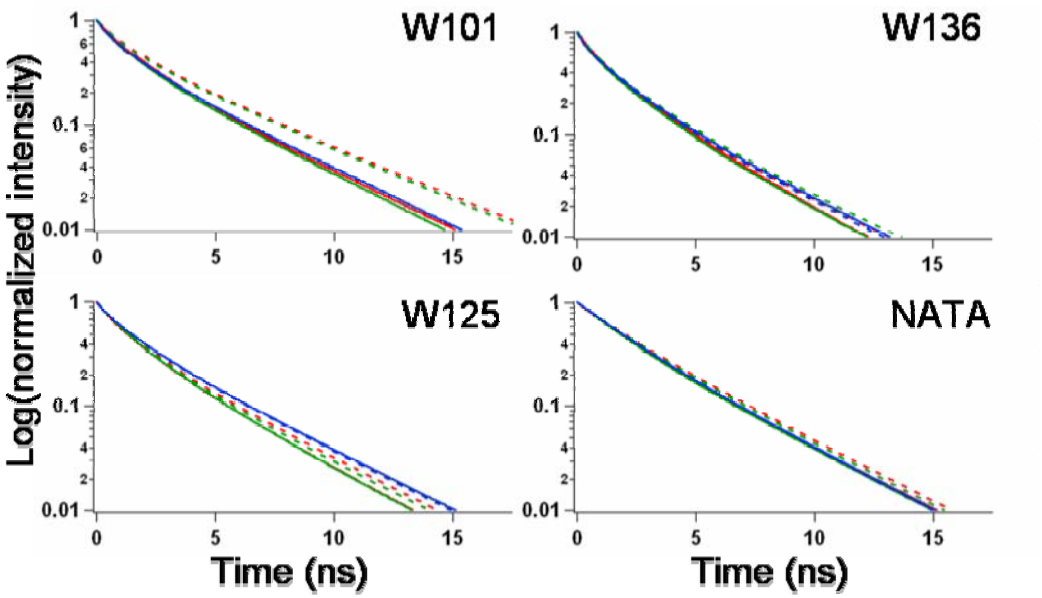

Figure 4.2. Time-resolved fluorescent decay of α-syn mutants W101 (top-left panel), W125 (bottom-left panel), W136 (top-right panel), and NATA (bottom-right panel) in the presence of HEPES (blue solid line), HEPES and Ca^{2+} (blue dotted line), 6,7-DiBr SUV (green solid line), DiBr SUV and Ca^{2+} (green dotted line), 1:1 POPC:POPA SUV (red solid line), and 1:1 POPC:POPA SUV and Ca^{2+} (red dotted line)

absence (solid traces) of calcium ions. W125 and W136 show time-resolved fluorescent decay comparable to NATA in the various environments described above.

Although W101 shows similar time-resolved fluorescent lifetimes in the absence of calcium ions, there is an increase in lifetimes when calcium ions are added into samples containing 1:1 POPC:POPA SUVs. The extended fluorescent lifetimes indicate that the Trp has displayed a higher quantum yield, thus implying that the Trp is in a more hydrophobic environment, such as the lipid bilayer. This experimental result demonstrates that W101 is more associated with the membrane in the presence both SUVs and calcium ions, but not W125 and W136.

We have previously employed SUVs incorporated with heavy atom (Br) and energy transfer (dinitrophenol) quenchers to predict the specific location of Trps when α-syn is folded into the membrane.[29,44] Again, we used the brominated lipid DiBr, where the quencher Br atoms are 9 Å away from the headgroup.[45] On the other hand, the dinitrophenol (DNP) has its quencher located on the lipid headgroup. By determining the amount of quenching of α-syn mutants in these quencher-containing SUVs, it is possible to elucidate how deep the C-terminal tail is inserted into the lipid bilayer in the presence of calcium ions.

As suggested by **Figure 4.2**, the fluorescent lifetimes for W101 are comparable when the α-syn mutant was placed in 1:1 POPC:POPA SUVs and DiBr SUVs. The lack of quenching by the brominated lipids implies that W101 was not inserted deeply into the membrane.

Previously we have also employed 10% DNP SUVs to investigate the position of these C-terminal mutants with respect to the surface of the vesicles.[29,44] The time-

resolved fluorescent kinetic traces were fitted using NNLS method, with special attention paid to the ultra-fast lifetimes (< 0.1 ns) related to the energy transfer from Trp to the dinitrophenol group. In our previous study, we have demonstrated that none of the C-terminal mutants have this ultra-fast lifetime component. However, based on the amplitude of the fast decay component (~ 1 x 10^{-9} s^{-1}), Trp101 (38%) displays the highest population, followed by W136 (14%) then W125 (2%).

In this study, we focus on the populations of the fast lifetime components (> 1 x 10^{-9} s^{-1}) of the Trp mutants in the presence of calcium ions and 10% DNP SUVs. If an increase of these fast lifetime components is observed, it can imply that calcium ions are mediating membrane association with the C-terminal tail region. **Figure 4.3** shows that the change of amplitude for the fast lifetime components of NATA and W136 is minimal when calcium ions were introduced. This agrees with the time-resolved fluorescence data, suggesting that W136 does not become closely associated with the lipid bilayer upon the addition of calcium ions.

Among the three Trp C-terminal mutants studied, W101 demonstrates the highest increase in the fast lifetime population (25%), indicating that the region around W101 is associated with the surface of the membrane fairly closely, but not deeply inserted. This result is not surprising as the time-resolved fluorescence data has already suggested that W101 forms a closer contact with the lipid bilayer, while the lack of quenching in the time-resolved fluorescent lifetimes of Trp101 with DiBr SUVs shows that the Trp is not deeply inserted into the membrane.

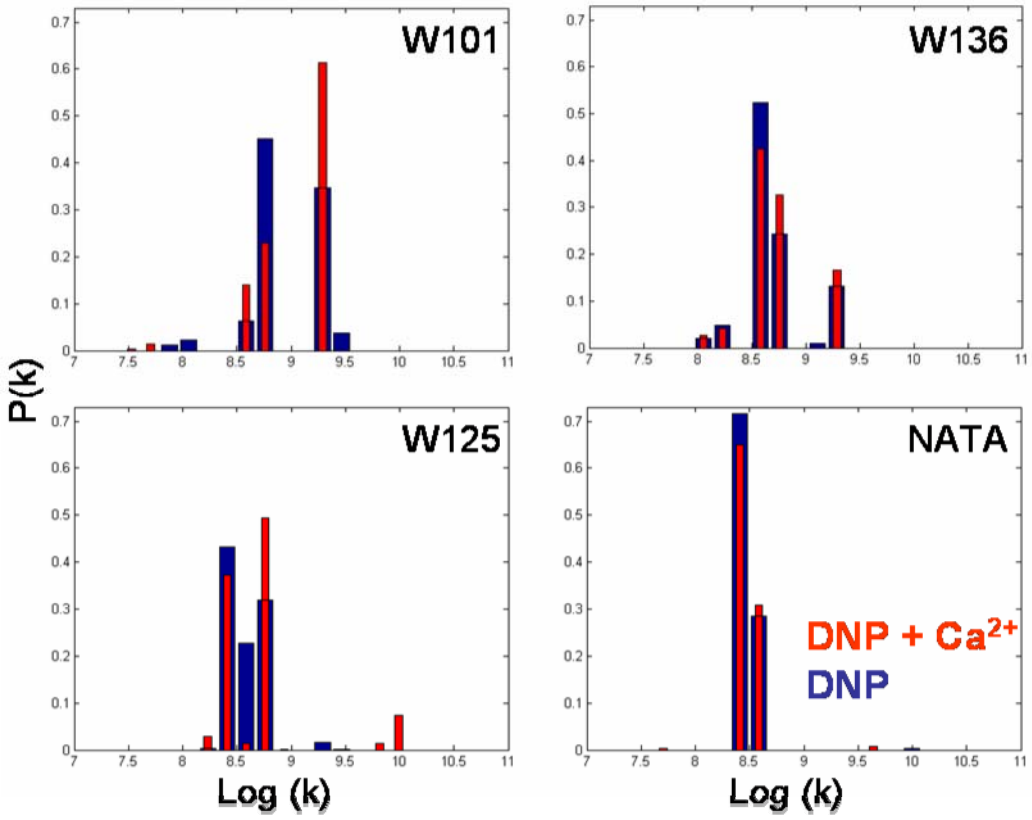

Figure 4.3. Distributions of tryptophan decay rate constants (k) for W101 (top left), W125 (bottom left), W136 (top right), and NATA (bottom right) α-syn mutants with 10 % DNP SUVs in the absence (blue) and presence (red) of Ca^{2+} (red)

What is interesting from this study is that W125 shows a modest increase of quenching (10 %) when calcium ions were added into the sample. A possible explanation is that the early segment of the C-terminal tail becomes closely associated with the lipid bilayer, mediated by the presence of the calcium ions. Therefore, W125 can be found closer to the membrane surface, although it is not directly associated with the membrane itself.

Time-resolved Anisotropy Studies.

The time-resolved fluorescent anisotropy decays for the three Trp-only mutants were carried out in the presence of 1:1 POPC:POPA SUVs with 1 mM of calcium ions (**Figure 4.4**). The anisotropy decays were fitted with biexponential decays. The rotation correlation times (θ) and anisotropies at time zero (r_0) were extrapolated to reveal the flexibility and the size of the Trps, thus providing information on how embedded the Trps are in different environments. These data were compared against the numbers obtained from Chapter 2 to determine the effect of calcium ions on the C-terminal mutants with respect to the membrane.

The three C-terminal Trp mutants display a dramatic increase of r_0 in the presence of calcium ions, with W101 (r_0 = 0.11 in SUVs and 0.23 in SUVs + Ca^{2+}) and W136 (r_0 = 0.10 in SUVs and 0.22 in SUVs + Ca^{2+}) doubling their r_0 values. On the other hand, W125 only shows a modest increase of r_0 value from 0.10 to 0.17 when calcium ions were added.

In addition, **Figure 4.4** exhibits a sharp decrease of r-value within 0.2 ns. Contrary to the anisotropy decay curves shown in **Figure 2.8**, the r-values of the C-

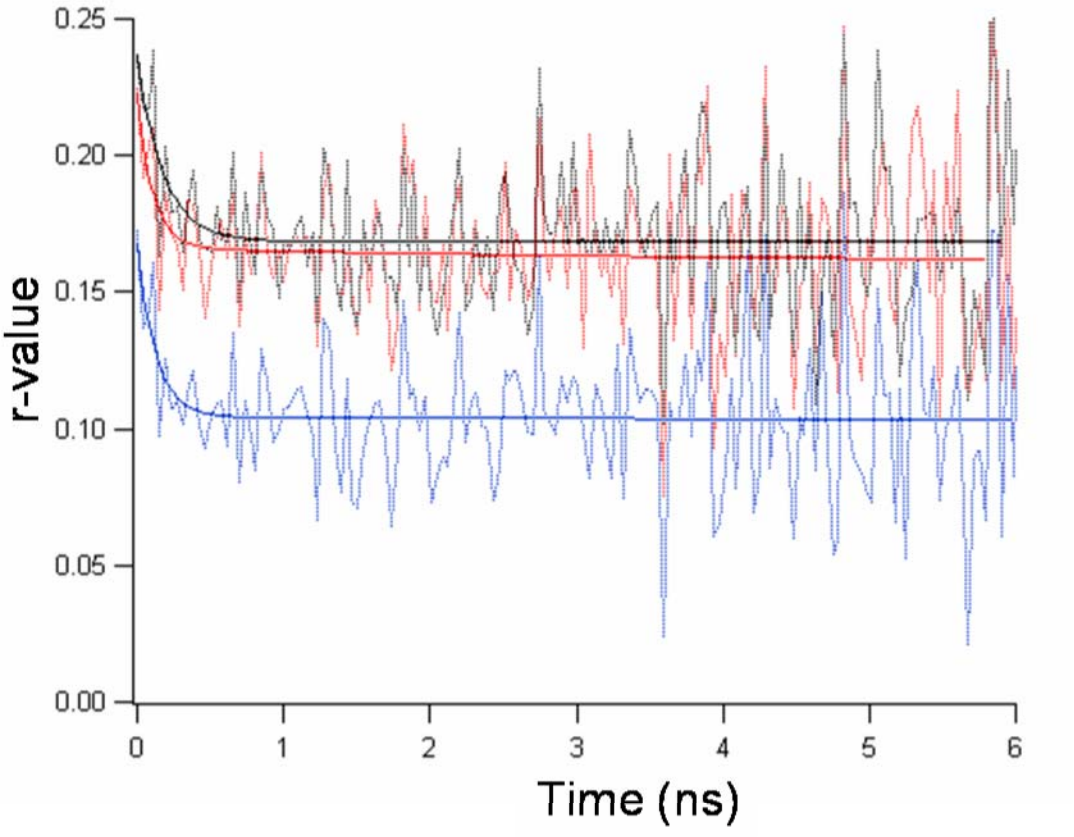

Figure 4.4. Time-resolved anisotropy decays for α-syn mutants W101 (red), W125 (blue), and W136 (black) in 1:1 POPC:POPA SUVs in 1 mM Ca^{2+}

terminal Trp mutants do not go to zero in the presence of calcium ions. It is possible to conclude that the all Trps in the C-terminal tail are now in a more rigid environment, caused by the calcium ions. Among the three C-terminal mutants, it is not surprising to note that W101 becomes more rigid with calcium ions. It has been shown previously that calcium ions mediate closer interaction between W101 and the membrane. However, W136 also demonstrates some degree of rigidity in the presence of calcium ions, so that region could possibly serve as a calcium binding region.

Electron Transfer Study.

The electron transfer rates between ^{3}Trp* and Tyr(NO_2) for the seven D-A pairs in solution and SUVs have been measured, either in the presence or the absence of calcium ions. The ET rates (**Table 4.1** and **Figure 4.5–4.7**) have been fitted using the NNLS protocol. If α-syn mutants are placed in an environment where Trp and Tyr(NO_2) become close in contact, the ET rate will decrease significantly. In addition, the ET rate is also dependent on the average D-A distances and the stiffness of the polypeptide chain joining D-A.[36] Therefore, the ET rates can also shed light on whether the various changes in the mutants' surroundings can cause the C-terminal sequence to stiffen.

In addition to measuring the ET rates for the seven D-A mutants, the rates for their non-nitrated counterparts were also investigated as a control experiment. As **Table 1** suggests, all seven nitrated mutants demonstrate similar ET rates compared to their controls, regardless of which environments (buffer, buffer with calcium ions,

Mutant	Environment	τ (μs)	Mutant	Environment	τ (μs)
W94/Y125	HEPES	20	W94/Y125(NO_2)	HEPES	21
	HEPES + Ca^{2+}	20		HEPES + Ca^{2+}	14
	SUV	20		SUV	14
	SUV + Ca^{2+}	17		SUV + Ca^{2+}	17
W94/Y136	HEPES	20	W94/Y136(NO_2)	HEPES	20
	HEPES + Ca^{2+}	18		HEPES + Ca^{2+}	20
	SUV	19		SUV	19
	SUV + Ca^{2+}	18		SUV + Ca^{2+}	18
W94/Y113	HEPES	22	W94/Y113(NO_2)	HEPES	18
	HEPES + Ca^{2+}	33		HEPES + Ca^{2+}	17
	SUV	20		SUV	18
	SUV + Ca^{2+}	18		SUV + Ca^{2+}	18
W101/Y125	HEPES	25	W101/Y125(NO_2)	HEPES	18
	HEPES + Ca^{2+}	16		HEPES + Ca^{2+}	17
	SUV	20		SUV	18
	SUV + Ca^{2+}	16		SUV + Ca^{2+}	17
W101/Y136	HEPES	16	W101/Y136(NO_2)	HEPES	15
	HEPES + Ca^{2+}	19		HEPES + Ca^{2+}	15
	SUV	17		SUV	15
	SUV + Ca^{2+}	19		SUV + Ca^{2+}	16
W101/Y74	HEPES	21	W101/Y74(NO_2)	HEPES	17
	HEPES + Ca^{2+}	16		HEPES + Ca^{2+}	17
	SUV	18		SUV	20
	SUV + Ca^{2+}	17		SUV + Ca^{2+}	16
W125/Y136	HEPES	18	W125/Y136(NO_2)	HEPES	16
	HEPES + Ca^{2+}	15		HEPES + Ca^{2+}	15
	SUV	16		SUV	18
	SUV + Ca^{2+}	16		SUV + Ca^{2+}	17

Table 4.1. The electron transfer rates (τ) of the α-syn mutants in the various environments

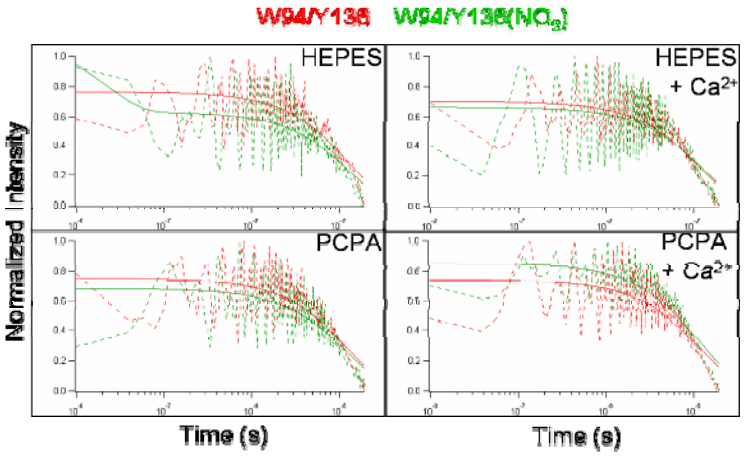

(a)

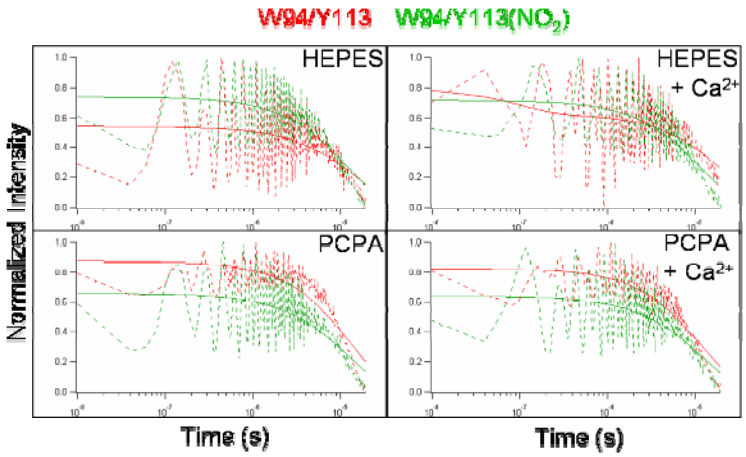

(b)

Figure 4.5. Electron transfer decay curves for **(a)** W94/Y136 (red) and W94/Y136(NO_2) (green) and **(b)** W94/Y113 (red) and W94/Y113(NO_2) (green) and in HEPES (top left), HEPES + Ca^{2+} (top right), 1:1 POPC:POPA SUVs (left bottom), and 1:1 POPC:POPA SUVs + Ca^{2+} (right bottom)

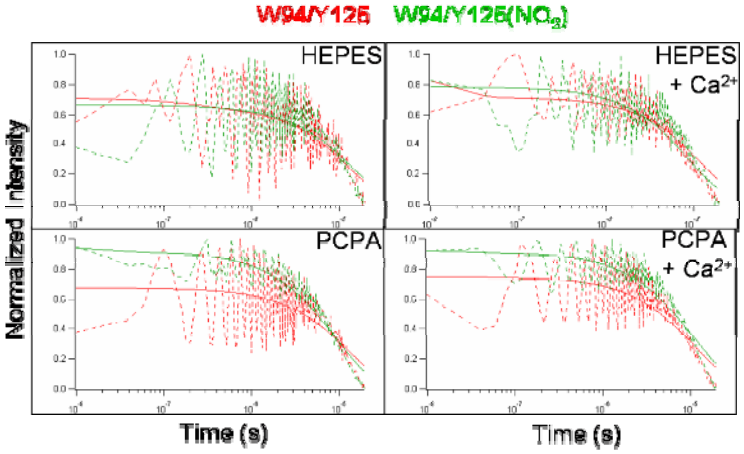

(a)

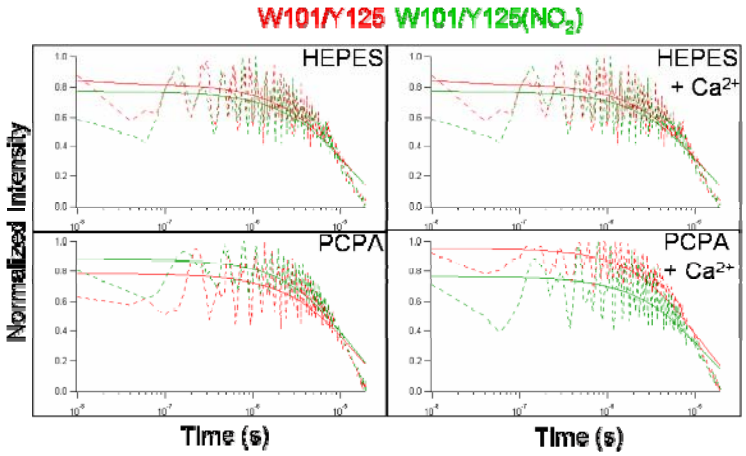

(b)

Figure 4.6. Electron transfer decay curves for **(a)** W94/Y125 (red) and W94/Y125(NO_2) (green) and **(b)** W101/Y125 (red) and W101/Y125(NO_2) (green) in HEPES (top left), HEPES + Ca^{2+} (top right), 1:1 POPC:POPA SUVs (left bottom), and 1:1 POPC:POPA SUVs + Ca^{2+} (right bottom)

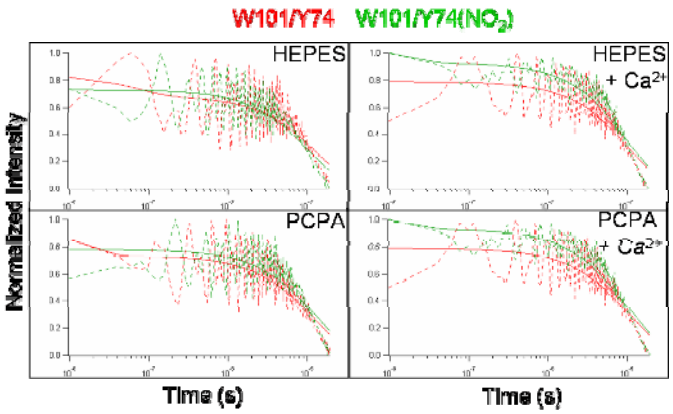

(a)

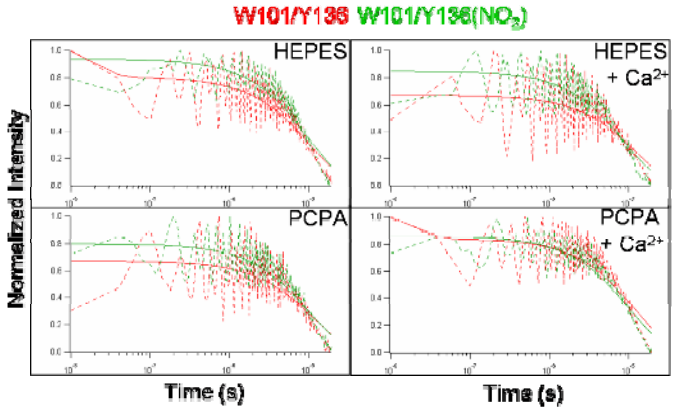

(b)

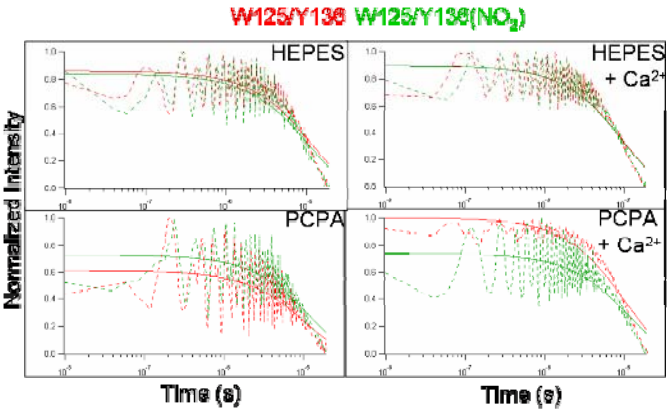

(c)

Figure 4.7 Electron transfer decay curves for **(a)** W101/Y74 (red) and W101/Y74(NO_2) (green), **(b)** W101/Y136 (red) and W101/Y136(NO_2) (green), and **(c)** W125/Y136 (red) and W125/Y136(NO_2) (green) in HEPES (top left), HEPES + Ca^{2+} (top right), 1:1 POPC:POPA SUVs (left bottom), and 1:1 POPC:POPA SUVs + Ca^{2+} (right bottom)

SUVs, and SUVs with calcium ions) these mutants were placed in. These experimental results imply that Trp and Tyr(NO_2) are not in close contact in any tested conditions. This phenomenon could be expected when calcium binding occurs, as the calcium ions preclude Trp and Tyr(NO_2) coming into close proximity. However, it comes as a surprise that ET between Trp and Tyr(NO_2) cannot be observed when these α-syn mutants were in solution-only environment. Lee et al. has previously shown that there are some predetermined structures when α-syn is in solution, even though it has been considered as natively unfolded.[36] Another potential cause of this phenomenon is the prevalence of acidic residues, as these negative charges repel each other, thus disallowing contact formation.

FET study.

Figure 4.8 and **Figure 4.9** show the distance distributions of four of the seven D-A α-syn mutants in solution in the presence/absence of calcium ions, extrapolated from time-resolved fluorescent energy transfer. In solution, W125/Y136(NO_2) mutant shows little quenching (decay curves not shown). However, with the addition of calcium ions, there is a small degree of quenching. The distance distribution of fitted data shows that there is formation of a population with smaller distance populations (~ 31 Å), implying there is a possible calcium binding region between residue 125 and 136. This phenomenon is also supported by the distributions obtained in W94/Y136(NO_2). For W94/Y136(NO_2), there is a shift from long distance distributions (> 40 Å) to shorter distance distributions (~ 37 Å) upon the addition of calcium ions.

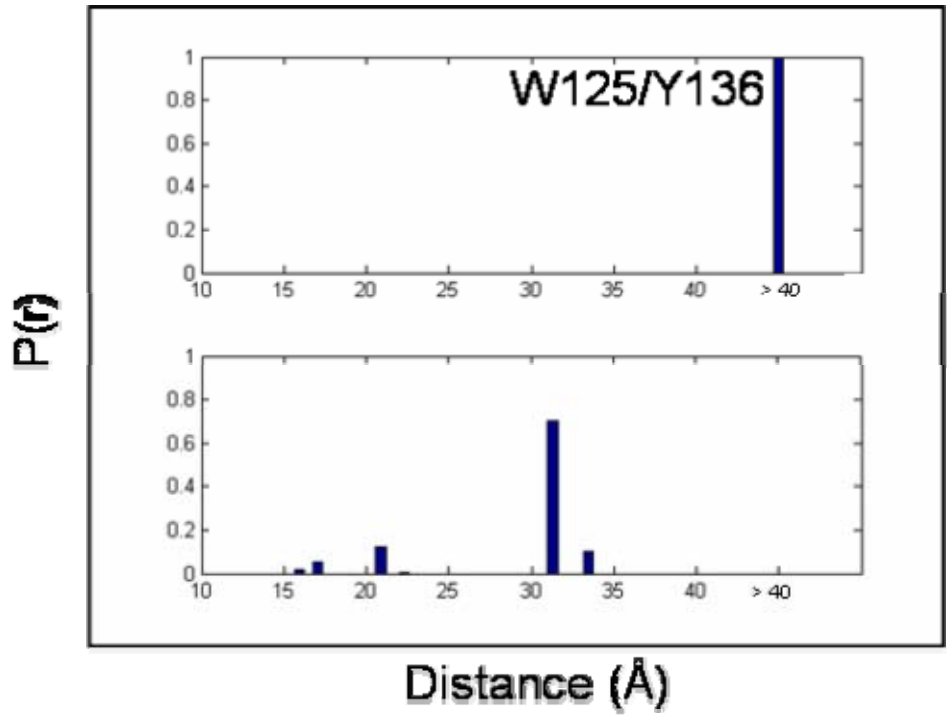

(a)

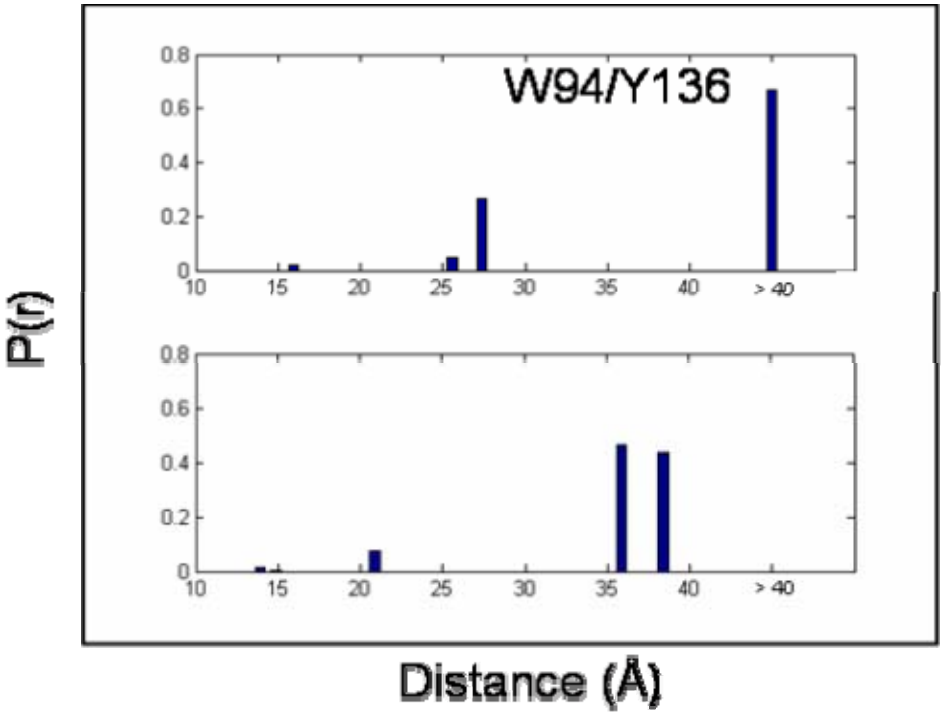

(b)

Figure 4.8. D-A distance distributions extrapolated from FET kinetics for **(a)** W125/Y136(NO_2) and **(b)** W94/Y136(NO_2) in 10 mM HEPES buffer (top panel), and 10 mM HEPES buffer with 1 mM Ca^{2+} (bottom panel)

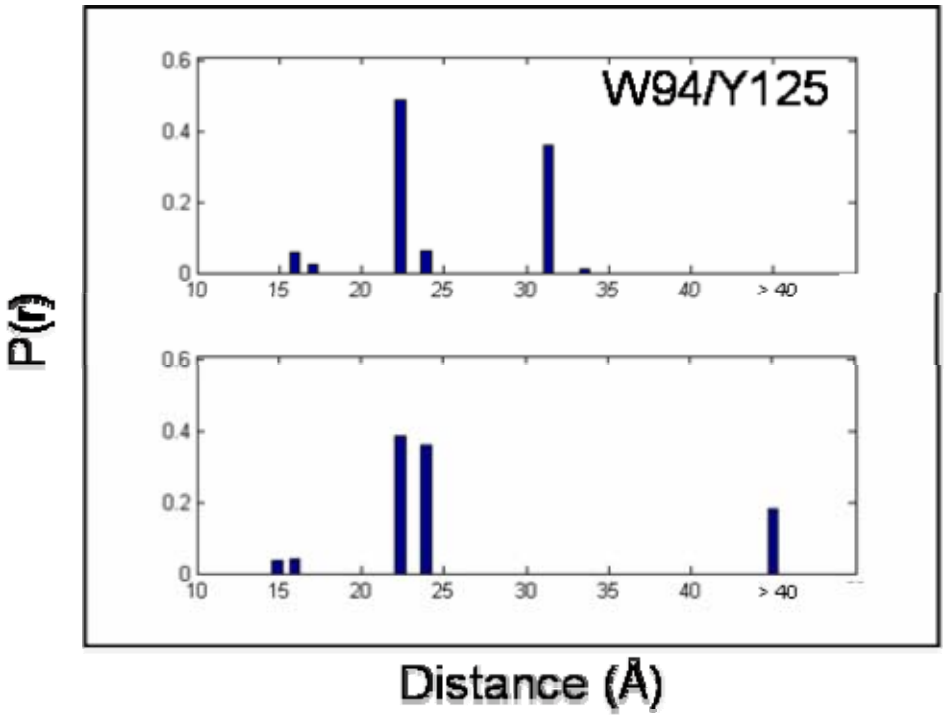

(a)

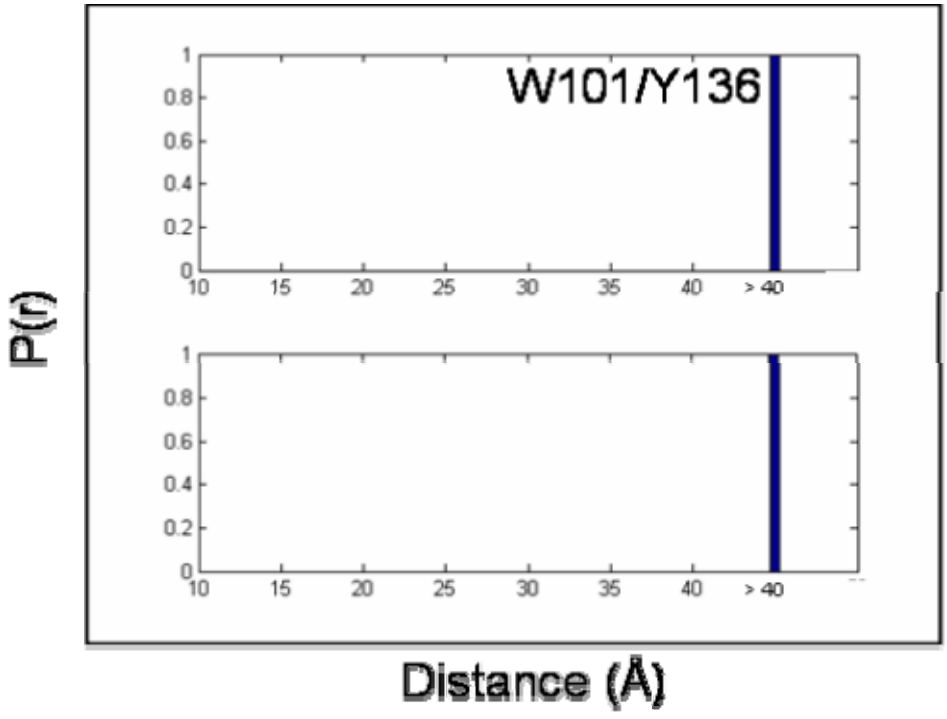

(b)

Figure 4.9. D-A distance distributions extrapolated from FET kinetics for **(a)** W94/Y125(NO_2) and **(b)** W101/Y136(NO_2) in 10 mM HEPES buffer (top panel), and 10 mM HEPES buffer with 1 mM Ca^{2+} (bottom panel)

This pair, however, does not discount the possibility that there could be another calcium binding region in another part of the C-terminal tail. Following this hypothesis, we expect that the distance distributions for W101/Y136(NO_2) should decrease upon the addition of calcium ions. However, the D-A distances in both environments are still over the experimental limits of 40 Å.

On the other hand, in **Figure 4.10**, W101/Y74(NO_2) has a distribution of long (~ 33 Å, ~ 85%) and medium distances (18 Å, ~ 15%). However, upon the addition of calcium ions, the α-syn mutant sees a shift to slightly longer distances (~ 34 Å, 80%; ~ 20 Å, 15%). This suggests that this region experiences some lengthening when calcium ions are added. This slight lengthening phenomenon can also be observed for W94/Y113(NO_2) mutant, only to a much shorter extent. The population of extended distances (> 40 Å) remains largely the same (~ 20%), while there is a shift of the distance populations from ~ 22 Å to ~ 23 Å (60%) and from ~ 16 Å to ~ 17 Å (20%). Since the distance shift is much smaller for W94/Y113(NO_2) than W101/Y74(NO_2), it is possible that another calcium region can be found between residue 101 and 113, compensating for the lengthening between residue 74 and 101.

This binding region between residue 101 and 113 can be further proven by the distance distributions in W94/Y125(NO_2) as it gives an ensemble of extended distances (~ 32 Å, ~ 40%), intermediate distances (~ 23 Å, ~ 50%), and short distances (~ 16 Å, 10%). Adding calcium ions increases the intermediate distances' population significantly (75%). Similarly, for W101/Y125(NO_2) (**Figure 4.11**), a distance distribution of 38 Å to 36 Å (60%). It is interesting to note that the distance contraction for this D-A pair is very modest when compared to the one shown in the

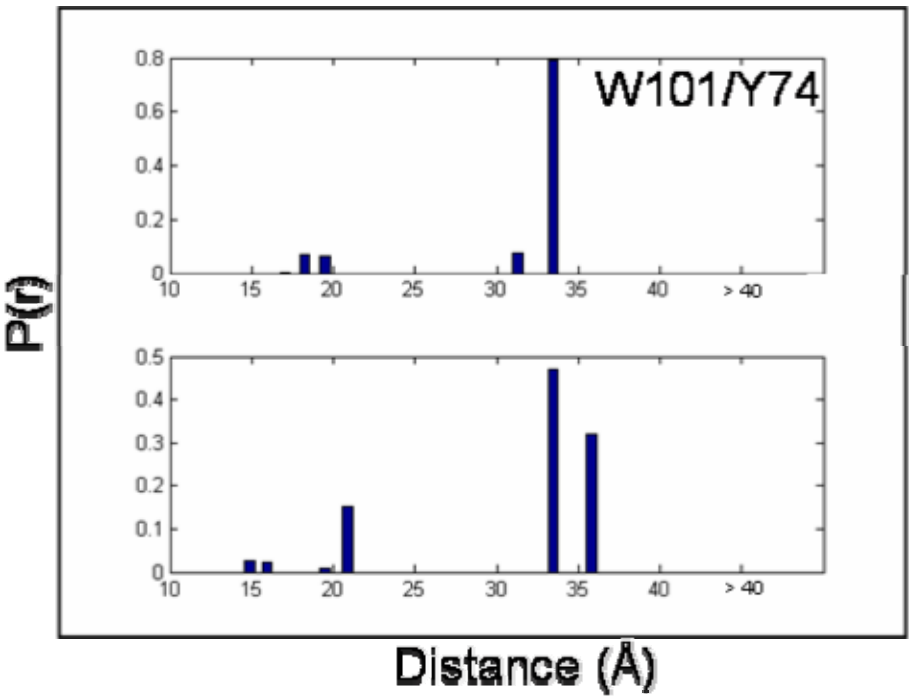

(a)

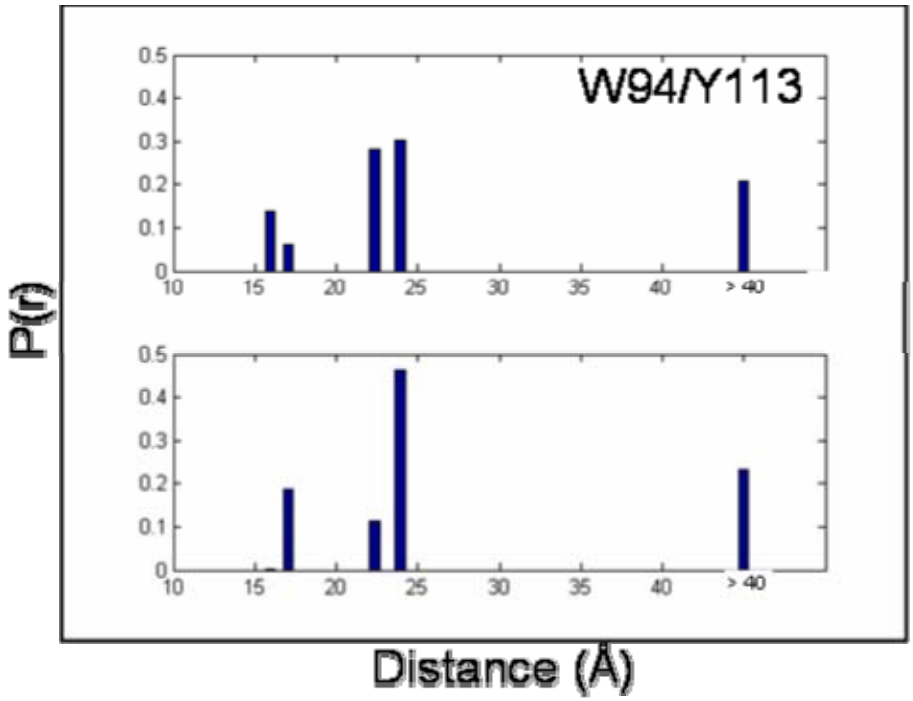

(b)

Figure 4.10. D-A distance distributions extrapolated from FET kinetics for **(a)** W101/Y74(NO_2) and **(b)** W94/Y113(NO_2) in 10 mM HEPES buffer (top panel), and 10 mM HEPES buffer with 1 mM Ca^{2+} (bottom panel)

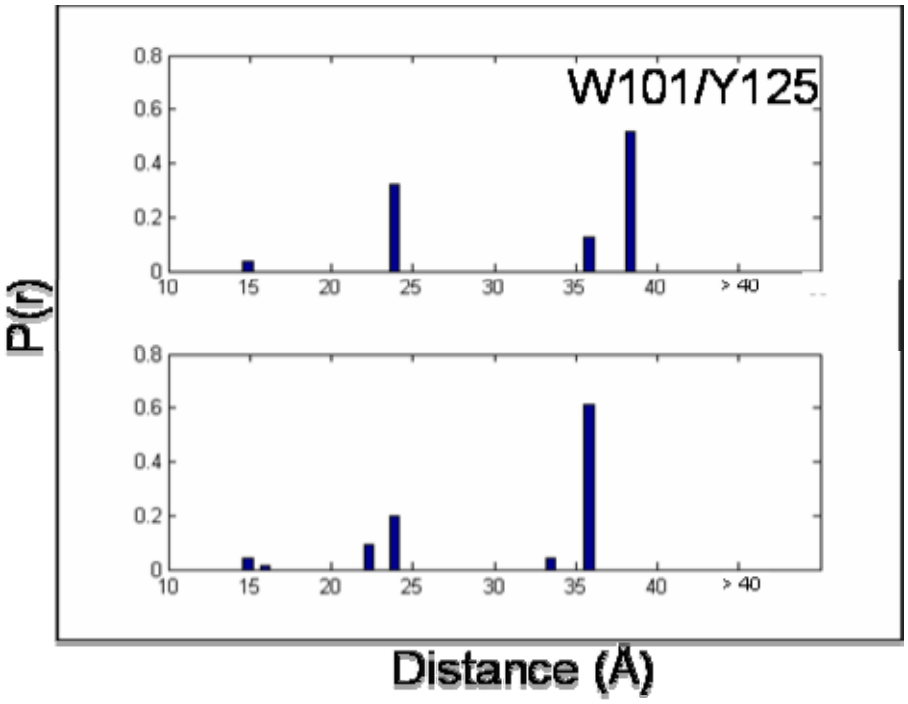

Figure 4.11. D-A distance distributions extrapolated from FET kinetics for W101/Y125(NO_2) in 10 mM HEPES buffer (top panel), and 10 mM HEPES buffer with 1 mM Ca^{2+} (bottom panel)

W125/Y136(NO_2) D-A pair. We can assign this phenomenon as an extending and rigidifying of the polypeptide between residues 113 and 125 upon the addition of calcium ions.

The C-terminal tail of α-syn behaves slightly differently when the mutants are in the presence of 1:1 POPC:POPA SUVs. For W101/Y74(NO_2) (**Figure 4.12**), the majority of the distance distribution slightly shifts from 33 Å to 31 Å upon the addition of calcium ions. A small population (10%) of short distance (19 Å) also emerges. Since this mutant belongs to part of the NAC region, it forms a helical structure in the presence of SUVs. Therefore, the slight decrease in distances is caused by a balance between the contraction due to helix formation and the lengthening between residues 94 and 101. This agrees with previous data as it is the region that has demonstrated association with the membrane when calcium ions and SUVs are present.

In **Figure 4.13**, for W101/Y125(NO_2), the distance distribution shifts from > 40 Å to 38 Å (~ 70%) when calcium ions were added. Similarly, W94/Y113(NO_2) shows a shift from > 40 Å to ~ 36 Å. These two D-A pairs show that some contraction is observed between residues 94 and 113. We have already concluded that there is a slight decrease in distances between residues 94 and 101. Therefore, there is a significant decrease of distances between residues 101 and 113. This region has already been identified as a calcium binding region in solution. This result reveals this calcium binding region is not affected when SUVs are present.

For W94/Y125(NO_2) (**Figure 4.14a**), there is a population of long polypeptide distance (> 40 Å, 40%) regardless of whether there are calcium ions present.

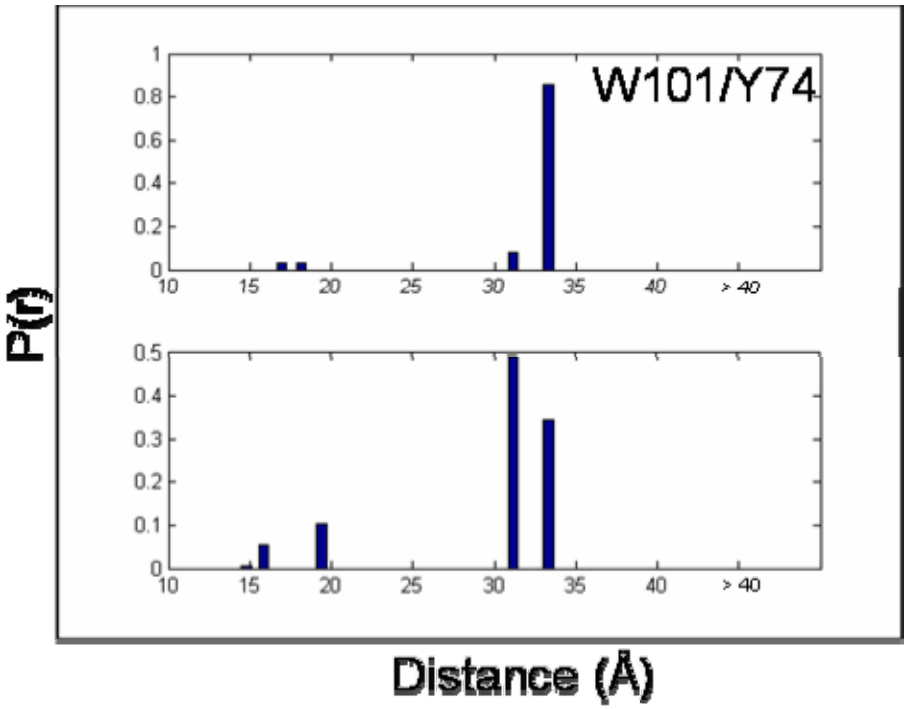

Figure 4.12. D-A distance distributions extrapolated from FET kinetics for W101/Y74(NO_2) in 1.4 mg/mL 1:1 POPC:POPA SUVs (top panel), and with 1 mM Ca^{2+} added (bottom panel)

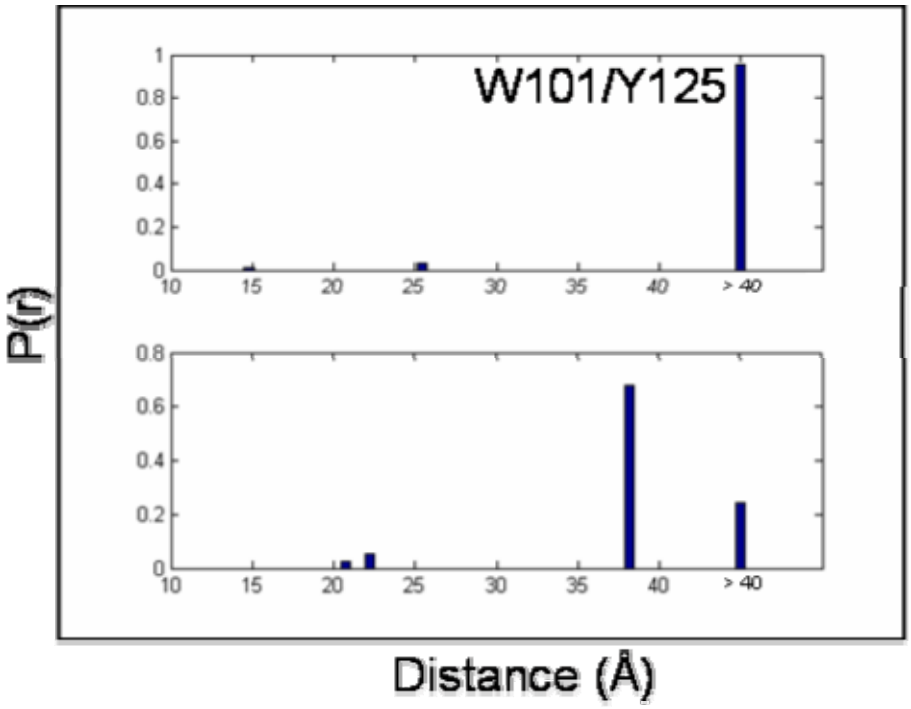

(a)

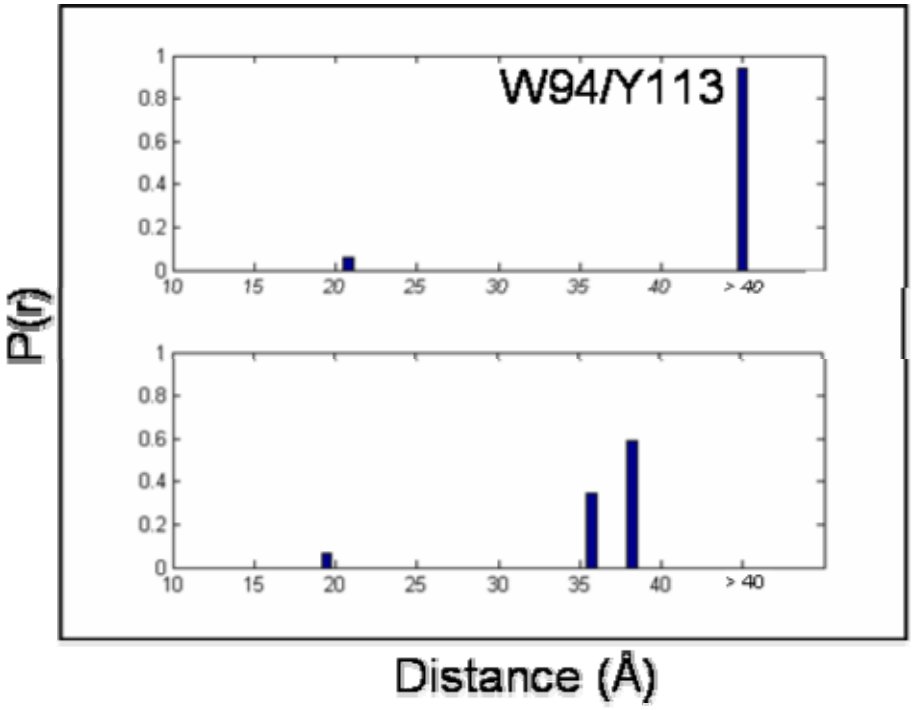

(b)

Figure 4.13. D-A distance distributions extrapolated from FET kinetics for **(a)** W101/Y125(NO_2) and **(b)** W94/Y113(NO_2) in 1.4 mg/mL 1:1 POPC:POPA SUVs (top panel), and with 1 mM Ca^{2+} added (bottom panel)

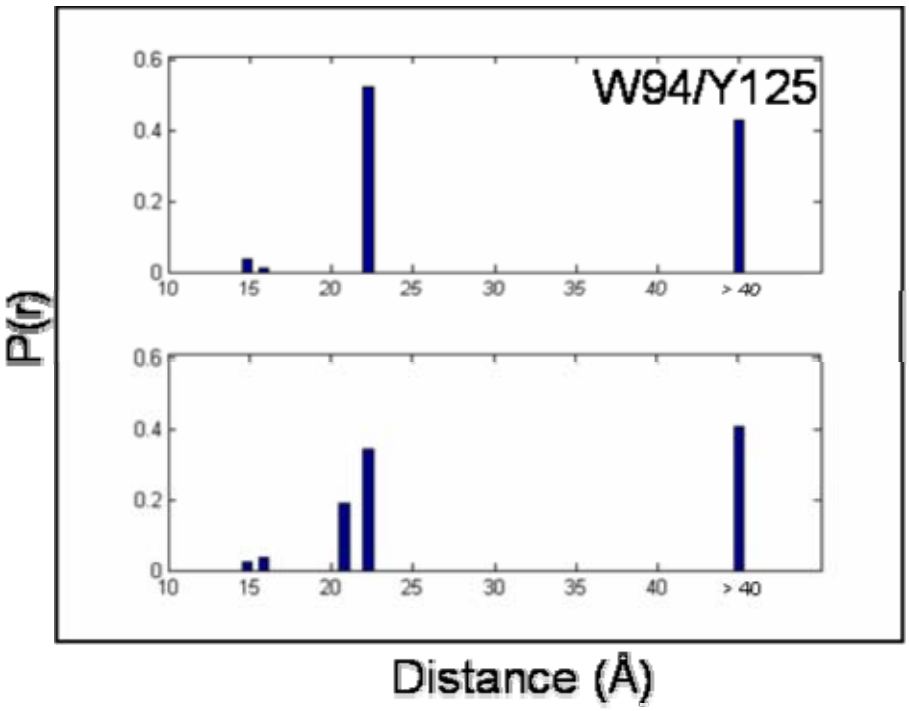

(a)

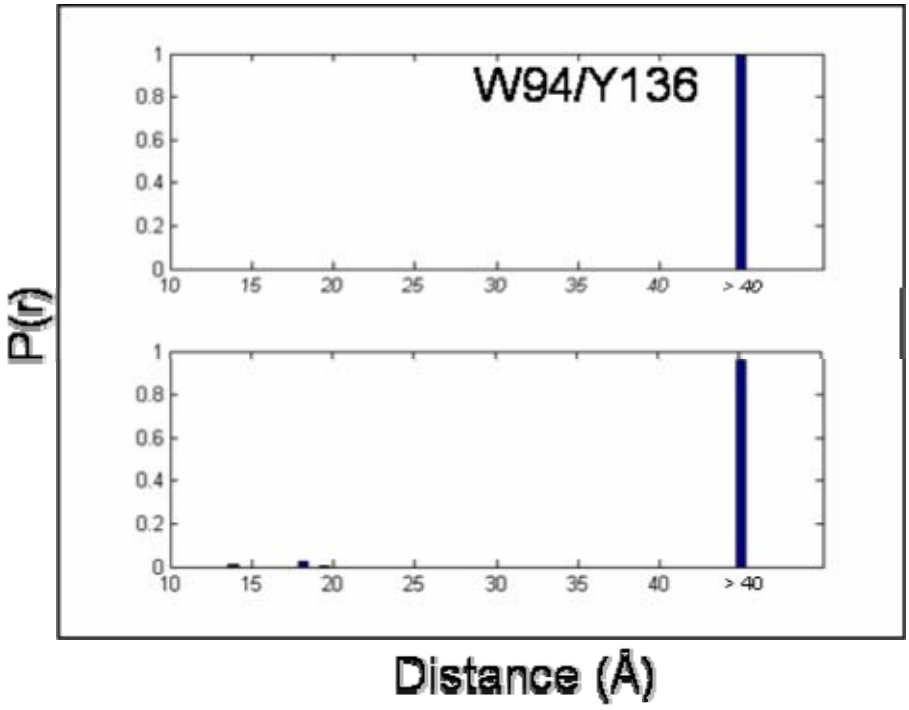

(b)

Figure 4.14. D-A distance distributions extrapolated from FET kinetics for **(a)** W94/Y125(NO_2) and **(b)** W94/Y136(NO_2) in 1.4 mg/mL 1:1 POPC:POPA SUVs (top panel), and with 1 mM Ca^{2+} added (bottom panel)

However, an intermediate polypeptide population (50%) shifts from 23 Å to 21 Å upon introducing calcium ions. This decrease of distances is much smaller than the one compared to W94/Y113(NO_2). Therefore, a lengthening site is required between residues 113 and 125 that will result in only a small decrease of distances in these two α-syn mutants.

In **Figure 4.14b** and **Figure 4.15**, the time-resolved fluorescent energy transfer kinetics curves for W94/Y136(NO_2), W101/Y136(NO_2), and W125/Y136(NO_2) show that there is no quenching in these experiments (decay curves not shown), implying that the Trp and Tyr(NO_2) were too far apart for energy transfer to be effective. This could imply the disappearance or weakening of the calcium binding region between residue 125 and 136 in the presence of SUVs. The steric bulk of the associated SUV is one possible cause.

Circular Dichroism Studies.

Figure 4.16 shows the CD spectra of our seven C-terminal α-syn mutants in the buffer (red lines) and SUVs (black lines), in the presence (dotted lines) or absence (solid lines) of calcium ions. It has been suggested previously that α-syn mostly lacks structure in solution. The addition of calcium ions does not seem to induce any structural change to the mutants in solution. Also previously stated in Chapter 1, the presence of acidic SUVs can produce a highly helical structure. However, as demonstrated by **Figure 4.16**, no extra structures, such as β sheets, were introduced when calcium ions were introduced.

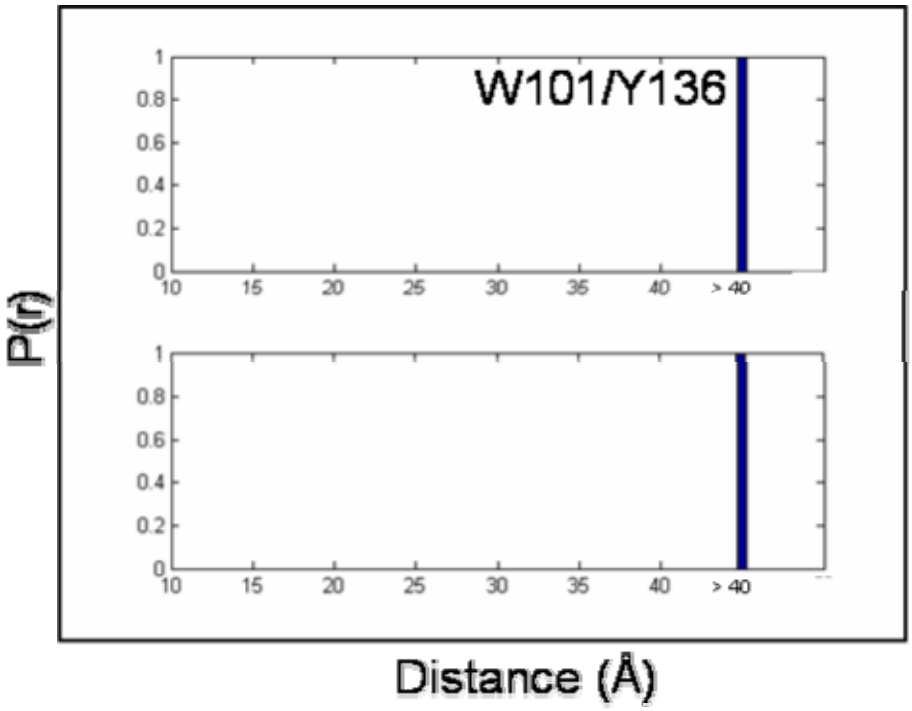

(a)

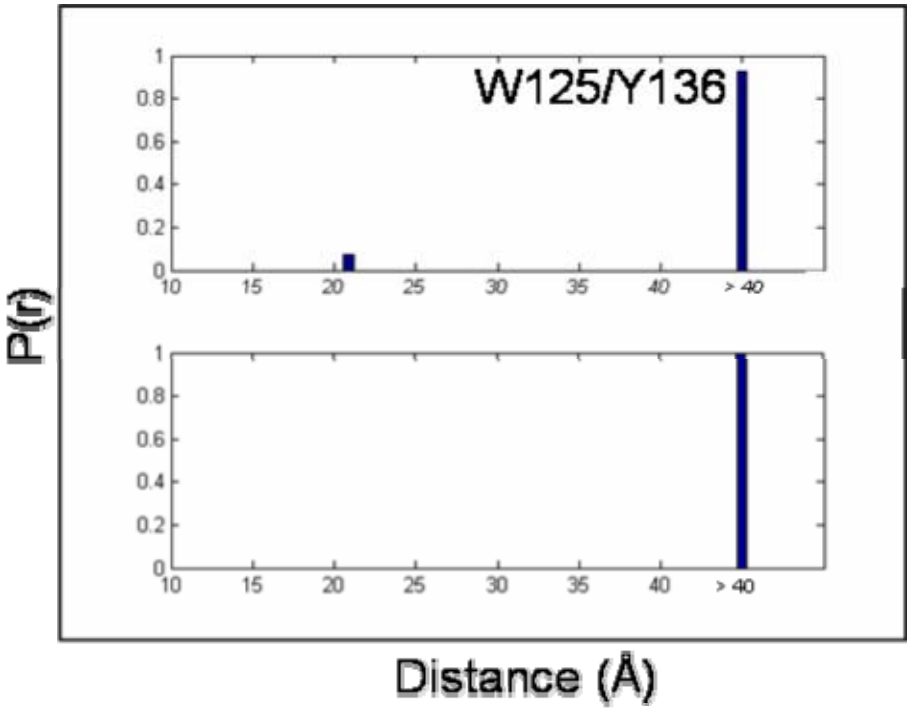

(b)

Figure 4.15. D-A distance distributions extrapolated from FET kinetics for **(a)** W101/Y136(NO_2) and **(b)** W125/Y136(NO_2) in 1.4 mg/mL 1:1 POPC:POPA SUVs (top panel), and with 1 mM Ca^{2+} added (bottom panel)

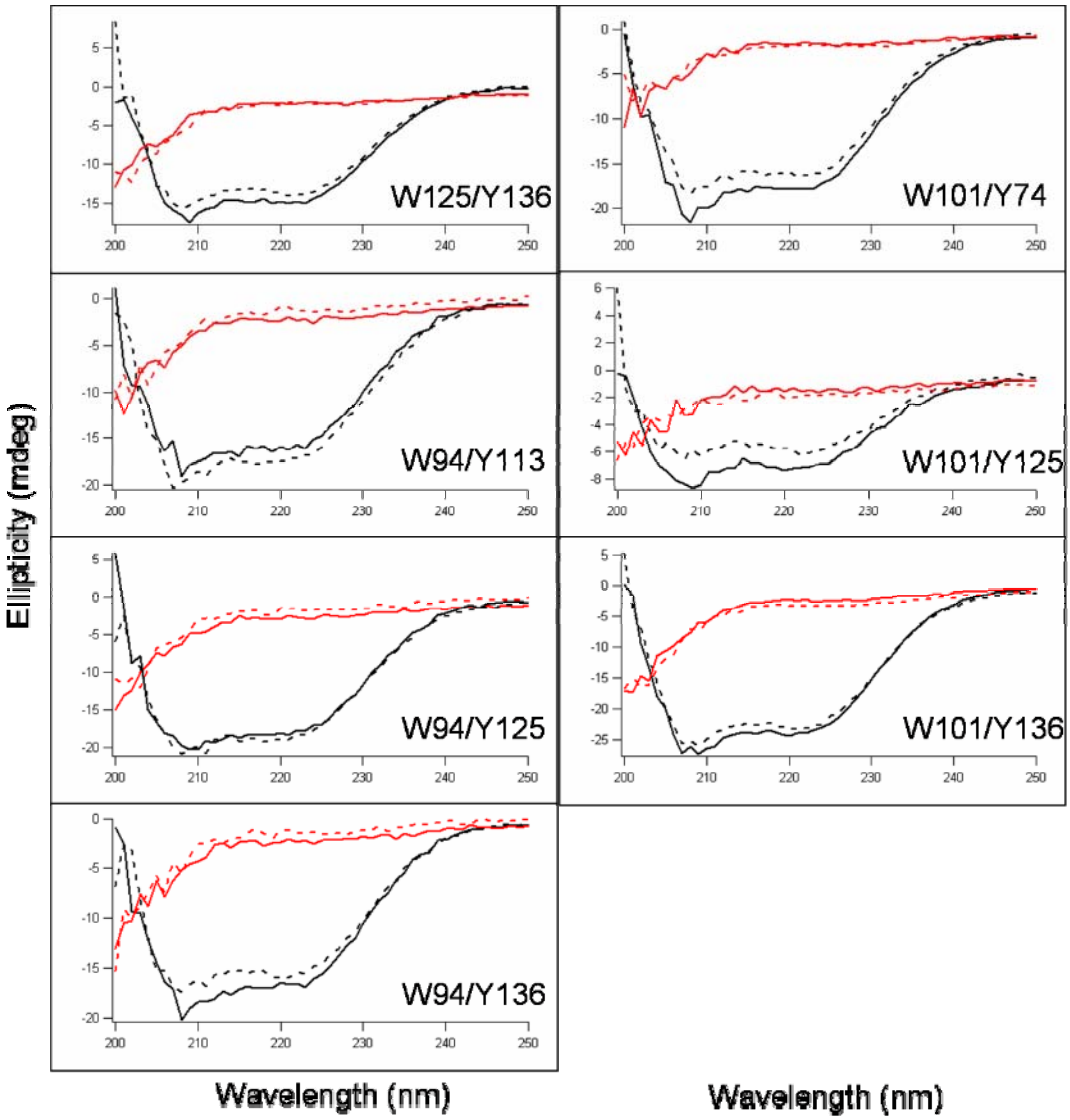

Figure 4.16. CD spectra of the seven C-terminal α-syn mutants in HEPES buffer (red solid line), HEPES + Ca^{2+} (red dotted line), 1:1 POPC:POPA SUVs (black solid line), and 1:1 POPC:POPA SUVs + Ca^{2+} (black dotted line)

Conclusion

Using all the results collected from this study, **Figure 4.17** shows a pictorial description of the C-terminal tail structure in solution and SUVs in the presence of calcium ions. In this study, we have employed steady-state fluorescence spectroscopy on single Trp α-syn mutants in the C-terminal tail to investigate the amount of calcium ions needed to induce association with membrane. By incorporating quencher-containing lipids into SUVs, we have also deduced that the insertion of the C-terminal tail into the lipid bilayer is minimal. In addition, we have also conducted FET and contact quenching studies on seven α-syn mutants with Trp and Tyr(NO_2) incorporated as donor and acceptor.

Calcium binding has been observed for the amino acid sequence DX(D/N)XD.[46] **Figure 4.18** shows the sequence of the C-terminal tail of α-syn. Although this exact calcium binding motif is not present in the sequence, there are several regions which contain an acidic amino acid at positions one/five or one/three/five in the sequence.

Using that motif, we can identify the following potential calcium binding regions: residues 110–114, 115–119, 119–123, 126–130, 131–135, and 135–139. However, the several prolines (Pro117, Pro120, Pro128, Pro138) may disrupt the calcium binding capability of those polypeptides. By eliminating those possible calcium binding sites containing a proline in the sequence, the only possible binding regions that remain are residues 110–114 and 131–135. These two regions have been predicted to be the calcium binding sites experimentally.

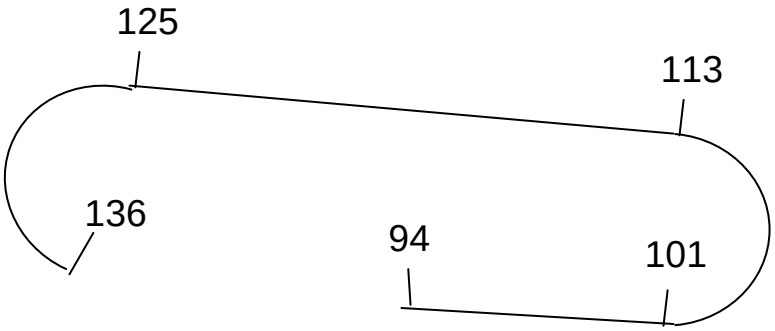

(a)

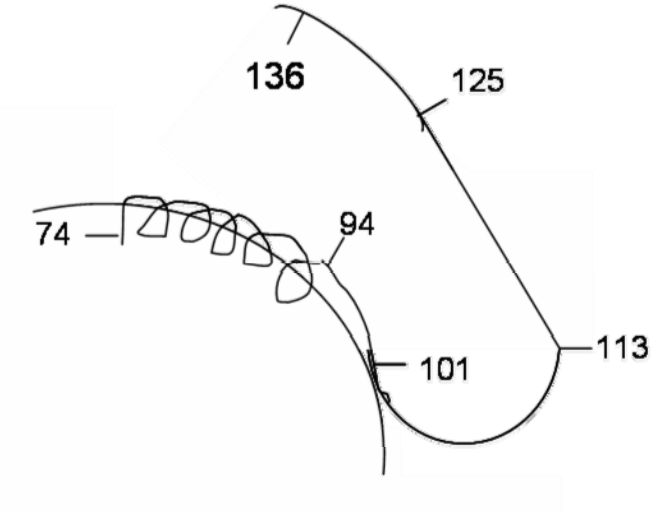

(b)

Figure 4.17. A pictorial representation of the proposed C-terminal tail structure associated with calcium ions **(a)** in the absence of 1:1 POPC:POPA SUVs and **(b)** in the presence of 1:1 POPC:POPA SUVs

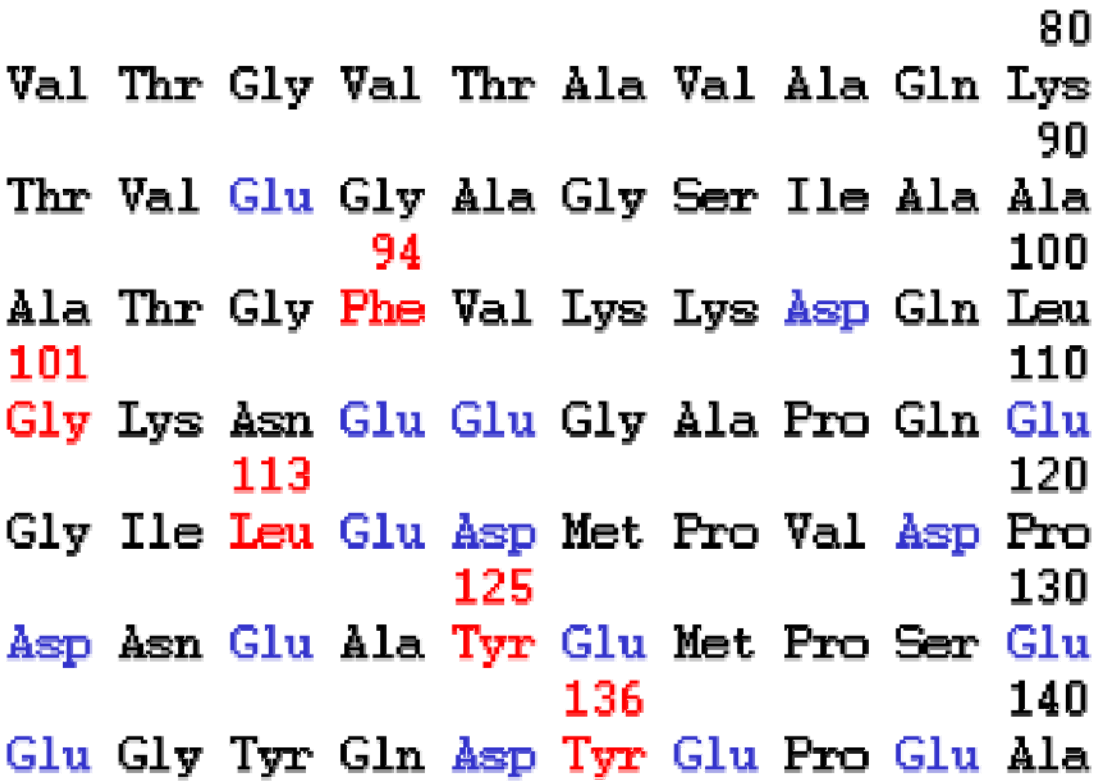

Figure 4.18. Amino acid sequence of the C-terminal tail of α-syn. The acidic residues (blue) and mutation sites (red) are highlighted

This study shows that the C-terminal tail of α-syn can bind to calcium ions. This binding process also induces some structural change to the protein. However, the binding mechanism of these calcium ions is still unclear. Therefore, future work will employ similar techniques to investigate whether this binding process is specific exclusively to calcium ions. First, we will look into the structural change of this C-terminal tail in an excess of protons (acidic environment). Second, we will study the effect of magnesium ions on the C-terminal tail structure as magnesium and calcium are similar in their electronic configurations.

4.5 ACKNOWLEDGEMENT.

This project was completed with the assistance of Ms. Stephanie S. E. Schulze and Mr. Matthew L. Robinson. Dr. Tetsunari Kimura also contributed in electron transfer experiment setup.

4.6 REFERENCES.

(1) Clayton, D. F.; George, J. M. *Trends Neurosci.* **1998**, *21*, 249–254.
(2) Lowe, R.; Pountney, D. L.; Jensen, P. H.; Gai, W. P.; Voelcker, N. H. *Protein Sci.* **2004**, *13*, 3245–3252.
(3) Jensen, P. H.; Nielsen, M. S.; Jakes, R.; Dotti, G.; Goedert, M. *J. Biol. Chem.* **1998**, *273*, 26292–26294.
(4) Nielsen, M. S.; Vorum, H.; Lindersson, E.; Jensen, P. H. *J. Biol. Chem.* **2001**, *276*, 22680–22684.
(5) Jensen, P. H.; Islam, K.; Kenney, J.; Nielsen, M. S.; Power, J.; Gai, W. P. *J Biol Chem* **2000**, *275*, 21500–21507.
(6) Fernandez, C. O.; Hoyer, W.; Zweckstetter, M.; Jares-Erijman, E. A.; Subramaniam, V.; Griesinger, C.; Jovin, T. M. *EMBO J.* **2004**, *23*, 2039–2046.
(7) Park, S. M.; Jung, H. Y.; Chung, K. C.; Rhim, H.; Park, J. H.; Kim, J. *Biochemistry* **2002**, *41*, 4137–4146.
(8) Kim, T. D.; Paik, S. R.; Yang, C. H.; Kim, J. *Protein Sci.* **2000**, *9*, 2489–2496.
(9) Park, S. M.; Jung, H. Y.; Kim, T. D.; Park, J. H.; Yang, C. H.; Kim, J. *J. Biol. Chem.* **2002**, *277*, 28512–28520.

(10) Souza, J. M.; Giasson, B. I.; Lee, V. M. Y.; Ischiropoulos, H. *Febs Letters* **2000**, *474*, 116–119.
(11) Kim, T. D.; Paik, S. R.; Yang, C. H. *Biochemistry* **2002**, *41*, 13782–13790.
(12) Serpell, L. C.; Berriman, J.; Jakes, R.; Goedert, M.; Crowther, R. A. *Proc. Natl. Acad. Sci.* **2000**, *97*, 4897–4902.
(13) Crowther, R. A.; Jakes, R.; Spillantini, M. G.; Goedert, M. *Febs Letters* **1998**, *436*, 309–312.
(14) Murray, I. V. J.; Giasson, B. I.; Quinn, S. M.; Koppaka, V.; Axelsen, P. H.; Ischiropoulos, H.; Trojanowski, J. Q.; Lee, V. M. Y. *Biochemistry* **2003**, *42*, 8530–8540.
(15) Giasson, B. I.; Duda, J. E.; Murray, I. V. J.; Chen, Q. P.; Souza, J. M.; Hurtig, H. I.; Ischiropoulos, H.; Trojanowski, J. Q.; Lee, V. M. Y. *Science* **2000**, *290*, 985–989.
(16) Fujiwara, H.; Hasegawa, M.; Dohmae, N.; Kawashima, A.; Masliah, E.; Goldberg, M. S.; Shen, J.; Takio, K.; Iwatsubo, T. *Nat. Cell Biol.* **2002**, *4*, 160–164.
(17) Crowther, R. A.; Daniel, S. E.; Goedert, M. *Neurosci. Lett.* **2000**, *292*, 128–130.
(18) Der-Sarkissian, A.; Jao, C. C.; Chen, J.; Langen, R. *J. Biol. Chem.* **2003**, *278*, 37530–37535.
(19) Miake, H.; Mizusawa, H.; Iwatsubo, T.; Hasegawa, M. *J. Biol. Chem.* **2002**, *277*, 19213–19219.
(20) Tamamizu-Kato, S.; Kosaraju, M. G.; Kato, H.; Raussens, V.; Ruysschaert, J. M.; Narayanaswami, V. *Biochemistry* **2006**, *45*, 10947–10956.
(21) Ischiropoulos, H.; Beckman, J. S. *J. Clin. Invest.* **2003**, *111*, 163–169.
(22) Denisova, N. A.; Strain, J. G.; Joseph, J. A. *J. Neurochem.* **1997**, *69*, 1259–1266.
(23) Schulz, J. B.; Lindenau, J.; Seyfried, J.; Dichgans, J. *Eur. J. Biochem.* **2000**, *267*, 4904–4911.
(24) Huang, C. L.; Huang, N. K.; Shyue, S. K.; Chern, Y. *J. Neurochem.* **2003**, *86*, 1247–1259.
(25) Cuschieri, J.; Bulger, E.; Garcia, L.; Maier, R. V. *Surgery* **2005**, *138*, 158–164.
(26) de Laureto, P.; Tosatto, L.; Frare, E.; Marin, O.; Uversky, V. N.; Fontana, A. *Biochemistry* **2006**, *45*, 11523–11531.
(27) Lai, B. T.; Lee, J. C.; Gray, H. B.; Winkler, J. R. (Manuscript in preparation).
(28) Forster, T. *Ann. Phys.-Berlin* **1948**, *2*, 55–75.
(29) Lai, B. T.; Lee, J. C.; Gray, H. B.; Winkler, J. R. (Manuscript in preparation).
(30) Lee, H. J.; Choi, C.; Lee, S. J. *J. Biol. Chem.* **2002**, *277*, 671–678.
(31) Beechem, J. M.; Haas, E. *Biophys. J.* **1989**, *55*, 1225–1236.
(32) Navon, A.; Ittah, V.; Landsman, P.; Scheraga, H. A.; Haas, E. *Biochemistry* **2001**, *40*, 105–118.
(33) Lyubovitsky, J. G.; Gray, H. B.; Winkler, J. R. *J. Am. Chem. Soc.* **2002**, *124*, 14840–14841.
(34) Wu, P. G.; Brand, L. *Anal. Biochem.* **1994**, *218*, 1–13.
(35) Lee, J. C.; Gray, H. B.; Winkler, J. R. *J. Am. Chem. Soc.* **2005**, *127*, 16388–16389.

(36) Lee, J. C.; Lai, B. T.; Kozak, J. J.; Gray, H. B.; Winkler, J. R. *J. Phys. Chem. B* **2007**, *111*, 2107–2112.
(37) Jakes, R.; Spillantini, M. G.; Goedert, M. *Febs. Lett.* **1994**, *345*, 27–32.
(38) Surrey, T.; Jahnig, F. *Proc. Natl. Acad. Sci. U. S. A.* **1992**, *89*, 7457–7461.
(39) Reshetnyak, Y. K.; Koshevnik, Y.; Burstein, E. A. *Biophys. J.* **2001**, *81*, 1735–1758.
(40) Kleinschmidt, J. H.; den Blaauwen, T.; Driessen, A. J. M.; Tamm, L. K. *Biochemistry* **1999**, *38*, 5006–5016.
(41) Doring, K.; Konermann, L.; Surrey, T.; Jahnig, F. *Eur. Biophys. J.* **1995**, *23*, 423–432.
(42) McIntosh, T. J.; Holloway, P. W. *Biochemistry* **1987**, *26*, 1783–1788.
(43) Winkler, G. R.; Harkins, S. B.; Lee, J. C.; Gray, H. B. *J. Phys. Chem. B* **2006**, *110*, 7058–7061.
(44) Arjara, G., California Institute of Technology, 2008.
(45) Bolen, E. J.; Holloway, P. W. *Biochemistry* **1990**, *29*, 9638–9643.
(46) Takada, Y.; Murphy, E.; Pil, P.; Chen, C.; Ginsberg, M. H.; Hemler, M. E. *J. Cell Biol.* **1991**, *115*, 257–266.

Chapter 5

Structural Effect on α-Synuclein Caused by Two Single-point Mutations Related to Familial Parkinson's Disease

5.1 ABSTRACT

Two single-point mutations in the α-synuclein sequence (A30P and A53T) have been linked to familial Parkinson's disease. These mutations are compelling evidence that α-synuclein is involved in the pathogenesis of this neurodegenerative disorder. Fluorescent energy transfer is yet again utilized to provide time-resolved fluorescent decays of eight of the previously studied tryptophan-3-nitrotyrosine donor-acceptor pairs. Distance distributions can be extrapolated from these decays to investigate whether these single point mutations can lead to any structural change in solution and various membrane mimics. The effect on the calcium binding ability of the C-terminal tail was also explored.

5.2 INTRODUCTION

Two missense mutations in the α-syn sequence, namely A30P[1] and A53T[2], have been linked to early onset Parkinson's disease. One of the roles of these two mutations is to accelerate the formation of protofibrils, which has been considered as the toxic species causing PD.[3] The rate of fibril formation between wild type, A30P, and A53T α-syn has been investigated.[4-8] Although it has been demonstrated that all three α-syn sequences are capable of producing fibrils that are similar to the ones extracted from Lewy bodies, the rate of fibril formation is the fastest for the A30P mutant, while A53T mutant is the slowest.[9] However, both mutations have demonstrated capability of generating protofibrils faster than wild type α-syn.[9-11] These evidence suggests that although both A30P and A53T could lead to PD, their pathogenesis pathways should be different.

AFM studies suggested that A53T α-syn can disrupt membranes more than wild type α-syn,[12] while other studies have shown that A30P α-syn has a weaker binding affinity toward lipid membranes.[12-15] Another AFM study showed that protofibrils are in the form of spheres, with A30P forming tighter spheres than wild type. On the other hand, A53T protofibrils contain a mixture of spheres, with the tight spheres resembling those commonly found in A30P.[16] These AFM studies showed that there should be differences in structures between wild type, A30P, and A53T α-syn. Therefore, it is in our interest to compare the structure of monomeric α-syn with these single point mutations to further understand the disease.

Previous studies completed by NMR and EPR have stated that the N-terminal region of α-syn demonstrates a highly helical structure in the presence of SDS micelles or acidic SUVs.[17-22] This region is also marked by characteristic seven eleven-residue repeats.[23] Since this region is highly structured in the presence of membrane mimics, the presence of these alanine mutations can possibly disrupt these structures. In Chapter 3, we have obtained the distance distributions for N-terminal mutants in solution, SDS micelles, and 1:1 POPC:POPA SUV using fluorescent energy transfer (FET).

In this study, we are interested in studying whether the introduction of these point mutations leads to any changes in the structure of monomeric α-syn. Previously studied D-A pairs were incorporated into A30P or A53T and fluorescent energy transfer (FET) was employed, where tryptophan has been utilized as the fluorescent donor, and 3-nitrotyrosine has been selected as the energy acceptor. Previously, Lee et al. has utilized similar techniques, using W4/Y19(NO_2)/A30P and Y19(NO_2)/W39/A30P, to conclude that the introduction of A30P can cause more relaxed structures to be formed in the N-terminal helix.[24] In this study, the effectsof A53T mutant on this helix were investigated using W4/Y19(NO_2)/A53T and Y19(NO_2)/W39/A53T. Furthermore, Y39(NO_2)/W94 and Y74(NO_2)/W94 were selected to the effect of both missense mutations on the C-terminal helix. W39/Y55(NO_2) was elected to study the linker region of α-syn.

In Chapter 4, the calcium binding ability of the α-syn C-terminal tail has been demonstrated. Therefore, three of the C-terminal mutants studied, namely W94/Y113(NO_2), W94/Y125(NO_2), and W125/Y136(NO_2), were also chosen to

compare the structural changes caused by the alanine point mutations in solution and SUVs. The effect of calcium ions on these mutants was also investigated.

5.3 METHODS

Protein expression, purification, nitration, and characterization have been outlined in Chapter 1. The data collection parameters for steady-state and time-resolved fluorescence measurements have also been previously described. However, it is important to note that spectroscopic studies on the N-terminal mutants were carried out in 20 mM NaP_i (pH 7.4), while 10 mM HEPES buffer (pH 7.4) was used for C-terminal mutants. SDS micelles and 1:1 POPC:POPA SUVs were made in the appropriate buffers, determined by the mutants to be studied.

5.4 RESULTS AND DISCUSSIONS

N-terminal Helix.

In **Figure 5.1a**, we can observe that the distance distributions extracted from W4/Y19(NO_2) (blue) and W4/Y19(NO_2)/A53T (green). A slightly tighter conformation was formed in W4/Y19(NO_2)/A53T when it was associated with membrane mimics. It can be extrapolated that a slightly tighter helix was formed when these mutants were in association with micelles than with SUVs. This trend is opposite from what A30P can affect the N-terminal helix.

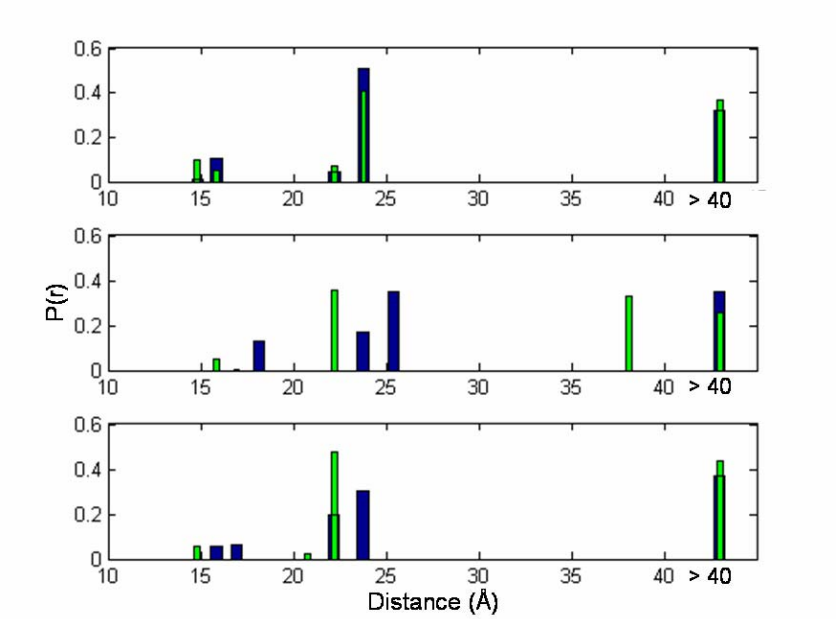

(a)

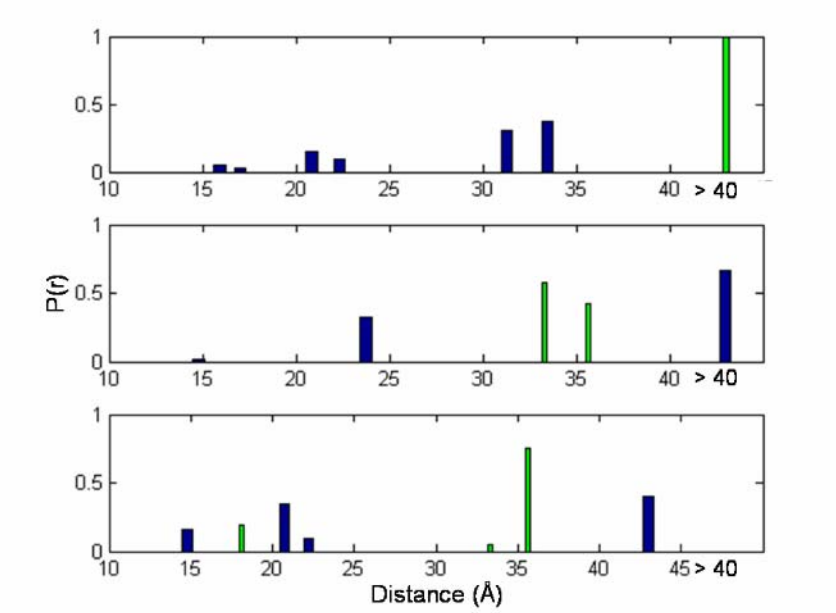

(b)

Figure 5.1. D-A distance distributions extrapolated from FET kinetics for **(a)** W4/Y19(NO_2) (blue) and W4/Y19(NO_2)/A30P (red), **(b)** Y19(NO_2)/W39 and Y19(NO_2)/W39/A53T (green) in 20 mM NaP_i buffer (top panel), 1:1 POPC:POPA (middle panel), and 31 mM SDS (bottom panel)

On the contrary, although Y19(NO_2)/W39 and W4/Y19(NO_2) are located within the same N-terminal helix, the effects caused by A53T are noticeably different (**Figure 5.1b**). When Y19(NO_2)/W39/A53T was placed in solution, only extended distances (> 40 Å) are found. When it was in association with SUVs, a shorter distance (~ 34 Å, 100%) in SUVs is formed. But, when the mutant was bound to the smaller membrane mimic, SDS micelles, a population (20%) of short distance (18 Å) emerges. Previously, we have shown that the N-terminal helix formed similar structures in micelles and SUVs. However, the distance distributions displayed by this A53T mutat in micelles show a much larger scale of contraction. This implies that A53T can possibly prevent this portion of the N-terminal helix from forming close contact in solution. However, in the presence of small membrane mimics, a much tighter helix can be formed.

Lee et al. has previously studied the effect of A30P on this mutant also.[24] They have concluded that the presence of that mutant allows a higher distribution of extended distances when the mutant was in association with micelles. Our results demonstrate that an opposite phenomenon is observed when A53T is incorporated into these N-terminal mutants. Therefore, we can conclude that A30P and A53T mutations affect the structure of monomeric α-syn quite differently.

C-terminal Helix.

In Chapter 3, we have postulated that C-terminal helix forms a tighter helix with the α-syn mutant is associated with SDS micelles than with SUVs. In **Figure 5.2**, the distance distributions for Y74(NO_2)/W94 (blue), Y74(NO_2)/W94/A30P (red), and Y74(NO_2)/W94/A53T (green) are shown. Y74(NO_2)/W94/A30P in solution is the only one that shows some intermediate distances (~ 23 Å, ~ 60%) and short distances (~ 15 Å, ~ 10%). All the other intermediate and short distance distributions in Y74(NO_2)/W94 in various environments have disappeared.

Although it is known that A30P and A53T mutants both form helices in these regions, it is possible that this C-terminal helix is now in a more relaxed conformation. This phenomenon is also supported by the data presented in **Figure 5.3**, where the only non-extended distances could only be observed when Y39(NO_2)/W94/A30P was placed in buffer. These results also suggest that the presence of the A30P and A53T mutations can prevent this polypeptide region from forming close contacts.

Linker Region.

W39/Y55(NO_2) is studied to investigate the behavior of the linker region and also the C-terminal helix. From **Figure 5.4b**, it shows that the A53T mutant provides longer distance distributions in solution when compared to the pseudo wild-type mutant. This implies that A53T could weaken any propensity for the unstructured protein from forming close contacts.

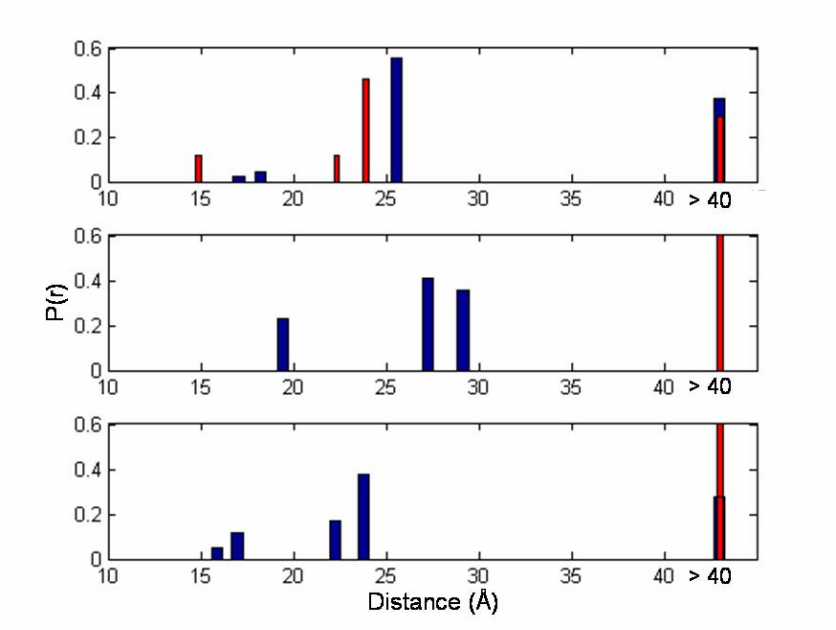

(a)

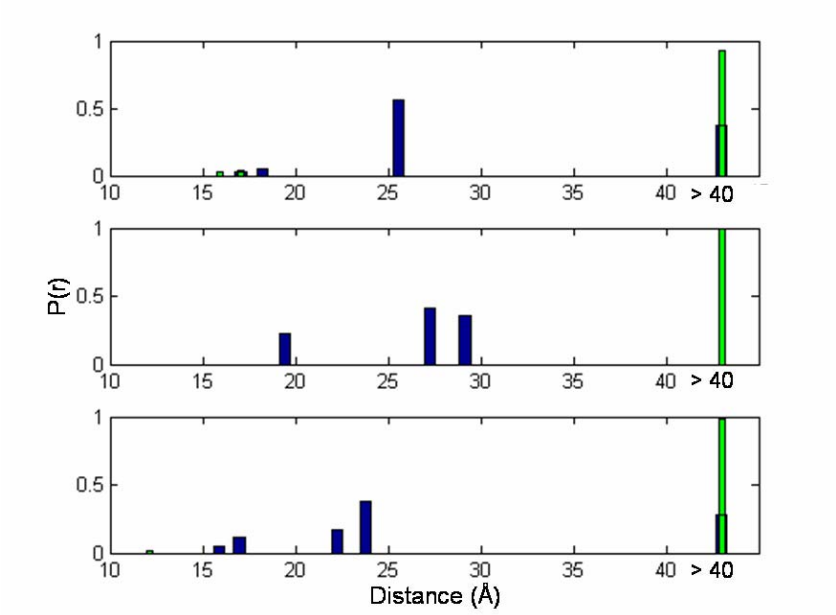

(b)

Figure 5.2. D-A distance distributions extrapolated from FET kinetics for Y74(NO_2)/W94 (blue), **(a)** Y74(NO_2)/W94/A30P (red), and **(b)** Y74(NO_2)/W94/A53T (green) in 20 mM NaP_i buffer (top panel), 1:1 POPC:POPA (middle panel), and 31 mM SDS (bottom panel)

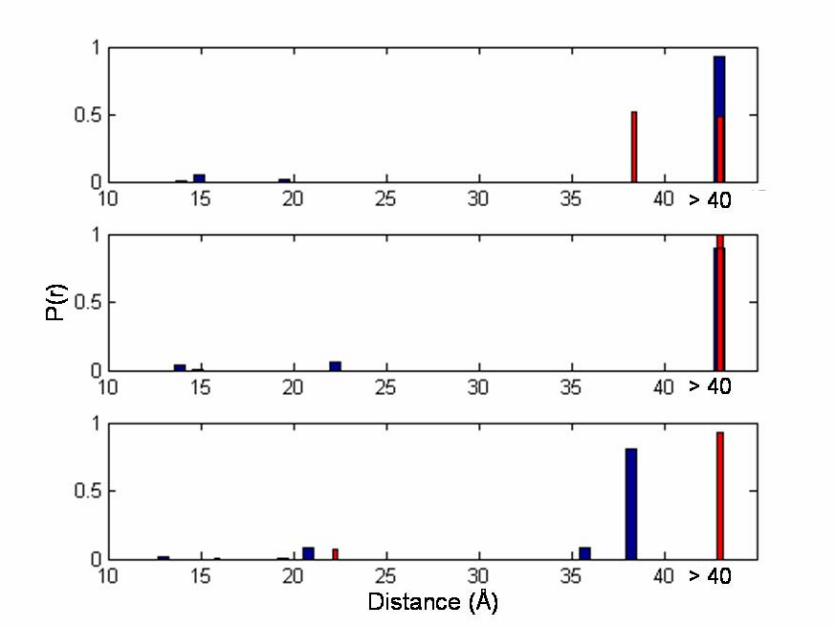

(a)

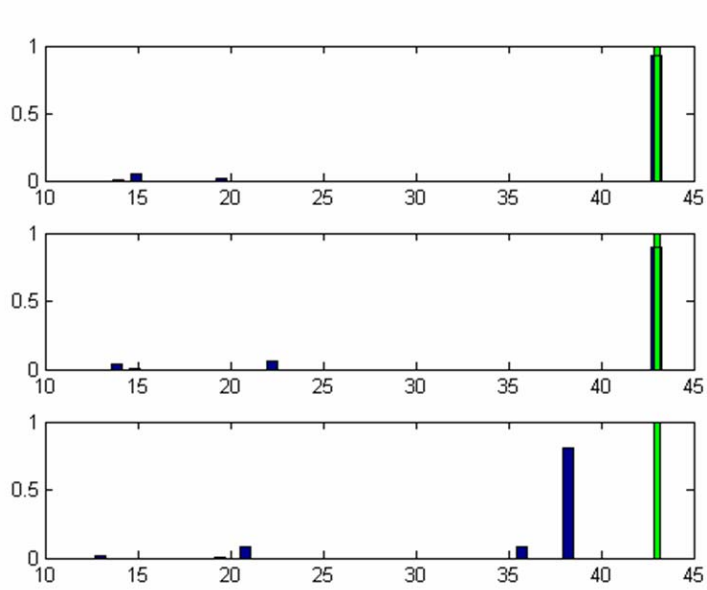

(b)

Figure 5.3. D-A distance distributions extrapolated from FET kinetics for Y39(NO_2)/W94 (blue), **(a)** Y39(NO_2)/W94/A30P (red), and **(b)** Y39(NO_2)/W94/A53T (green) in 20 mM NaP_i buffer (top panel), 1:1 POPC:POPA (middle panel), and 31 mM SDS (bottom panel)

On the other hand, the extended distance population (> 40 Å) has increased from ~ 40% to ~ 60% in membrane mimics. Conversely, the intermediate distance populations (~ 20 Å) have shifted to smaller distances. The presence of the A53T mutant can shorten the turn region, thus justifying the shortening of the intermediate distance populations. On the other hand, the lengthening of the extended distance population can further confirm that the C-terminal helix becomes more relaxed when the A53T mutation is introduced.

In the pseudo wild-type mutant, the distance distribution shows that a tighter helix is formed in the presence of SDS micelles when compared to SUVs. This similar trend is still observed for the A53T mutant, only the distance reduction is at a smaller extent. This also implies that the C-terminal helix of the A53T mutant could still be folding into similar motif like its pseudo wild type counterpart, only with a looser helix and tighter turn area. On the other hand, for W39/Y55(NO_2)/A30P (**Figure 5.4a**), an opposite trend can be observed, where a more compact distance distribution is found when the mutant is bound to SUVs than to micelles.

It is also interesting to note that in solution, the A30P mutant gives a shorter distance for the compact distances region (~ 20 Å) when compared to the non-disease mutant, possibly implying the effect of A30P in the turn region (**Figure 5.4a**). On the contrary, the extended distances distribution (> 33 Å) becomes more extended when the A30P mutant is introduced. Previously, we have shown that the introduction of the A30P can discourage close contacts from forming for the C-terminal mutants (Y74/Y94(NO_2) and Y39/W94(NO_2)), thus causing this lengthening phenomenon.

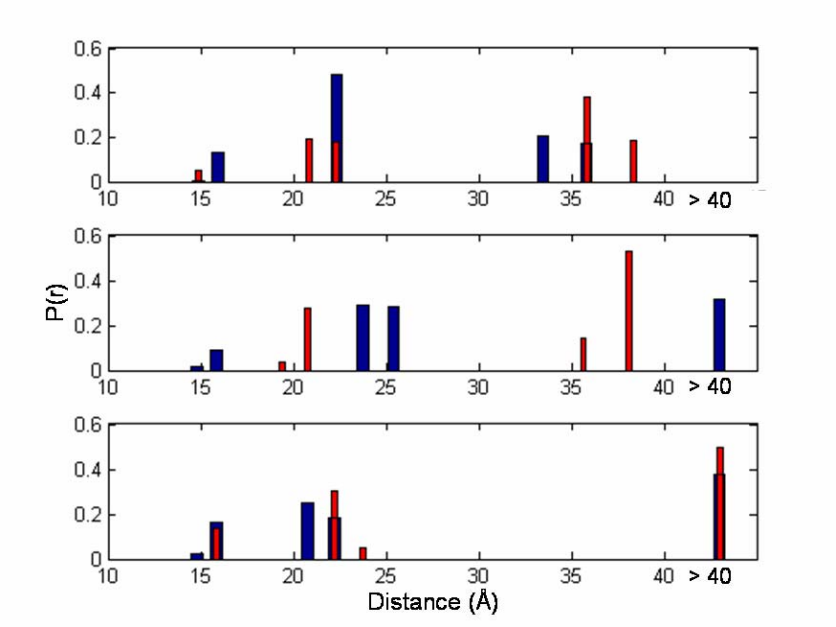

(a)

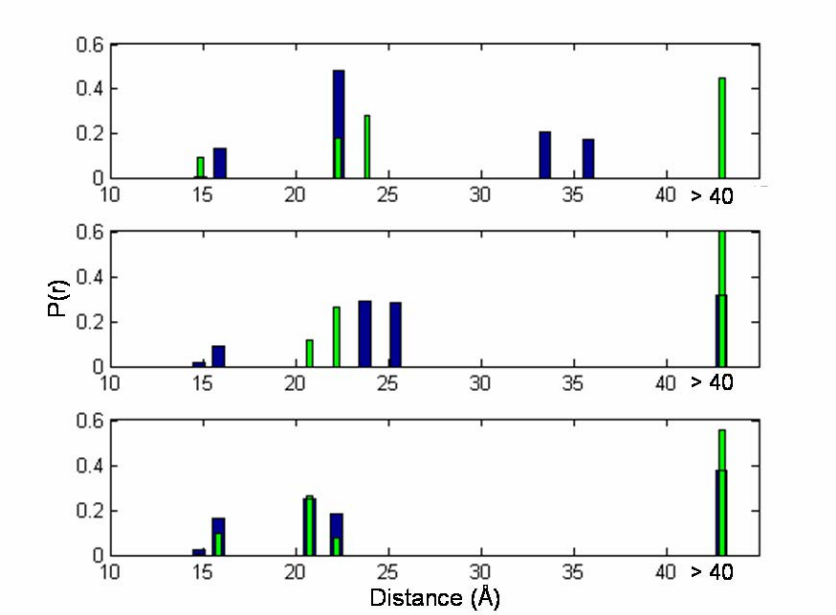

(b)

Figure 5.4. D-A distance distributions extrapolated from FET kinetics for W39/Y55(NO_2) (blue), **(a)** W39/Y55(NO_2)/A30P (red), and **(b)** W39/Y55(NO_2)/A53T (green) in 20 mM NaP_i buffer (top panel), 1:1 POPC:POPA (middle panel), and 31 mM SDS (bottom panel)

Summary on the helical region.

Figure 5.5a shows a summary on the effect of A30P (red arrows) and A53T (green arrows) mutations on the structure in solution, when compared to their non-disease related counterpart. It shows that both mutations discourage the formation of close contacts in the second half of the N-terminal mutant. On the other hand, A30P allows the C-terminal helix to form close contact easier, while preventing it in the turn region and the second part of the N-terminal helix. However, opposing phenomenon can be observed for the A53T mutant.

Figure 5.5b and **Figure 5.5c** show that the effect of A30P and A53T are quite similar when the mutants are in association with SUVs and micelles. They both cause the C-terminal helix to lengthen and the turn region to contract. The only difference is that it does not seem that the A30P can cause shortening of distances in the second half of the N-terminal helix in SUVs, while A53T has that effect on that region for both membrane mimics. From these results, it can suggest that the contraction in the second half of the N-terminal helix could be a culprit for the seeding the aggregation reaction. Since the NAC region (residues 61–95) is suspected of being involved in the pathogenesis of the PD, the lengthening of the C-terminal helix could also affect aggregation.

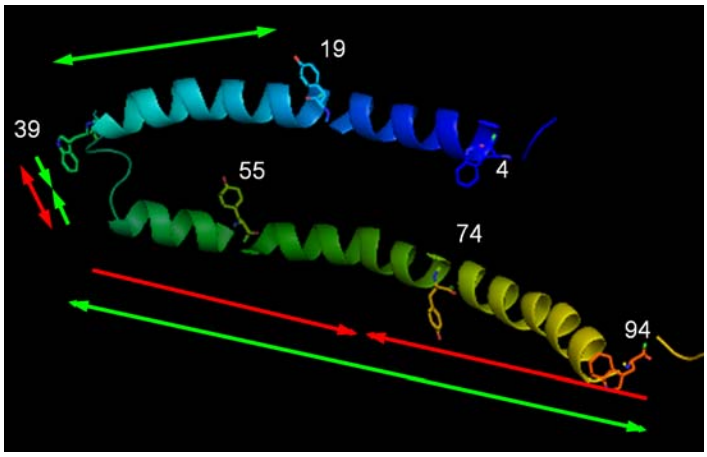

(a)

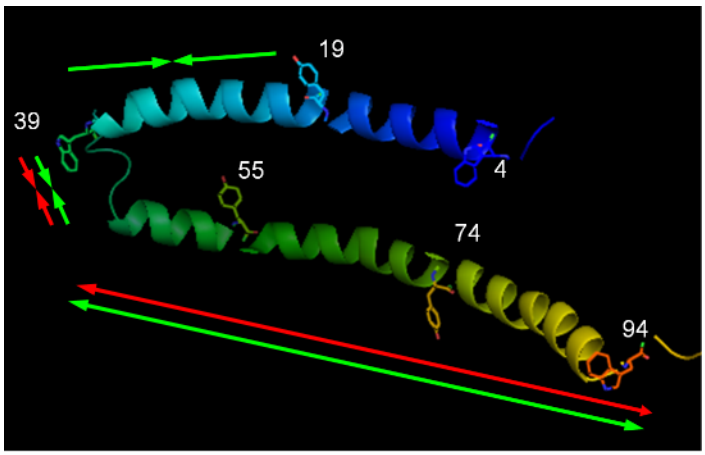

(b)

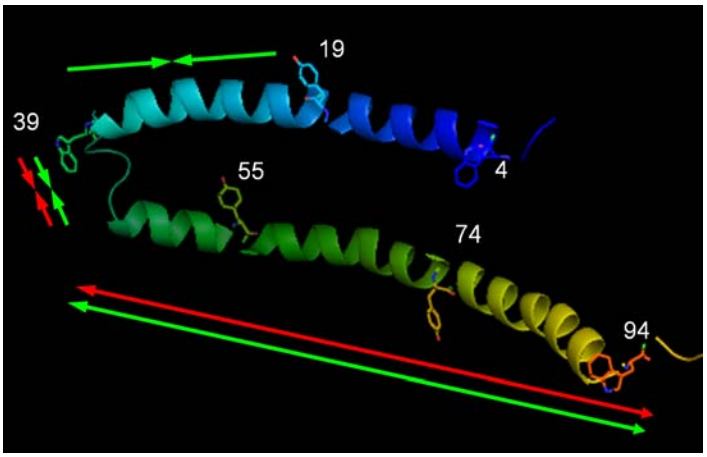

(c)

Figure 5.5. The effect of A30P (red) and A53T (green) mutants on the structure of α-syn in **(a)** NaPi, **(b)** SUVs, and **(c)** SDS micelles, when compared with their pseudo-wild-type counterpart

C-terminal Tail in Solution.

For the mutant W125/Y136(NO_2), more compact structures formed when the A30P and A53T mutations were introduced (**Figure 5.6**). There is also a small contraction of distance distributions (60%) from 22 Å to 21 Å for the A30P mutant when calcium ions were added. Similar shortening of distances (23 Å to 21 Å, 60%) can be observed in W125/Y136(NO_2)/A53T. However, these decreases in distances are smaller in scale compared to the mutants without these single-point mutations. Previously in Chapter 4, we have elucidated a calcium binding pocket between residues 125 and 136 in solution; it seems like this binding motif is maintained with the introduction of A30P or A53T, with the possibility that they weaken the calcium binding ability.

Figure 5.7 shows the addition of A30P and A53T into the W94/Y113(NO_2) mutation causes an increase in the population of extended distances (> 40 Å), with A30P showing a more dramatic change (60%) compared to A53T (10%). In addition, a more dramatic shift of the short distance distribution is observed for A30P than A53T. These general trends can be observed regardless of whether calcium ions are present, implying that A30P and A53T can lead to more compact structures.

It is also interesting to note although there is no change in the population of the extended distances when calcium ions are introduced, there is a contraction observed on the short distance population, with the A30P mutant shifting ~ 3 Å, while the A53T mutant only yields a ~ 1 Å change. We have previously assigned a calcium binding region between residues 101 and 113 in solution. From this set of data, it suggests that this calcium binding region remains with the A30P/A53T mutations.

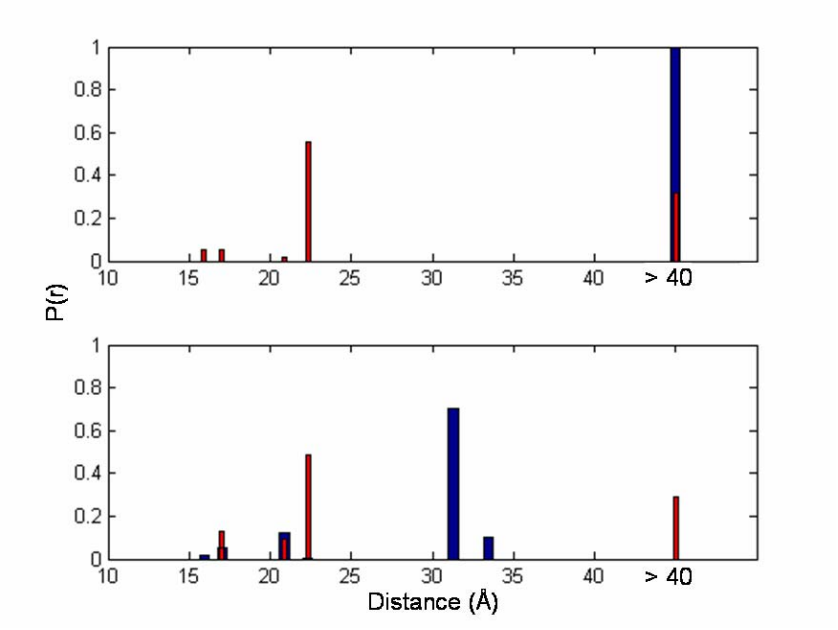

(a)

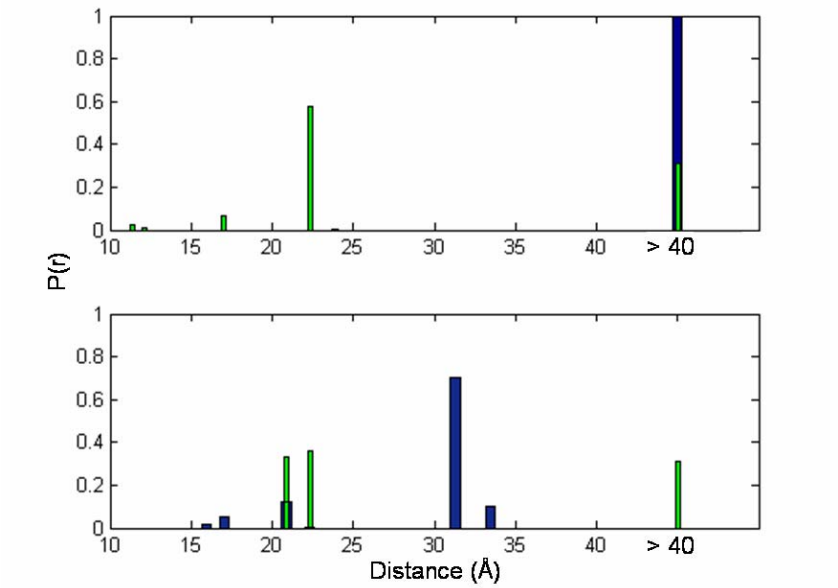

(b)

Figure 5.6. D-A distance distributions extrapolated from FET kinetics for W125/Y136(NO_2) (blue), **(a)** W125/Y136(NO_2)/A30P (red), and **(b)** W125/Y136(NO_2)/A53T (green) in 10 mM HEPES buffer (top panel), and 10 mM HEPES buffer with 1 mM Ca^{2+} (bottom panel)

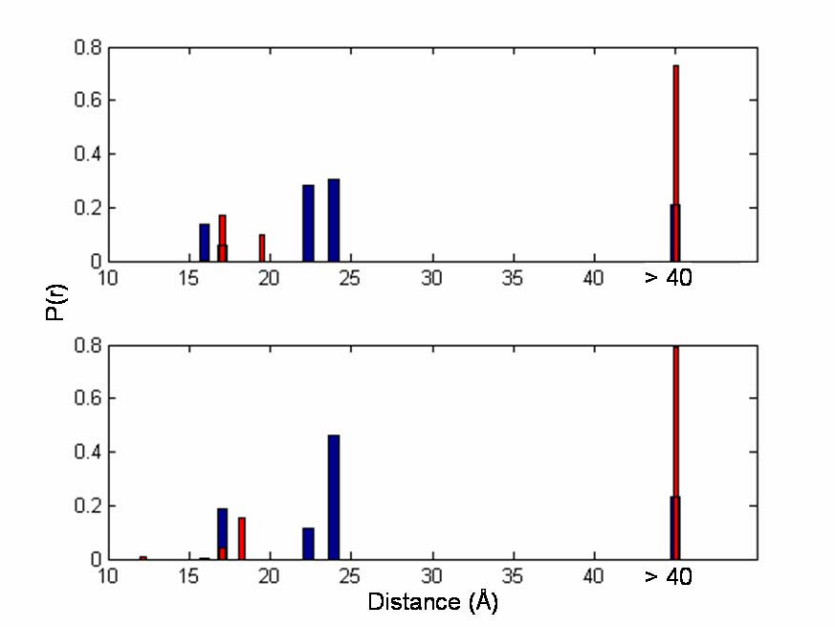

(a)

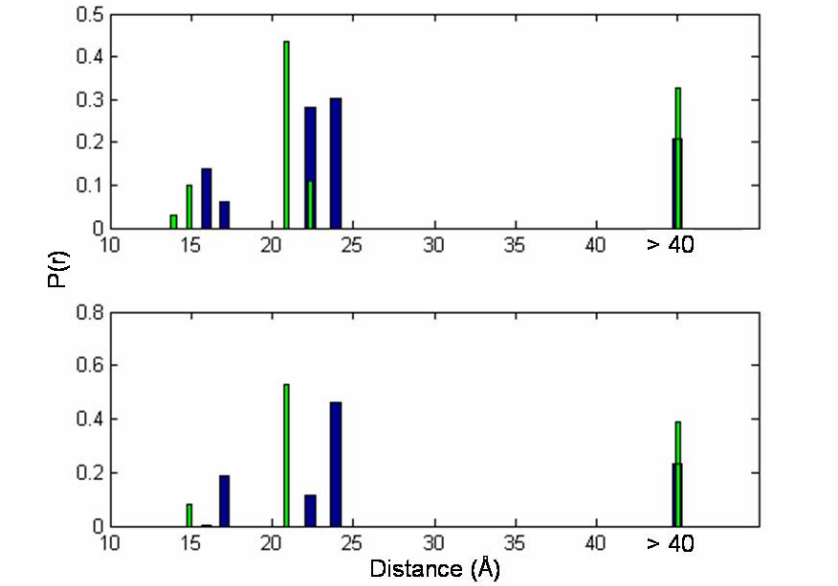

(b)

Figure 5.7. D-A distance distributions extrapolated from FET kinetics for W94/Y113(NO_2) (blue), **(a)** W94/Y113(NO_2)/A30P (red), and **(b)** W94/Y113(NO_2)/A53T (green) in 10 mM HEPES buffer (top panel), and 10 mM HEPES buffer with 1 mM Ca^{2+} (bottom panel)

The distance distributions between W94/Y125(NO_2) and W94/Y125(NO_2)/A30P are almost overlapping with each other, except that a higher population of extended distances (> 40 Å) is observed (**Figure 5.8a**). The lengthening caused by the addition of calcium ions observed in W94/Y125 is also demonstrated in W94/Y125(NO_2)/A30P. On the other hand, the presence of A53T mutants causes the mutant to shift to shorter distances when calcium ions are present (**Figure 5.8b**). Thus, an opposite trend is observed when calcium ions were added to A53T. This could suggest that while the presence of A30P and A53T mutants can cause more extended structures to form in solution, the A53T mutant can weaken the rigidity of the polypeptide 113–125, which was previously extrapolated in Chapter 4.

C-terminal Tail in SUVs.

In Chapter 4, it was suggested that there is a calcium binding region between residues 94 and 113, while a lengthening region can be found between residues 113 and 125. For W94/Y125(NO_2)/A30P (**Figure 5.9a**), there is an increase in the distance distribution, from 22 Å to 23 Å, when calcium ions are introduced. On the other hand, the distances extrapolated from the decay curves (not shown) for W94/Y125(NO_2)/A53T (**Figure 5.9b**), W94/Y113(NO_2)/A30P (**Figure 5.10a**), and W94/Y113(NO_2)/A53T (**Figure 5.10b**) when they are associated with SUVs show that all the distance populations can be found > 40 Å, demonstrating that there is negligible quenching, regardless of whether calcium ions were added. These distance distributions suggests that the lengthening region between 113 and 125 still persists when the single-point mutations were added. Therefore, calcium ions could still be

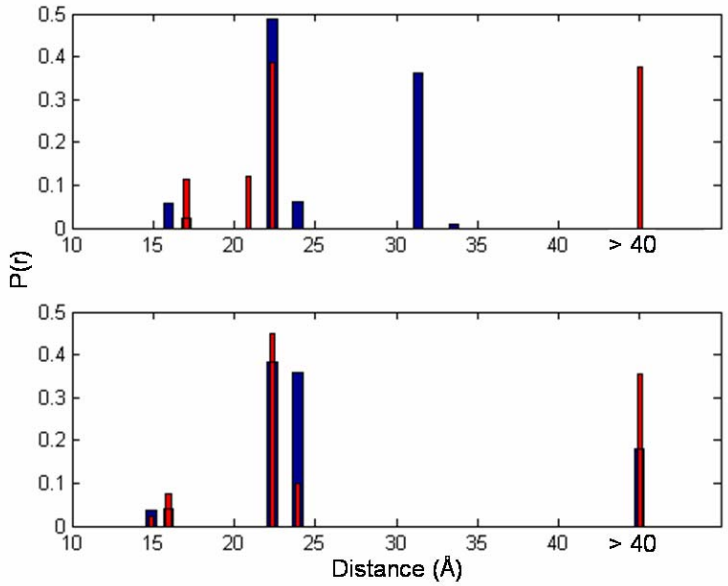

(a)

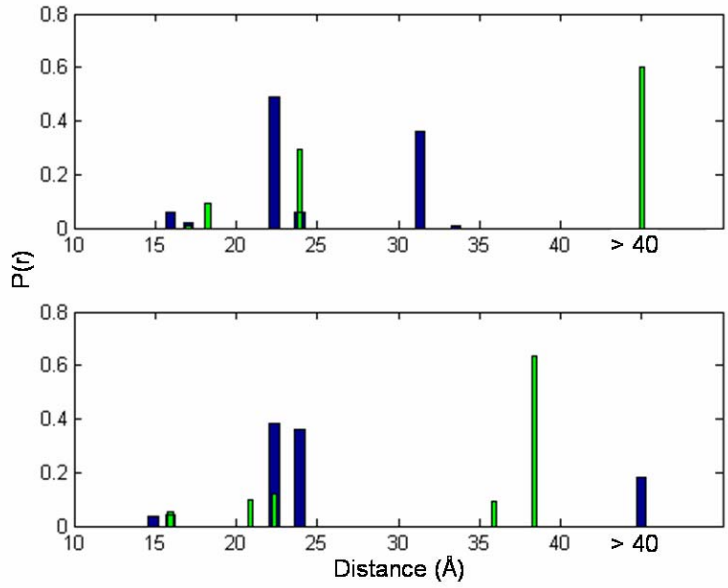

(b)

Figure 5.8. D-A distance distributions extrapolated from FET kinetics for W94/Y125(NO_2), **(a)** W94/Y125(NO_2)/A30P (red), and **(b)** W94/Y125(NO_2)/A53T (green) in 10 mM HEPES buffer (top panel), and 10 mM HEPES buffer with 1 mM Ca^{2+} (bottom panel)

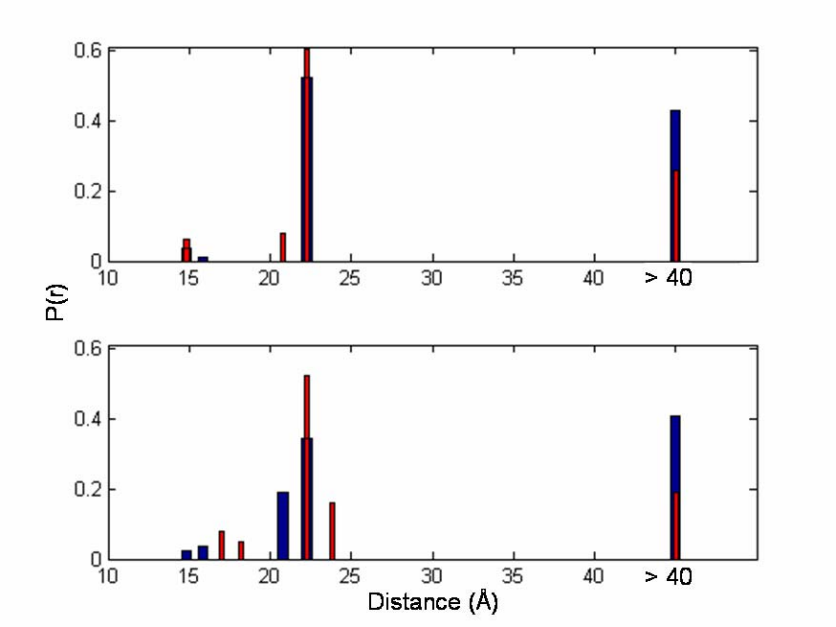

(a)

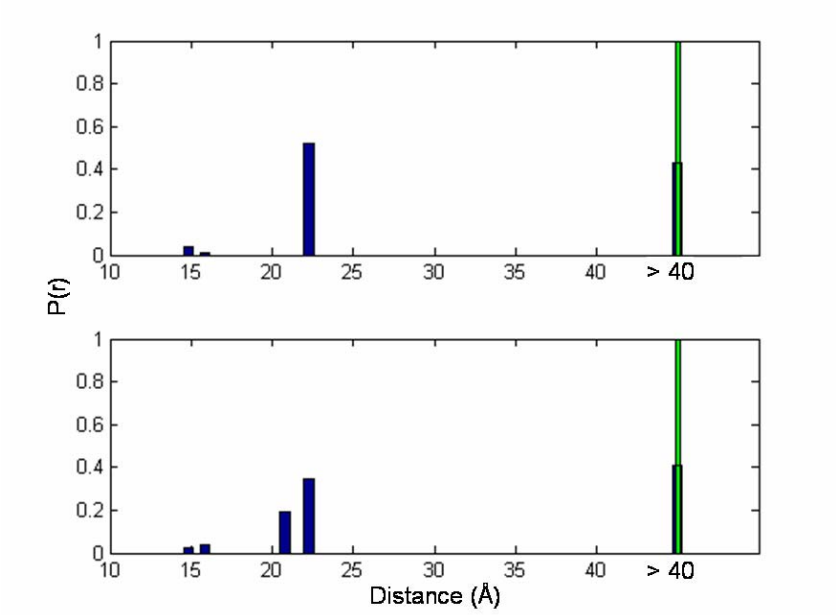

(b)

Figure 5.9. D-A distance distributions extrapolated from FET kinetics for W94/Y125(NO_2) (blue), **(a)** W94/Y125(NO_2)/A30P (red), and **(b)** W94/Y125(NO_2)/A53T (green) in 1:1 POPC:POPA (1.4 mg/mL)in 10 mM HEPES buffer (top panel), and with 1 mM Ca^{2+} (bottom panel)

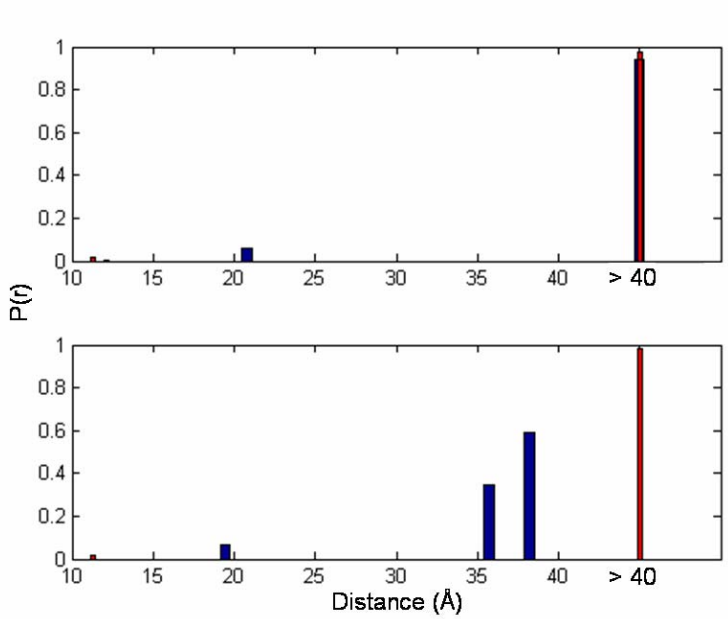

(a)

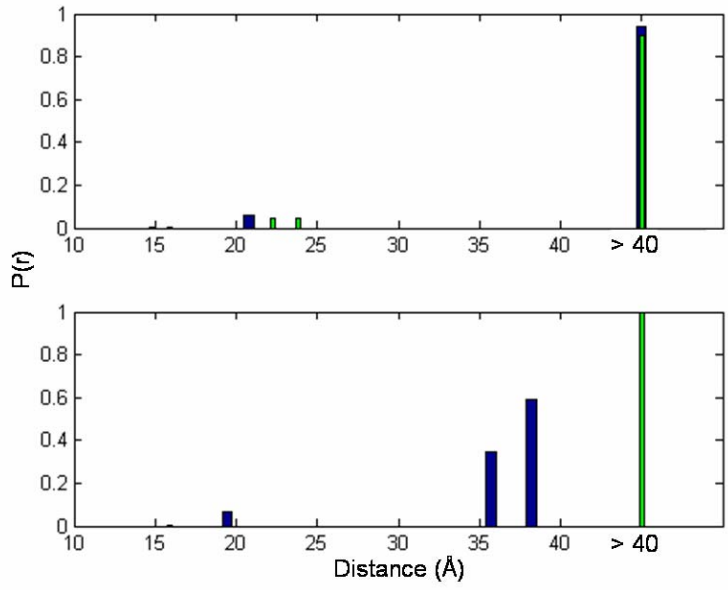

(b)

Figure 5.10. D-A distance distributions extrapolated from FET kinetics for W94/Y113(NO_2) (blue), **(a)** W94/Y113(NO_2)/A30P (red), and **(b)** W94/Y113(NO_2)/A53T (green) in 1:1 POPC:POPA (1.4 mg/mL)in 10 mM HEPES buffer (top panel), and with 1 mM Ca^{2+} (bottom panel)

affecting the C-terminal tail. However, the calcium binding region between 101 and 113 could be severely weakened with the introduction of the A30P or A53T mutations.

The distance distributions for W125/Y136(NO_2) in the presence of SUVs (**Figure 5.11**) suggest that there is a disappearance of calcium binding region between residues 125–136, as no intermediate or short distances emerge when calcium ions were added. However, a population (~ 60%) starts to appear when W125/ Y136(NO_2)/A30P (22 Å) and W125/Y136(NO_2)/A53T (21 Å) are associated with SUVs. What is more interesting is that upon the addition of calcium ions, a small degree of distance contraction can be observed.

Summary on the C-terminal Tail Region.

In conclusion, both the A30P and A53T mutations seem to generate more compact structures in solution and in SUVs, regardless of whether calcium ions were present. These single point mutations also affect the calcium binding ability of the first calcium binding region (polypeptide 101–113) when SUVs were present. On the contrary, the weak second calcium binding region (residues 125–136) seems to be enhanced slightly with these single-point mutations. In solution, the first calcium binding region seems to be maintained, while the second binding region is enhanced.

Since more compact structures are formed with the mutations, these structures could encourage the formation of protofibrils. The two calcium binding regions could serve a different role in the pathogenesis of the disease, as one of them is enhanced in the presence of SUVs, while the other one is weakened. However, the

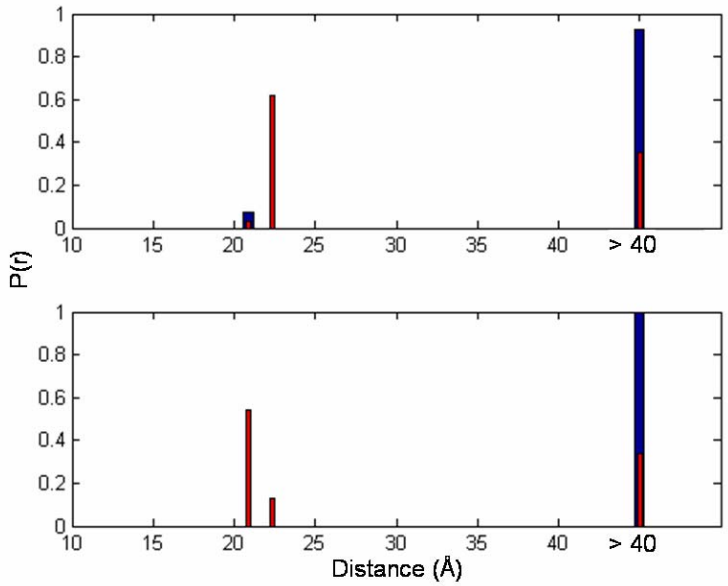

(a)

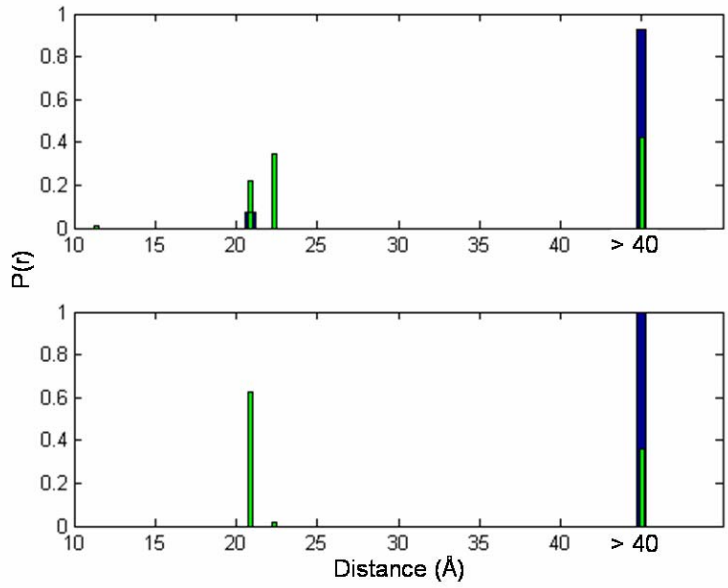

(b)

Figure 5.11. D-A distance distributions extrapolated from FET kinetics for W125/Y136(NO_2) (blue), **(a)** W125/Y136(NO_2)/A30P (red), and **(b)** W125/Y136(NO_2)/A53T (green) in 1:1 POPC:POPA (1.4 mg/mL)in 10 mM HEPES buffer (top panel), and with 1 mM Ca^{2+} (bottom panel)

change in the calcium binding ability of this C-terminal tail caused by these mutations can show that calcium ions are also quite important in determining the monomeric structure of α-syn, possibly influencing the rate of plaque formation.

5.5 ACKNOWLEDGEMENTS

This project was completed with the assistance of Ms. Stephanie S. E. Schulze, Mr. Matthew L. Robinson, and Ms. Debbie G. Tseng.

5.6 REFERENCES

(1) Kruger, R.; Kuhn, W.; Muller, T.; Woitalla, D.; Graeber, M.; Kosel, S.; Przuntek, H.; Epplen, J. T.; Schols, L.; Riess, O. *Nat. Genet.* **1998**, *18*, 106–108.

(2) Polymeropoulos, M. H.; Lavedan, C.; Leroy, E.; Ide, S. E.; Dehejia, A.; Dutra, A.; Pike, B.; Root, H.; Rubenstein, J.; Boyer, R.; Stenroos, E. S.; Chandrasekharappa, S.; Athanassiadou, A.; Papapetropoulos, T.; Johnson, W. G.; Lazzarini, A. M.; Duvoisin, R. C.; Di Iorio, G.; Golbe, L. I.; Nussbaum, R. L. *Science* **1997**, *276*, 2045–2047.

(3) Rochet, J. C.; Outeiro, T. F.; Conway, K. A.; Ding, T. T.; Volles, M. J.; Lashuel, H. A.; Bieganski, R. M.; Lindquist, S. L.; Lansbury, P. T. *J. Mol. Neurosci.* **2004**, *23*, 23–33.

(4) Narhi, L.; Wood, S. J.; Steavenson, S.; Jiang, Y. J.; Wu, G. M.; Anafi, D.; Kaufman, S. A.; Martin, F.; Sitney, K.; Denis, P.; Louis, J. C.; Wypych, J.; Biere, A. L.; Citron, M. *J. Biol. Chem.* **1999**, *274*, 9843–9846.

(5) Conway, K. A.; Harper, J. D.; Lansbury, P. T. *Nat. Med.* **1998**, *4*, 1318–1320.

(6) El-Agnaf, O. M. A.; Jakes, R.; Curran, M. D.; Wallace, A. *Febs Letters* **1998**, *440*, 67–70.

(7) Hashimoto, M.; Hsu, L. J.; Sisk, A.; Xia, Y.; Takeda, A.; Sundsmo, M.; Masliah, E. *Brain Res.* **1998**, *799*, 301–306.

(8) Giasson, B. I.; Uryu, K.; Trojanowski, J. Q.; Lee, V. M. Y. *J. Biol. Chem.* **1999**, *274*, 7619–7622.

(9) Conway, K. A.; Harper, J. D.; Lansbury, P. T. *Biochemistry* **2000**, *39*, 2552–2563.

(10) Li, J.; Uversky, V. N.; Fink, A. L. *Biochemistry* **2001**, *40*, 11604–11613.

(11) Li, J.; Uversky, V. N.; Fink, A. L. *Neurotoxicology* **2002**, *23*, 553–567.

(12) Jo, E. J.; McLaurin, J.; Yip, C. M.; St George-Hyslop, P.; Fraser, P. E. *J. Biol. Chem.* **2000**, *275*, 34328–34334.

(13) McLean, P. J.; Kawamata, H.; Ribich, S.; Hyman, B. T. *J. Biol. Chem.* **2000**, *275*, 8812–8816.
(14) Perrin, R. J.; Woods, W. S.; Clayton, D. F.; George, J. M. *J. Biol. Chem.* **2000**, *275*, 34393–34398.
(15) Jensen, P. H.; Nielsen, M. S.; Jakes, R.; Dotti, G.; Goedert, M. *J. Biol. Chem.* **1998**, *273*, 26292–26294.
(16) Ding, T. T.; Lee, S. J.; Rochet, J. C.; Lansbury, P. T. *Biochemistry* **2002**, *41*, 10209–10217.
(17) Bussell, R.; Eliezer, D. *J. Mol. Biol.* **2003**, *329*, 763–778.
(18) Chandra, S.; Chen, X. C.; Rizo, J.; Jahn, R.; Sudhof, T. C. *J. Biol. Chem.* **2003**, *278*, 15313–15318.
(19) Eliezer, D.; Kutluay, E.; Bussell, R.; Browne, G. *J. Mol. Biol.* **2001**, *307*, 1061–1073.
(20) Jao, C. C.; Der-Sarkissian, A.; Chen, J.; Langen, R. *Proc. Natl. Acad. Sci. U. S. A.* **2004**, *101*, 8331–8336.
(21) Ramakrishnan, M.; Jensen, P. H.; Marsh, D. *Biochemistry* **2003**, *42*, 12919–12926.
(22) Ulmer, T. S.; Bax, A.; Cole, N. B.; Nussbaum, R. L. *J. Biol. Chem.* **2005**, *280*, 9595–9603.
(23) George, J. M.; Jin, H.; Woods, W. S.; Clayton, D. F. *Neuron* **1995**, *15*, 361–372.
(24) Lee, J. C.; Langen, R.; Hummel, P. A.; Gray, H. B.; Winkler, J. R. *Proc. Natl. Acad. Sci. U. S. A.* **2004**, *101*, 16466–16471.

Chapter 6

Highly Fluorescent Dye for α-Synuclein Aggregation Studies

6.1 ABSTRACT

A characteristic of Parkinson's disease is the presence of Lewy bodies in surviving neurons of the *substantia nigra* region of the brain. Lewy bodies are insoluble protein deposits comprised mostly of α-synuclein (α-syn). Measurements of fluorescent energy-transfer (FET) kinetics can provide site-specific information about the structure, dynamics, degree of aggregation, and fibrillogenesis mechanisms of α-syn. Dyes with high quantum yields, I-SHark and phI-SHark, were synthesized for use as fluorescent labeling reagents on protein cysteine residues. The labeling protocol between these fluorescent dyes and a cysteine residue was created using commercially available *Saccharomyces cerevisiae* Iso-1 cytochrome *c* (cyt *c*). Successful labeling was confirmed by absorption spectroscopy, mass spectrometry, and peptide mapping of tryptic digestion fragments. To further enhance the overlap integral for future study on α-syn intermolecular aggregation, an acceptor, nitrophenol, was also designed to couple with phI-SHark.

6.2 INTRODUCTION

In PD patients, abnormal protein aggregates with mostly α-syn have been found. Unfortunately, the usual tools used in determining protein structure, such as x-ray crystallography and NMR spectroscopy, provide little insight into the structure of these soluble oligomers.[1] Measurements of FET kinetics can provide site-specific information about the structure, dynamics, degree of aggregation, and fibrillogenesis mechanisms of amyloid forming proteins.[2] This powerful tool can be employed to obtain a distribution of distances between a fluorescent donor (D) and an energy acceptor (A),[3-7] as the dipole-dipole energy transfer rates are inversely proportional to the sixth power of the fluorescent D-A distance.[8] Hence, this technique may extend the understanding of the mechanism of many misfolding diseases, including Alzheimer's [9] and Parkinson's diseases.[10]

To successfully extract distance information between a fluorescent donor and an acceptor, Förster distance (R_0) is an important factor to be considered. Förster distance (**Equation 1**) is dependent on the orientation factor of the transition dipoles of donor and acceptor (κ^2), the refractive index of the surrounding medium (n), the donor fluorescent quantum yield (Φ_D), the normalized donor fluorescence spectrum (F_D), the acceptor molar absorption spectrum (ε_A), and the wavelength (λ).

$$R_0^{\,6} = 8.785 \times 10^{-5} \frac{\kappa^2}{n^4} \Phi_D \int F_D(\lambda) \varepsilon_A(\lambda) \lambda^4 d\lambda \qquad (1)$$

Currently, we have been using tryptophan and 3-nitrotyrosine as our fluorescent donor and energy acceptor (D-A), respectively, to characterize the

monomeric structure of α-syn.[2] However, the Förster distance between tryptophan and 3-nitrotyrosine may be too short to measure the distances for aggregation studies.[11] Therefore, there is a need to develop a fluorescent label with a higher quantum yield. The biexponential fluorescence decay of tryptophan[12] also complicates data interpretation. Therefore, this chapter describes the development of FET labels with a single exponential decay.

It is also particularly important that the fluorescent label is small enough to not interfere with the native protein structure, and also allow for the maximal rotational freedom of the attached probes.[1] Other requirements of FET labels for protein folding studies include a site-specific labeling reaction and an easy purification protocol for the labeled protein.

In addition, a new energy acceptor was also developed. An iodine is engineered in the label to undergo S_N2 reaction with the sulfhydryl group in the cysteine. Cyt *c*, a well-studied protein with a native cysteine residue, was successfully labeled with the new dyes to prove that they are promising probes for FET studies.

In studying α-synuclein aggregation, an α-synuclein mutant was used to illustrate that it is feasible to label protein with the new energy acceptor. Furthermore, a double cysteine mutant was expressed to investigate whether it is possible to selectively label α-synuclein at two separate sites, one with a fluorescent donor and one with an energy acceptor. This chapter reports the synthesis and spectroscopic characterization of new fluorescent labels and energy acceptor, along with their model compounds (**Figure 6.1**).

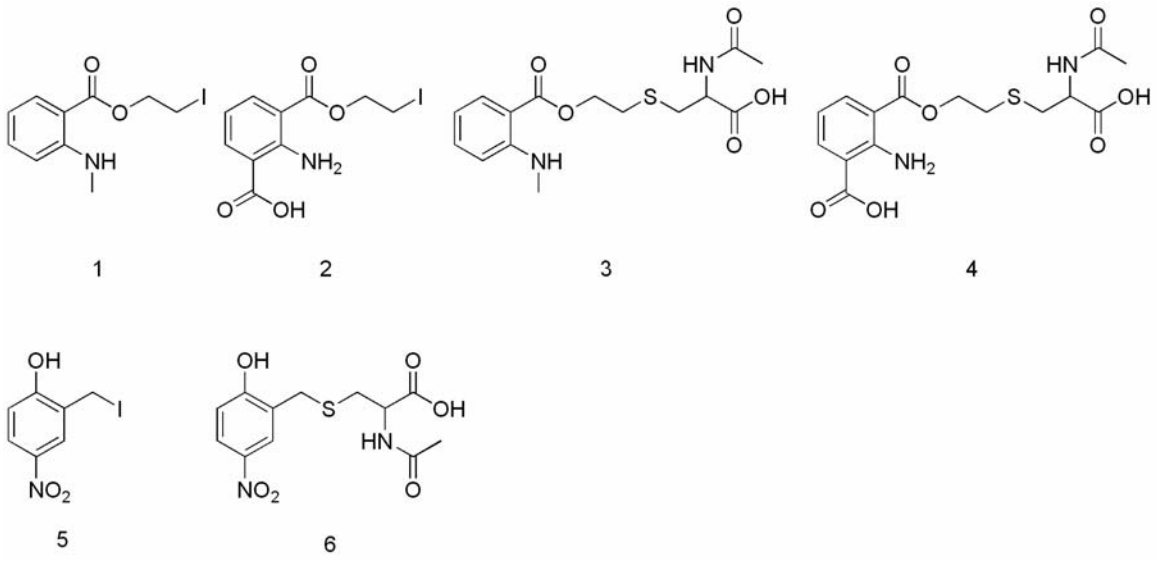

Figure 6.1. Chemical structures of fluorescent labels and their model complexes: I-SHark **(1)**, phI-SHark **(2)**, I-SHark model complex **(3)**, phI-SHark model complex **(4)**, nitrophenol **(5)**, and nitrophenol model complex **(6)**

6.3 MATERIALS AND METHODS

Materials.

Unless specified otherwise, all the reagents and solvents were purchased from Sigma and VWR, respectively. Thin Layer Chromatography (TLC) was carried out on silica gel plates (Merck 60-F254). The compounds were visualized using UV light (254 nm and 365 nm). Flash chromatography was carried out using silica gel 60 (EMD Chemicals, 40-63 μm). ^{1}H- and ^{13}C-NMR spectra were collected in CD_3OD with a Varian Inova 300 MHz spectrometer. Mass analyses were conducted by a ThermoQuest LCQ ion trap mass spectrometer by the California Institute of Technology Protein/Peptide Microanalytical Laboratory. All elemental analyses were carried out by Desert Analytics, Inc. (Tucson, AZ).

Synthesis of I-SHark (1) [2-iodoethyl 2-(methylamino)benzoate].

2-(methylamino)-benzoic acid was first recrystallized from CH_2Cl_2. The recrystallized 2-(methylamino)-benzoic acid (2.55 g, 16.9 mmol), 4-dimethylaminopyridine (DMAP, 320 mg, 2.62 mmol), and 2-iodoethanol (8.56 g, 49.8 mmol) were dissolved in dry CH_2Cl_2 (30 mL). To this mixture, a solution of dicyclohexylcarbodiimide (DCC, 3.80 g, 18.4 mmol) in dry CH_2Cl_2 (10 mL) was added dropwise. The mixture was stirred under Ar at room temperature for 5 h. The solution was filtered through celite, washed with CH_2Cl_2, dried over Na_2SO_4, and concentrated under vacuum. The concentrated solution was purified under flash column chromatography (hexanes/ethyl acetate 10:1). The purified green oil was

then acidified with concentrated HCl. The chloride salt was crystallized from methanol/ether. Yield: 1.56 g, 30%. R_f = 0.62 (hexanes/ethyl acetate 10:1). ^{1}H NMR (300 MHz, CD_3OD): δ 8.17 (1H, dd, J = 8.1, 1.2 Hz), 7.70 (1H, dt, J = 8.4, 1.5 Hz), 7.28-7.34 (2H, m), 4.61 (2H, t, J = 6.6 Hz), 3.54 (2H, t, J = 6.6 Hz), 3.07 (3H, s). ^{13}C NMR (300 MHz, CD_3OD): -0.8, 35.5, 66.1, 119.9, 121.6, 127.2, 132.2, 135.4, 140.7, 165.5. ESI-MS *m/z* 306 (M + 1). Anal. Calcd. for $C_{13}ClH_{13}INO_2$: C, 35.16; Cl, 10.38; H, 3.84; I, 37.15; N, 4.10; O, 9.37. Found: C, 35.23; H, 3.88; I, 37.61; N, 4.11.

Synthesis of phI-SHark (2) [2-amino-3-[(2-iodoethoxy)carbonyl]benzoic acid].

DMAP (27 mg, 0.2 mmol) and 2-iodoethanol (781 mg, 4.45 mmol) were added to a stirring solution of 2-aminoisophthalic acid (274 mg, 1.50 mmol) in THF (20 ml). A solution of DCC (340 mg, 1.65 mmol) was then added dropwise. After stirring for 4 h at room temperature, the mixture was dried under vacuum. The residue was redissolved in diethyl ether and extracted with 5% aqueous $NaHCO_3$ (3 × 30 mL). The aqueous layers were combined and acidified with 6M HCl to pH 5–6 and then extracted with ethyl acetate (3 × 30 mL). Further acidification of the aqueous layer to pH < 4 permitted recovery of the starting material, 2-aminoisophthalic acid. The organic phases were combined and dried over $MgSO_4$, filtered, and concentrated under reduced pressure to yield a pale yellow solid. The crude product was purified by chromatography (diethyl ether/hexanes 3:1), dissolved again in methanol by adding 6M NH_4OH, and crystallized from methanol/dichloromethane. Yield: 48 mg, 14%. R_f = 0.56 (ethyl acetate/hexanes/acetic acid 3:1:0.01). ^{1}H NMR (300 MHz, CD_3OD): δ 8.05 (1H, dd,

J = 7.5, 1.8 Hz), 7.96 (1H, dd, J = 7.8, 1.8 Hz), 6.50 (1H, t, J = 7.8 Hz), 4.49 (2H, t, J = 6.6 Hz), 3.48 (2H, t, J = 6.6 Hz). ^{13}C NMR (300 MHz, CD_3OD): -0.2, 64.8, 111.0, 112.1, 113.4, 137.2, 138.1, 149.1, 167.1, 176.9. ESI-MS *m/z* 334 (M – 1). Anal. Calcd. for $C_{10}H_9INNaO_4$: C, 33.64; H, 2.54; I, 35.54; N, 3.92; Na, 6.44; O, 17.92. Found: C, 33.58; H, 2.72; I, 34.97; N, 3.86.

Synthesis of I-SHark Model Compound (3) [2-(acetylamino)-3-[(2-[[2-(methylamino)benzoyl]oxyethyl)thio]propanoic acid].

To a stirring solution of **1** (305 mg, 1.00 mmol) and N-acetyl-cysteine (326 mg, 2.00 mmol) in dry DMF (20 ml), 1,8-Diazabicyclo[5.4.0]undec-7-ene (DBU, 608 mg, 4.00 mmol) in DMF was added dropwise. The mixture was stirred under Ar for 1 h. The solution was reduced to dryness under vacuum and redissolved in 1M HCl. The solution was then extracted with ethyl acetate (3 × 30 mL). The organic layers were reduced to dryness under vacuum and redissolved in methanol. After adding 10 µl of 30% NH_4OH solution, the product was crystallized from methanol/ether. Yield: 92 mg, 27%. R_f = 0.46 (dichloromethane/methanol/acetic acid 4:1:0.1); ^{1}H NMR (300 MHz, CD_3OD): δ 7.87 (1H, dd, J = 8.1, 1.8 Hz), 7.36 (1H, dt, J = 8.4, 1.8 Hz), 6.70 (1H, d, J = 8.4 Hz), 6.56 (1H, dt, J = 8.4, 1.2 Hz), 4.47 (1H, dd, J = 7.2, 4.2 Hz), 4.37 (2H, t, J = 6.6 Hz), 3.15 (1H, dd, J = 13.8, 4.5 Hz), 2.89-2.98 (6H, m), 1.99 (3H, s). ^{13}C NMR (300 MHz, CD_3OD): 21.6, 28.4, 30.7, 34.9, 54.5, 63.1, 109.7, 110.6, 114.2, 118.1, 131.5, 134.6, 152.2, 171.6, 175.8. ESI-MS *m/z* 363 (M + Na). Anal. Calcd. for $C_{15}H_{23}N_3O_5S$: C, 50.41; H, 6.49; N, 11.76; O, 22.38; S, 8.97. Found: C, 49.61; H, 6.24; N, 11.49; S, 8.37.

Synthesis of phI-SHark Model Compound (4) [3-[(2-[[2-(acetylamino)-2-carboxyethyl]thio]ethoxy)carbonyl]-2-aminobenzoic acid].

To a stirring solution of **2** (108 mg, 0.3 mmol) in dry DMF (6 ml), DBU (182 mg, 1.2 mmol) and N-acetyl-cysteine (98 mg, 0.6 mmol) were added. After stirring for 18 h under Ar at room temperature, the mixture was concentrated under reduced pressure and redissolved in water. The solution was acidified with 37% HCl (100 µl) and extracted with ethyl acetate (3 × 30 mL). The organic extracts were washed with water and dried with $MgSO_4$. The solution was dried under reduced pressure and redissolved in methanol. After adding 30% NH_4OH (20 µl), the product was crystallized by methanol/ethyl ether. Yield: 32 mg, 32%. R_f = 0.66 (dichloromethane/methanol/acetic acid 4:1:0.1). ^{1}H NMR (300 MHz, CD_3OD): δ 8.10 (1H, dd, *J* = 6.6, 1.8 Hz), 8.07 (1H, dd, *J* = 6.6, 1.8 Hz), 6.57 (1H, t, *J* = 7.8 Hz), 4.51 (1H, dd, *J* = 7.8, 4.5 Hz), 4.42 (2H, t, *J* = 6.6 Hz), 3.16 (1H, dd, *J* = 13.8, 4.5 Hz), 2.90-2.97 (3H, m), 2.00 (3H, s). ESI-MS *m/e* 393 (*M* + Na). Anal. Calcd. for $C_{15}H_{17}N_2O_7S$: C, 46.51; H, 5.46; N, 10.85; O, 28.91; S, 8.28. Found: C, 45.51; H, 5.40; N, 9.55; S, 8.31.

Synthesis of Nitrophenol (5).

Sodium iodide (660 mg, 4.4 mmol) was dissolved in minimal amount of dry acetone. Under Ar, 2-hydroxy-5-nitrobenzyl bromide (1.031g, 4 mmol) was dissolved in minimal amount of dry acetone in a 100 mL round bottom flask. The sodium iodide solution was then added dropwise into the round bottom flask. The mixture was stirred under Ar for 30 min. Dichloromethane (30 mL) was added to the

reaction mixture. The mixture was then filtered and concentrated to dryness. The dried solid was redissolved in minimal amount of benzene for recrystallization. After recrystallization was completed, the solution was filtered and dried, yielding brown crystals. Yield: 0.935 g (87%) ^{1}H-NMR (d_4-CH_3OH), δ: 8.221 (d, 1H, J = 3.0 Hz), 8.029 (dd, 1H, J = 8.8 Hz, 3.0 Hz), 6.872 (d, 1H, J = 9.0 Hz), 4.528 (m, 2H).

Synthesis of Nitrophenol Model Complex (6).

Nitrophenol (861 mg, 3.08 mmol) and N-acetyl-L-cysteine (1 g, 6.16 mmol) were dissolved in minimal amount of anhydrous DMF. A solution of DBU (1.88 g, 0.0123 mmol) in anhydrous DMF was added dropwise into the stirring solution of starting material under Ar. The reaction was allowed to proceed for 2 hr. The DMF was then concentrated under reduced pressure to yield a brown oil. 5 mL of ethyl acetate was added and the solution was then acidified with concentrated HCl until the brown oil was dissolved. The solution was extracted with water (2 × 30 mL). The aqueous layer was extracted with ethyl acetate (3 × 30 mL). The combined organic extracts were dried with $MgSO_4$. The dried solution was concentrated to 2 mL under reduced pressure and a white precipitate was observed. NH_3OH was added to redissolve the white precipitate and a yellow oil was yielded. The oil was dried and ammonia was removed under reduced pressure. Methanol (5 mL) was added to redissolve the oil and ethyl acetate was added to recrystallize the product. ^{1}H-NMR (d_4-CH_3OH), δ: 8.221 (d, 1H, J = 3.0 Hz), 8.029 (dd, 1H, J = 8.8 Hz, 3.0 Hz), 6.872 (d, 1H, J = 9.0 Hz), 4.528 (m, 2H). ESI-MS *m/e* 293 (*M* + Na).

Purification of Cyt c.

Commerically available cyt *c* was dissolved in 20 mM NaP_i (pH 7.0) buffer. The 100 μM cyt *c* solution was treated with 1 mM $Na_2S_2O_4$ and 1 mM DTT. Protein was then purified by ion-exchange chromatography using a Mono S column on a Fast Protein Liquid Chromatography (FPLC) system (Pharmacia). The column was equilibrated with 20 mM NaP_i buffer (pH 7.0) and the protein was eluted using a stepwise salt gradient (0–1 M NaCl), with both buffers containing 1 mM dithiothreitol (DTT). Pure fractions were then combined and concentrated to 50–100 μM. Purity of protein was confirmed using absorption and electrospray mass spectrometry.

Purification of α-Synuclein.

A single cysteine mutant, V40C, was expressed to develop the labeling protocol for nitrophenol on α-synuclein. For the double labeling studies, a double cysteine mutant, V26C/E57C, was selected. The purification protocol for α-synuclein from other chapters, with the addition of 1 mM DTT, was adopted to purify the protein. The purity of the mutant was proved by UV-Vis, SDS-PAGE and mass spectrometry.

Fluorescent Dye Labeling Procedures.

Purified cyt *c* (50–100 μM in NaP_i, pH 7.0) was exchanged into 20 mM NaPi (pH 7.6) buffer. It was then denatured with 4 M guanidinium chloride (GuHCl) and reduced by the same concentration of Tris(2-carboxy-ethyl)phosphine hydrochloride

(TCEP). The reaction mixture was deoxygenated by repeated evacuation/Ar-fill cycles on a Schlenk line for 30 min. phI-SHark (twentyfold molar excess) was dissolved in the same buffer (1 ml) and added dropwise to the stirring solution of the protein. The reaction was performed in the dark to minimize deleterious photochemical side reactions. The procedures for I-SHark labelling were slightly modified. Twentyfold molar excess of I-SHark was dissolved in 10% DMSO. The concentrated dye solution was added in two portions (at beginning of the reaction and after 12 h) in order to enhance the solubility of the dye.

The labelling reaction was stirred at room temperature for 40 h. Prior to purification, the solution was centrifuged at 10000 × *g* for 30 min to remove the insoluble dye. The protein was then oxidized with a tenfold excess of $K_3[Fe(CN)_6]$ for 30 min. The reaction mixture was desalted on a gel filtration column (HiPrep Desalting 26/10) using FPLC run in 20 mM NaP_i (pH 7.0). Dye-labeled protein was separated by ion-exchange chromatography (Mono S column) using a shallow stepwise salt gradient (0–1 M NaCl) in 20 mM NaP_i (pH 7.0). All the dye-labeled proteins were stored in the dark at 4 °C.

The labeling reaction was proven successful by UV-Vis spectroscopy, ESI-MS and SDS-PAGE. Trypsin digestion was also performed with the labeled protein by the California Institute of Technology Protein/Peptide Microanalytical Laboratory. The peptide fragments were then analyzed by MALDI-MS. The results demonstrate that the dye was correctly labeled onto the desired cysteine residue.

Energy Acceptor Labeling Procedures.

Concentrated α-synuclein mutant V40C (~100 μM) was stirred in the dark with a twentyfold molar excess of TCEP for 30 min. A twentyfold excess of nitrophenol was then added to the stirring protein. The reaction was stopped by applying the reaction mixture to the gel filtration column (HiPrep 26/10) on FPLC. The desalted protein solution was then purified by ion-exchange chromatography (Mono Q). The purity of the labelled protein was confirmed by UV-Vis and ESI-MS.

Double Cysteine Labeling Procedures.

In the dark, a twentyfold molar excess TCEP was stirred with concentrated α-synuclein mutant V26C/E57C (~ 100 μM) for 30 min. A tenfold molar excess of 1,5-I-AEDANS was then added to the stirring protein. The reaction was stopped by applying the reaction mixture to the gel filtration column (HiPrep 26/10) on FPLC. The desalted protein solution was then purified by ion-exchange chromatography (Mono Q). The singly labelled protein was characterized by UV-Vis and ESI-MS. It was then concentrated and labelled with nitrophenol using the same protocol as above.

Steady-State Spectroscopy.

Spectroscopic measurements for folded protein were recorded at room temperature with samples dissolved in phosphate buffer (20 mM NaP_i, pH 7.4), while 6 M guanidinium chloride (GuHCl) was added for the unfolded samples. Samples were deoxygenated by repeated evacuation/Ar-fill cycles during a period of 30 min

and sealed in fused-silica fluorescence cuvettes (1 cm × 1 cm). Absorption and luminescence spectra were measured on a Hewlett-Packard 8452 diode array spectrophotometer and a Spex Fluorolog2 spectrofluorimeter, respectively.

Evaluation of the Förster distance.

The value of overlap integral (*J*, **Equation 2**) for the donor-acceptor pairs (I-SHark/heme and phI-SHark/heme) was determined using the absorption spectrum for cyt *c* and normalized emission spectra of compounds **3** and **4**. The solution refractive index (*n*) was taken to be 1.34,[13] while the orientation factor (κ^2) was averaged to be 2/3 for the random dynamic orientation of the donor and acceptor.

$$J = \int F_D(\lambda)\varepsilon_A(\lambda)\lambda^4 d\lambda \qquad (2)$$

Time-Resolved Fluorescence Spectroscopy.

Samples for time-resolved fluorescence spectroscopy measurements were prepared as described above. Samples were excited by a 355 nm polarized pulse (35° from vertical) generated from a mode-locked Nd:YAG laser regenerative amplifier. Emission above 420 nm was selected by cutoff filters. Decay kinetics were measured with a picosecond streak camera (Hamamatsu C5680) in single photon counting mode. All experiments were controlled by a temperature-controlled cuvette holder at 25 °C. Control experiments were conducted using the model complexes **3** and **4**.

Data Analysis.

The measured fluorescence decay kinetics by non negative linear least-squares (NNLS) protocol, and were thoroughly described in Chapter 1.[14]

6.4 RESULTS AND DISCUSSION

Dye Synthesis.

The new labels and their corresponding model compounds (cysteinic conjugates) were successfully synthesized by one-step reactions. The products were easily purified by either flash column chromatography or recrystallization.

When designing the structure of new FET labels, minimal perturbation of the native protein structure and high rotational freedom of the dyes were considered. Therefore, I-Shark, phI-SHark and nitrophenol were designed to cause minimal steric hindrance. Iodoacetamide is frequently used as the reactive site for cysteine labeling. However, iodine was chosen instead in designing these labels to provide higher conformational freedom. The fluorophore conformational freedom was further enhanced by the ethylenic chain linking the cysteine and fluorophore.

Protein Labeling.

The functionalization of cyt *c* involves a linker between the fluorescent probe and Cys102 of the protein. However, the thiol of Cys102 is not solvent-exposed enough to react with the labels. Therefore, the protein was unfolded by GuHCl to encourage protein derivatization. TCEP was also added to avoid the oxidation of

sulphur groups. The reaction was carried out at a pH = 7.6 to where the thiol group was partially deprotonated, while the amine side chain of lysine, which is a main reactive agonist of cysteine, was almost fully protonated. The duration of protein labeling was optimized at 40 h, as protein denaturation and the oxidation of thiolic groups reduce labeling yields at longer reaction times.

Labeling α-synuclein has proven to be much easier as the protein is unstructured. Only 3 h of reaction was needed to yield labeled protein. After successfully labeling α-synuclein at one site, double cysteine labeling was attempted to investigate the possibility of tagging a fluorescent donor and an energy acceptor onto the same protein molecule. The dually labeled protein could be used to extract long-range intramolecular distances. The two cysteine labeling dyes chosen for this experiment were dansyl (Dns) and nitrophenol (NP). Dns and NP were chosen as robust cysteine labeling protocols have been developed previously.

Figure 6.2 shows the FPLC traces during the protein purification process after dansyl labeling was completed. Proteins from both peaks were submitted for UV-Vis and mass spectrometry analysis. The first peak was identified as the singly dansyl-labeled protein, while both cysteine sites were labeled by dansyl in the second peak. Protein fractions from the first peak were subjected to nitrophenol labeling.

Figure 6.3 shows the FPLC traces after nitrophenol labeling. Two peaks were again identified. Mass spectrometry and UV-Vis have confirmed that proteins from both peaks were labeled with dansyl and nitrophenol. It will require mass spectrometry on the tryptic digest product of those fractions to see which one contains V26C-Dns/E57C-NP and V26C-NP/E57C-Dns.

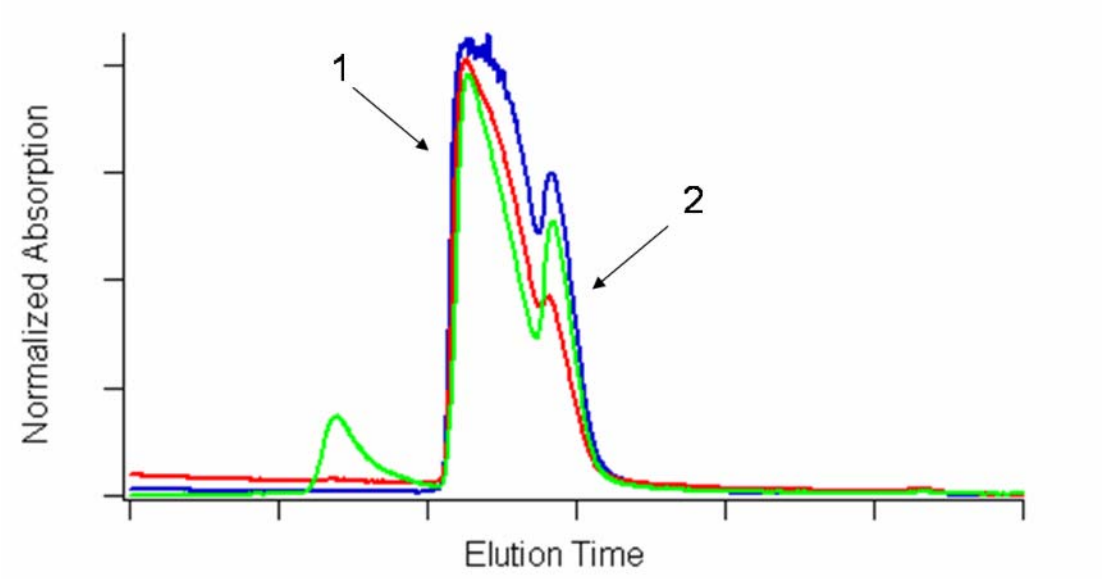

Figure 6.2. The FPLC traces during the protein purification process after dansyl labeling was completed. Peak (1) was identified as the singly dansyl-labeled protein, while both cysteine sites were labeled by dansyl in the second peak. Absorptions were monitored at 215 nm (blue), 280 nm (red), and 355 nm (green).

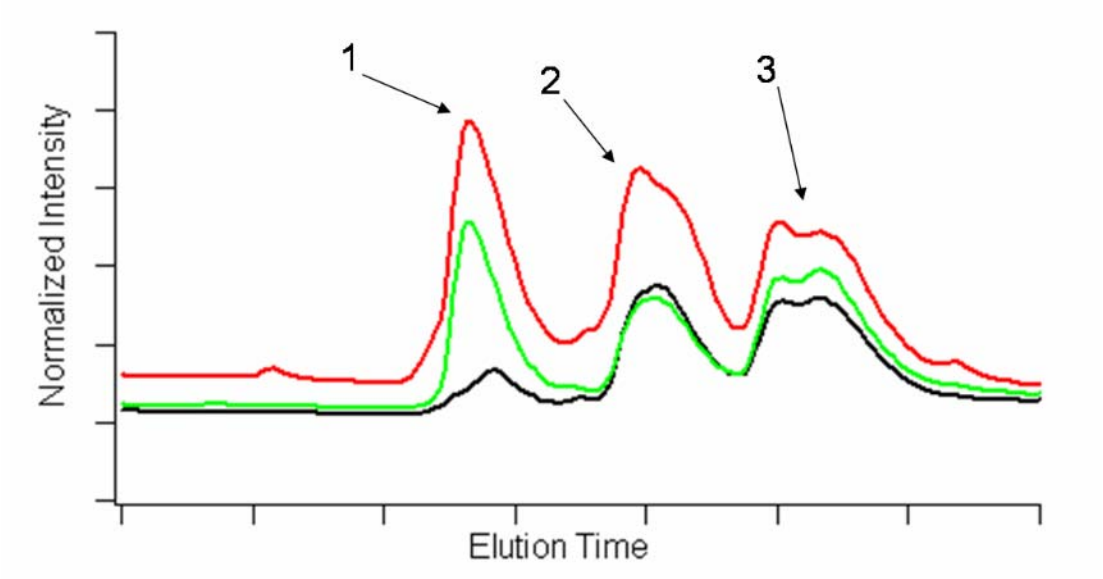

Figure 6.3. The FPLC traces after nitrophenol labeling, with absorption detected at 280 nm (red), 355 nm (green), and 400 nm (black). Peak (1) corresponds to protein that was not labeled with nitrophenol. Peak (2) and Peak (3) highlighted could be V26C-Dns/E57C-NP and V26C-NP/E57C-Dns.

Spectroscopic Characterization.

Previously, the fluorescent quantum yields of the labels, calculated overlap integral, and Förster distances between I-SHark/phI-SHark and cyt *c* heme group have been determined (**Table 6.1**). The overlap between the absorption of cyt *c* and phI-SHark is better than that of cyt *c* and I-SHark (**Figure 6.4**). It is also demonstrated that the fluorescence of phI-SHark has a higher quantum yield and longer Förster distance with cyt *c* than I-SHark. Another distinct disadvantage of I-SHark is its poor water solubility. DMSO was added to enhance dye solubility in the labeling reaction. However, the amount of DMSO added (10% v/v) was limited to avoid protein precipitation. On the contrary, the second carboxylic acid group makes phI-SHark more soluble than I-SHark in the aqueous labelling environment. Since phI-SHark has been shown to be a better label, our following discussion will be focused on the spectroscopic characterization of phI-SHark.

The phI-SHark-labeled cyt *c* was characterized spectroscopically in its native and denatured conformation to illustrate the ability of the label to provide distance information. When the protein is folded, the distance between Cys102 to the iron heme center is 13.9 Å. Therefore, when the protein is folded, the fluorescence emitted by the label should be quenched by the heme group.

On the other hand, when the protein is unfolded, the distance between the heme group and fluorophore should be too large for the quenching to be effective. In fact, steady-state fluorescence spectra show a significantly reduced emission for the folded protein compared to the unfolded protein (**Figure 6.5**). FET kinetics (**Figure 6.6**) also show a much faster decay for the folded protein (6×10^{-9} s^{-1}, 80%), when

	Quantum Yield	Förster Distance (Å)	Overlap Integral (M^{-1} cm^{-1} nm^4)
I-Shark	0.32	50	$8.7x10^{14}$
phI-SHark	0.48	60	$8.1x10^{15}$

Table 6.1. Fluorescent quantum yields of I-SHark and phI-SHark, calculated overlap integral and Förster distances between I-SHark/phI-SHark and heme group

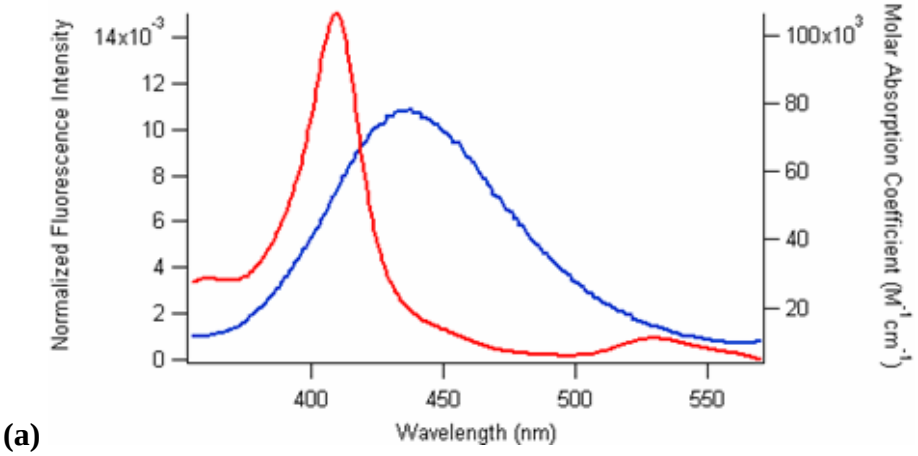

(a)

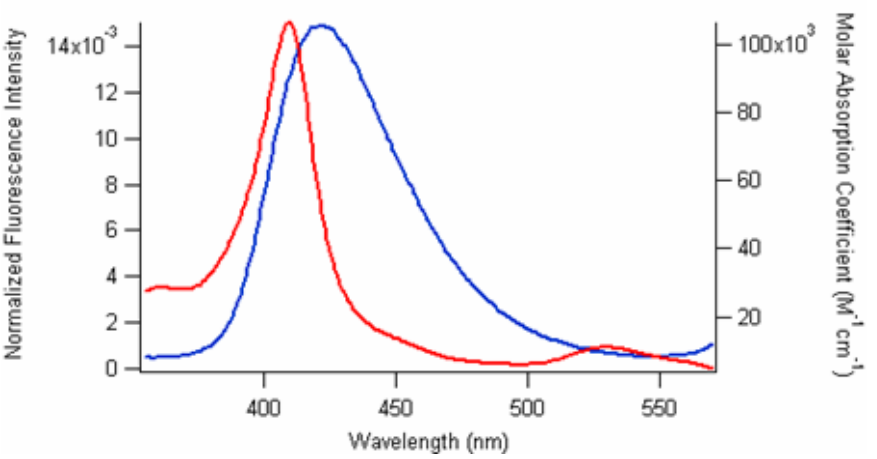

(b)

Figure 6.4. Molar absorption spectra of cyt c (red line), and fluorescence spectra (blue line) of **(a)** I-SHark and **(b)** phI-SHark

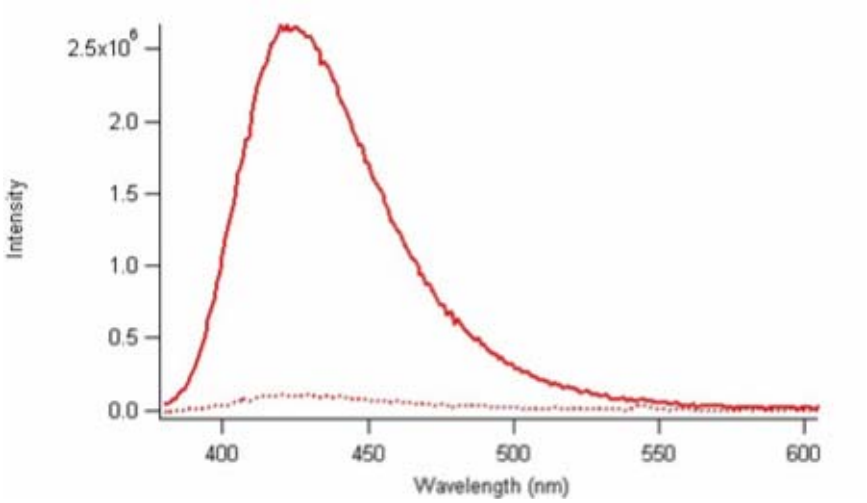

Figure 6.5. Steady-state fluorescence spectra for 5 μM phI-SHark labeled cyt *c* in 20 mM NaP_i (dotted line) and 6 M GuHCl (solid line), pH 7.4 at 25 °C

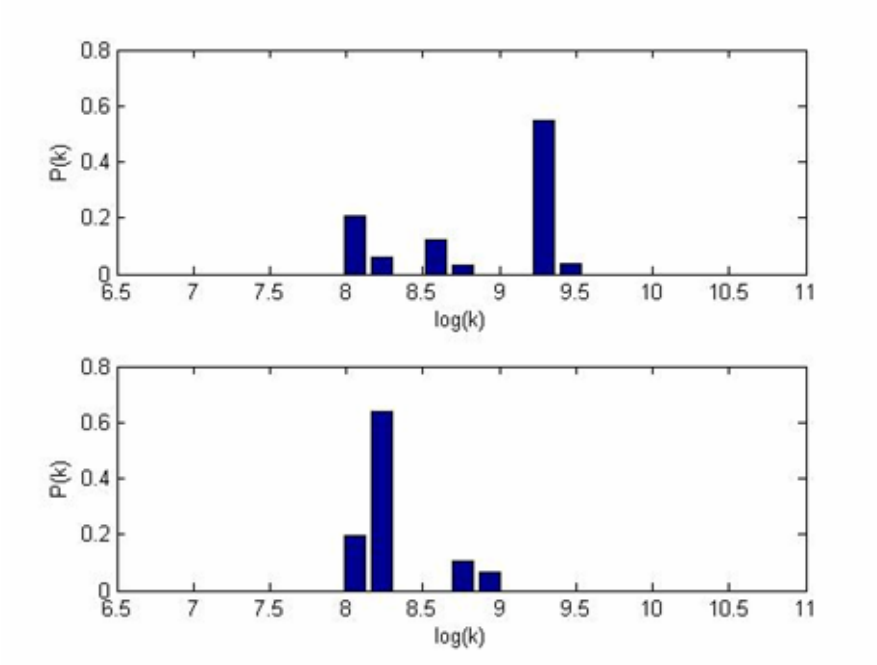

Figure 6.6. Distribution of fluorescence decay rates, *P(k)*, for 5 μM phI-SHark labeled cyt *c* in 20 mM NaP_i (top panel) and 6 M GuHCl (bottom panel) at pH 7.4 and 25°C, from NNLS analyses of the FET kinetics

compared to the unfolded protein (8×10^{-9} s^{-1}, 30%, 5×10^{-10} s^{-1}, 60%).

Control experiments using the phI-SHark model complex in NaP_i buffer and 6 M GuHCl were conducted. Comparable steady-state fluorescence emissions (**Figure 6.7**) and time-resolved lifetimes (**Figure 6.8**) show that phI-SHark behaves similarly in buffer (8×10^{-9} s^{-1}, 90%) and high concentration of GuHCl (7×10^{-9} s^{-1}, 90%). It can also be noted that the unquenched emission of phI-SHark is singly exponential.

Finally, phI-SHark and nitrophenol were developed as the fluorescent donor and energy acceptor for intermolecular FET studies during aggregation events. **Figure 6.9** shows the overlap between the fluorescence of phI-SHark (blue line) and absorption of nitrophenol (red line). The Förster distance was calculated to be 42 Å for this D-A pair, allowing us to measure distances between 13 and 65 Å.

In summary, two highly fluorescent dyes, I-SHark and phI-SHark, and an energy acceptor, nitrophenol, were synthesized and characterized. Spectroscopic characterization of phI-SHark-labeled cyt *c* shows that phI-SHark fulfills the requirements needed for an excellent label for FET studies. The overlap integral between phI-Shark and nitrophenol also allows for a large Förster distance which allows study of α-synuclein aggregation. Minimal steric hindrance, high rotational freedom, single exponential fluorescent lifetime, high quantum yield, ease of synthesis, and high solubility in water make phI-SHark-nitrophenol attractive as a fluorescent donor-energy acceptor pair to provide long-range distance information during protein folding events.

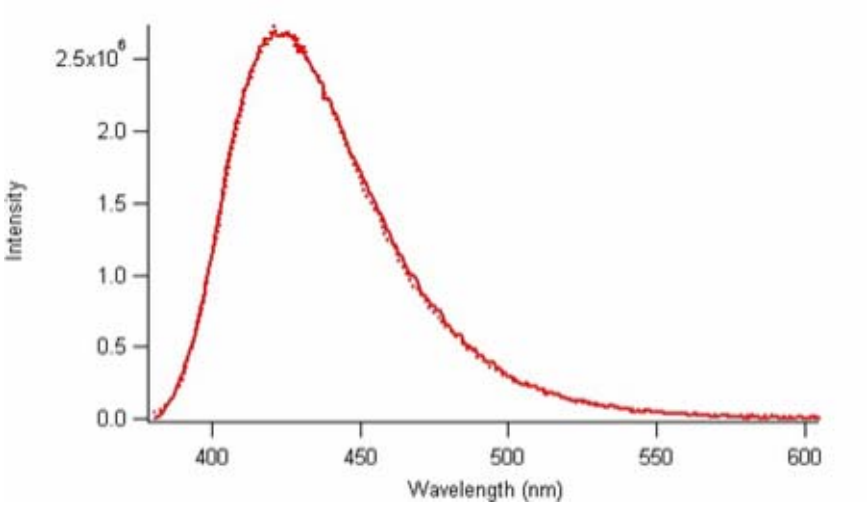

Figure 6.7. Steady-state fluorescence spectra for 5 μM phI-SHark model complex (**4**) in 20 mM NaP_i (dotted line) and 6 M GuHCl (solid line), pH 7.4 at 25 °C.

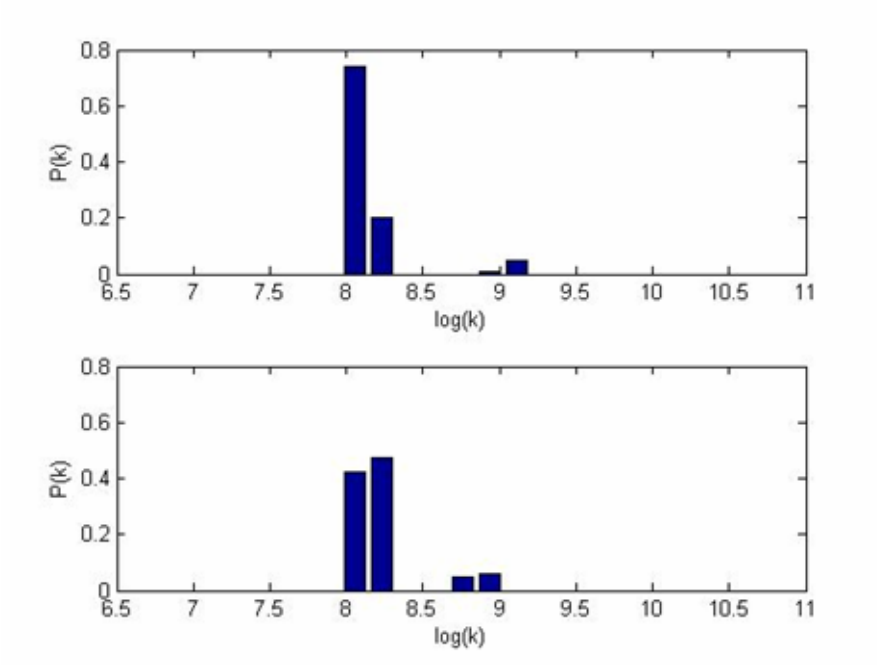

Figure 6.8. Distribution of fluorescence decay rates, *P(k)*, for 5 μM phI-SHark model complex (**4**) in 20 mM NaP_i (top panel) and 6 M GuHCl (bottom panel) at pH 7.4 and 25 °C, from NNLS analyses of the FET kinetics

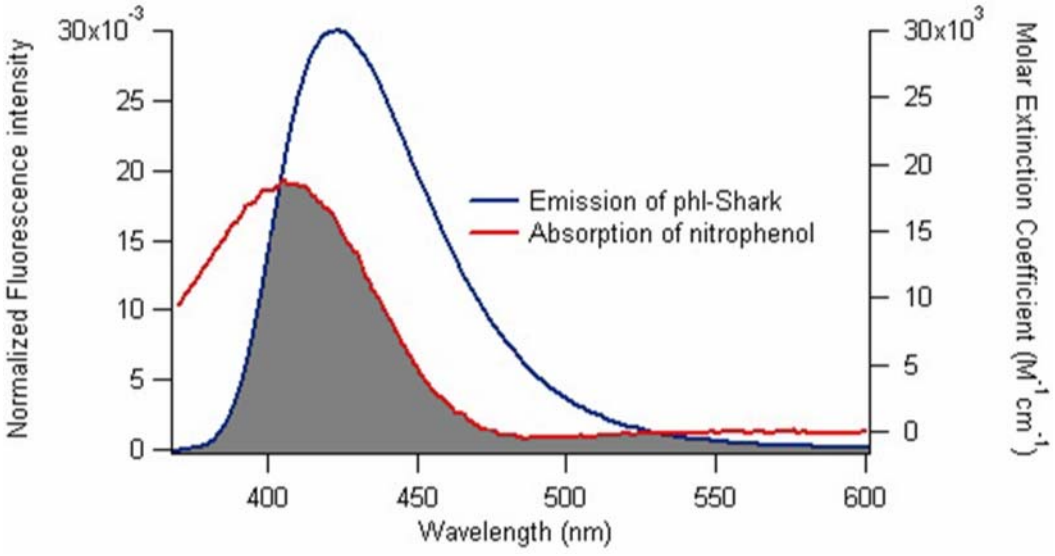

Figure 6.9. Molar absorption spectra of nitrophenol (red line), and fluorescence spectra (blue line) of phI-SHark

6.5 ACKNOWLEDGEMENT

Synthetic and labeling protocols for I-SHark and phI-SHark were developed by Dr. Seth B. Harkins, Dr. Francesco Bellia, and Dr. Jennifer C. Lee. This work was performed in collaboration with Mr. Dustin D. Hawker.

6.6 REFERENCES

(1) Duus, J. O. *J. Phys. Chem. B* **1998**, *102*, 6413–6418.
(2) Lee, J. C.; Langen, R.; Hummel, P. A.; Gray, H. B.; Winkler, J. R. *Proc. Natl. Acad. Sci. U. S. A.* **2004**, *101*, 16466–16471.
(3) Lyubovitsky, J. G.; Gray, H. B.; Winkler, J. R. *J. Am. Chem. Soc.* **2002**, *124*, 14840–14841.
(4) Lee, J. C.; Engman, K. C.; Tezcan, F. A.; Gray, H. B.; Winkler, J. R. *Proc. Natl. Acad. Sci. U. S. A.* **2002**, *99*, 14778–14782.
(5) Wu, P. G.; Brand, L. *Anal. Biochem.* **1994**, *218*, 1–13.
(6) Navon, A.; Ittah, V.; Landsman, P.; Scheraga, H. A.; Haas, E. *Biochemistry* **2001**, *40*, 105–118.
(7) Pletneva, E. V.; Gray, H. B.; Winkler, J. R. *J. Am. Chem. Soc.* **2005**, *127*, 15370–15371.
(8) Forster, T. *Ann. Phys.-Berlin* **1948**, *2*, 55–75.
(9) Phu, M. J.; Hawbecker, S. K.; Narayanaswami, V. *J. Neurosci. Res.* **2005**, *80*, 877–886.
(10) Winkler, G. R.; Harkins, S. B.; Lee, J. C.; Gray, H. B. *J. Phys. Chem. B* **2006**, *110*, 7058–7061.
(11) Callis, P. R. *J. Phys. Chem. B* **2004**, *108*, 4248–4259.
(12) Szabo, A. G.; Rayner, D. M. *J. Am. Chem. Soc.* **1980**, *102*, 554–563.
(13) Thormahlen, I. *J. Phys. Chem. Ref. Data* **1985**, *14*, 933–946.
(14) Lee, J. C.; Lai, B. T.; Kozak, J. J.; Gray, H. B.; Winkler, J. R. *J. Phys. Chem. B* **2007**, *111*, 2107–2112.

Chapter 7

α-Synuclein Intramolecular Aggregation Studies

7.1 ABSTRACT

Understanding the formation of α-syn protofibril can allow more profound discovery on the pathogenesis of Parkinson's Disease. An α-syn mutant, Y19/W39, was mixed with wild type and A30P α-syn. Aggregation was then induced at elevated temperature. The aim was to extract distance distributions of this fluorescent donor-acceptor pair during the aggregation event using fluorescence energy transfer. The effect of the point mutation A30P, which has been suggested in causing familial Parkinson's Disease, was also probed. Proteolysis of α-syn, possibly by the presence of bacteria, caused irreproducible aggregation, thus preventing extrapolation of D-A distances. Despite this, we have learned that the presence of A30P α-syn leads to a faster aggregation rate.

7.2 INTRODUCTION

Parkinson's Disease is characterized by the presence of Lewy bodies in the *substantia nigra* region in the brain.[1] A major component of the Lewy bodies is of α-syn.[2,3] Protofibrils have been known to be the toxic species that causes the aggregation event.[4-6] Therefore, in order to understand the pathogenesis of α-syn, it is crucial to provide thorough understanding on the structures of protofibrils. The goal of this study is to employ fluorescent energy transfer (FET) to study the change of distance distribution during the formation of these protofibrils. Trp is again utilized as the fluorescent donor and Tyr(NO_2) as an energy acceptor. Y19/W39 has been chosen as the donor-acceptor pair.

In this aggregation study, the D-A α-syn mutant was mixed with wild type and A30P mutant in a 1:15 ratio. The point mutation A30P was studied because it is one of the mutations linked to familial PD.[7,8] Other techniques, such as absorption, Trp fluorescence, thioflavin T (ThT) fluorescence, circular dichorism, and SDS-PAGE were also employed to monitor the progress of aggregation.

7.3 METHODS

Protein Preparation.

Any necessary mutations for α-syn were introduced through site-directed mutagenesis and confirmed with DNA sequencing. Proteins used for this study were expressed, purified, and nitrated according to protocols outlined in Chapter 1. The purified protein solutions were concentrated using Amicon YM-3 (molecular weight

cutoff 3 kD; Millipore) and stored at -80 °C until the day before the experiment. The protein solutions were then exchanged into filtered 100 mM NaP_i buffer (pH 7.4) using HiPrep Desalting 26/10 column by the FPLC. The protein solutions were then stored in the cold room (4 °C) until the experiment. The protein concentrations were then determined using UV-Vis. All the oligomeric materials were removed by filtration using YM-100 (molecular weight cutoff 100 kD; Millipore) prior to use.

Aggregation Experiment Setup.

16 × 125 mm (VWR) test tubes were utilized for the aggregation studies. Test tubes and magnetic stir bars were cleaned with freshly made *aqua regia*, and then washed thoroughly with Milli-Q water. The test tubes were subsequently dried under reduced pressure. Concentrated protein solutions were then added into these dried test tubes, along with a cleaned magnetic stir bar. All samples had a final protein concentration of 80 μM. For the Trp or Trp/Tyr(NO_2) mutants, each sample consisted of 5 μM of either the Y19/W39 or Y19/W39(NO_2). The rest of the proteins were furnished by WT or A30P. The test tubes were capped and incubated in a water bath shaker (New Brunswick Scientific) at 37 °C under 200 rpm.

Characterization of Aggregation Process.

Prior to withdrawing solutions from the aggregation samples, the test tubes were placed on the magnetic stir plate. The protein solutions were stirred gently for 5 min to allow even distribution of materials inside the test tubes. 200 μL aliquots of aggregation samples were withdrawn periodically for characterization.

Absorption of the protein solution was measured in a small-volume cuvette (200 μL) using a Hewlett-Packard 8452 diode array spectrophotometer. Trp fluorescence was measured following procedures outlined in Chapter 1. For ThT fluorescence studies, a 1 mM ThT stock was made. The ThT experimental sample consisted of 4 μL ThT stock, 20 μL protein solution, and 176 μL 100 mM NaP_i buffer. The absorption of this solution was measured. The steady-state fluorescence spectra between 420 nm and 680 nm (2 nm band pass, 0.5 s integration) were obtained by exciting the samples at 400 nm (1 nm band pass). An average of three scans for each sample was obtained to improve signal-to-noise ratio.

If aggregates were present, further studies were performed to investigate the soluble protein remaining in the sample. Turbidity of the samples can be characterized by the elevation of the baseline in the UV-Vis spectra. When that was observed, the samples were then spun at 16 100 × *g* for 1 hr. The supernatant solutions were removed and their absorption and fluorescent characteristics were then probed.

The protein solution was also subjected to CD analysis on Day 0 and 6, with experimental parameters outlined in Chapter 1. The original protein solutions and their supernatants were also studied under SDS-PAGE and size-exclusion chromatography on Day 6 and 9. The protein sample was applied to a Superdex 75/300 size exclusion column on a FPLC. The column was previously calibrated by a mixture of protein containing Bovine Serum Albumin, Ribonuclease A, Cytochrome *c*, and Aproprotein.

7.4 RESULTS AND DISCUSSIONS

UV-Vis.

The aggregation event was monitored by a variety of techniques. UV-Vis spectroscopy provides a good tool to determine the presence of aggregates. The formation of multimers can shift the baseline higher. From **Figure 7.1a**, it shows that the baseline was rather flat and uniform at the beginning of the aggregation experiment. However, by Day 3, **Figure 7.1b** demonstrates a wide range of baselines from all the samples, implying that different amount of aggregates were formed. It is also noticeable that the baselines for the same type of samples, such as WT + Y19(NO_2)/W39, also vary. Since it has been our assumption that introducing the Trp/Tyr(NO_2) mutants will not cause any changes in the aggregation event, all the WT containing solution should produce similar absorption at a certain time point. This is the first evidence that protein aggregation is not reproducible.

When aggregates were first obtained, protein solutions were centrifuged to obtain the supernatant. The resultant solutions were screened with UV-Vis and the concentrations were tracked throughout the time course of experiment. We expected that **Figure 7.2** would illustrate that supernatant concentration decreases as aggregation events increase over time. This result did not typically agree, hence implying that the protein aggregation events between samples are not reproducible. However, A30P containing samples have demonstrated a faster rate of aggregate formation. This could be evidence that the presence of the A30P mutation could potentially speed up aggregation.

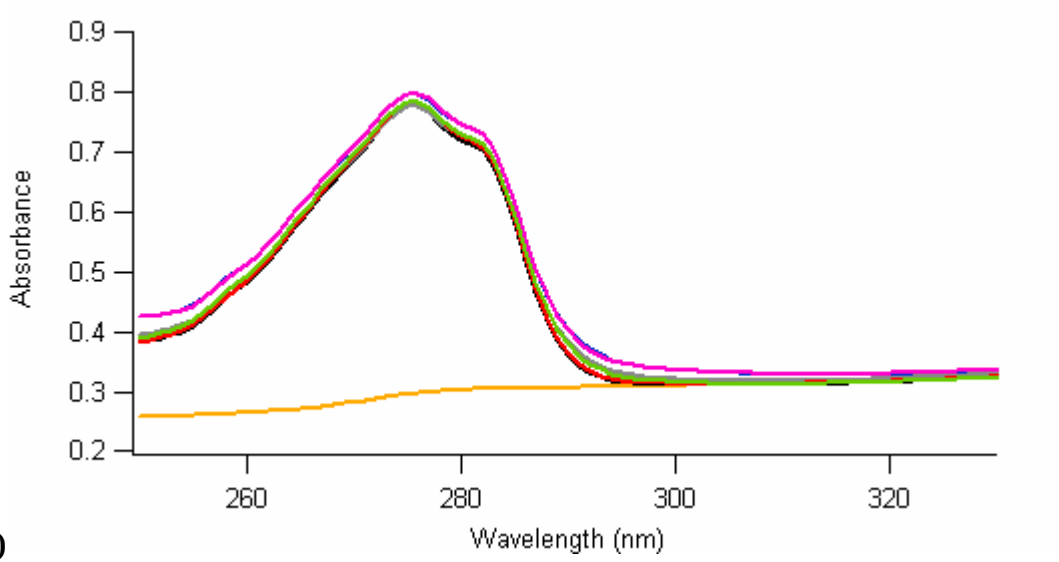

(a)

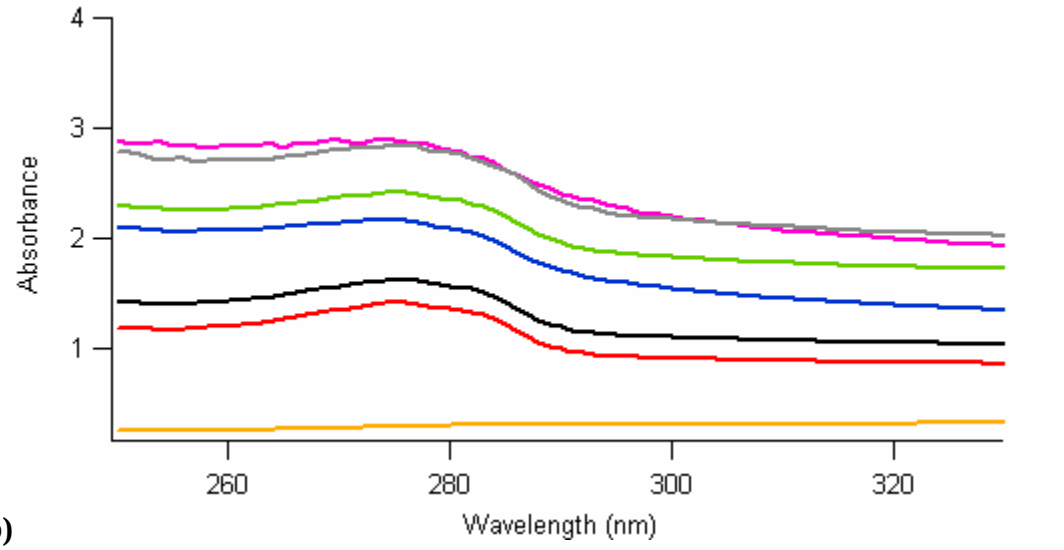

(b)

Figure 7.1. Absorption spectra of NaP_i buffer (orange), WT only (red), A30P only (black), WT + Y19/W39 (green), WT + Y19(NO_2)/W39 (blue or pink), and A30P + Y19/W39 (grey) at **(a)** Day 0 and **(b)** Day 3

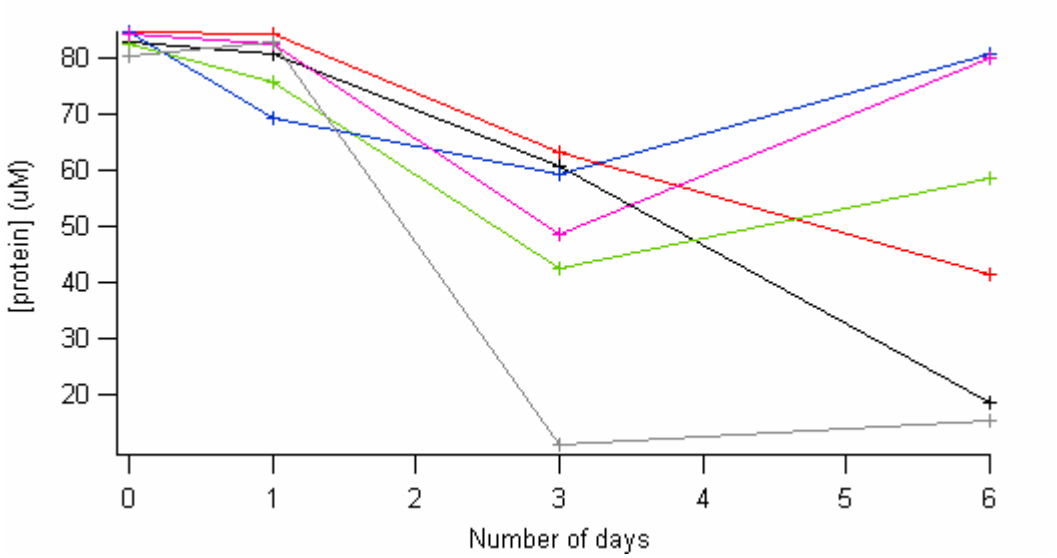

Figure 7.2. Supernatant protein concentration of WT only (red), A30P only (black), WT + Y19/W39 (green), WT + Y19(NO_2)/W39 (blue or pink), and A30P + Y19/W39 (grey) during the aggregation experiment, determined by UV-Vis spectroscopy

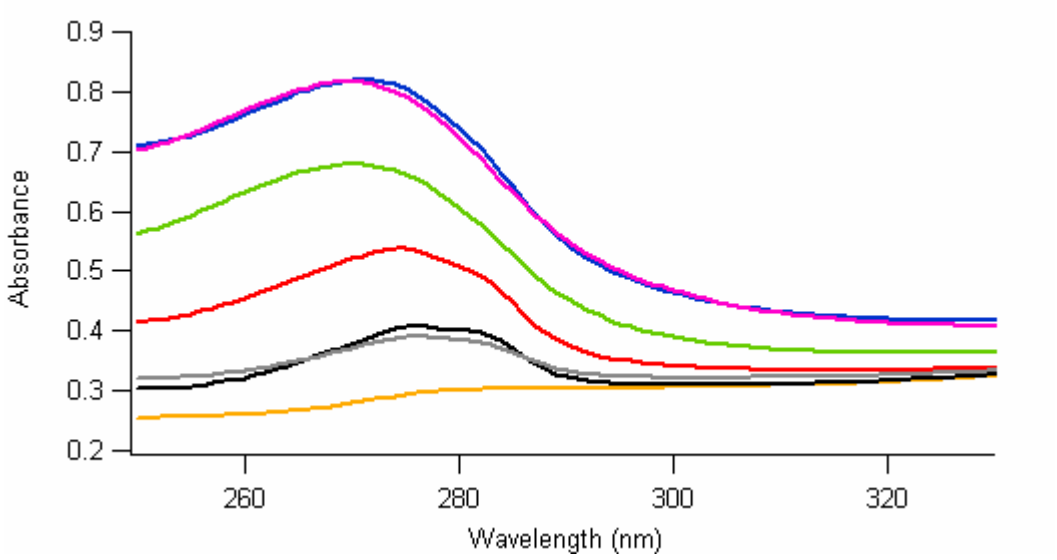

Figure 7.3. Absorption spectra for the supernatant of NaP_i buffer (orange), WT only (red), A30P only (black), WT + Y19/W39 (green), WT + Y19(NO_2)/W39 (blue or pink), and A30P + Y19/W39 (grey) at Day 6

Another interesting observation is that absorption traces between proteins in Day 0 (**Figure 7.1**) and the supernatants in Day 6 (**Figure 7.3**) are quite different. This could imply that protein materials in the supernatant in our experimental samples were altered during the aggregation event.

ThT Assay.

ThT is commonly known to bind to fibrils and exhibit birefringence.[9] Therefore, it is a common tool for characterizing the amount of fibrils during aggregation experiments.[10,11] **Figure 7.4a** illustrates that when ThT was mixed with monomeric α-syn, the emission was rather weak. After nine days of incubation, ThT emissions in all the samples became much more intense, by 10- to 40-fold (**Figure 7.4b**). This suggests that aggregates were developed during the incubation process.

However, the amount of ThT fluorescence within the WT-containing samples is not in agreement among each other. Similar phenomena have been observed for the A30P-containing samples, suggesting that the aggregation events studied here are not reproducible. This phenomenon can be further supported by **Figure 7.5**, where the normalized intensity has been plotted for individual samples to track the amount of aggregates formed over time. The rate of aggregation and the amount of aggregates formed are not uniform among samples.

As suggested by the results obtained by UV-Vis, A30P seems to form more aggregates at a faster rate. This can be confirmed with **Figure 7.4b**, as it displays that a higher ThT fluorescence was attained when A30P mutants were used. However, this faster aggregation rate cannot be conclusively verified by **Figure 7.5.**

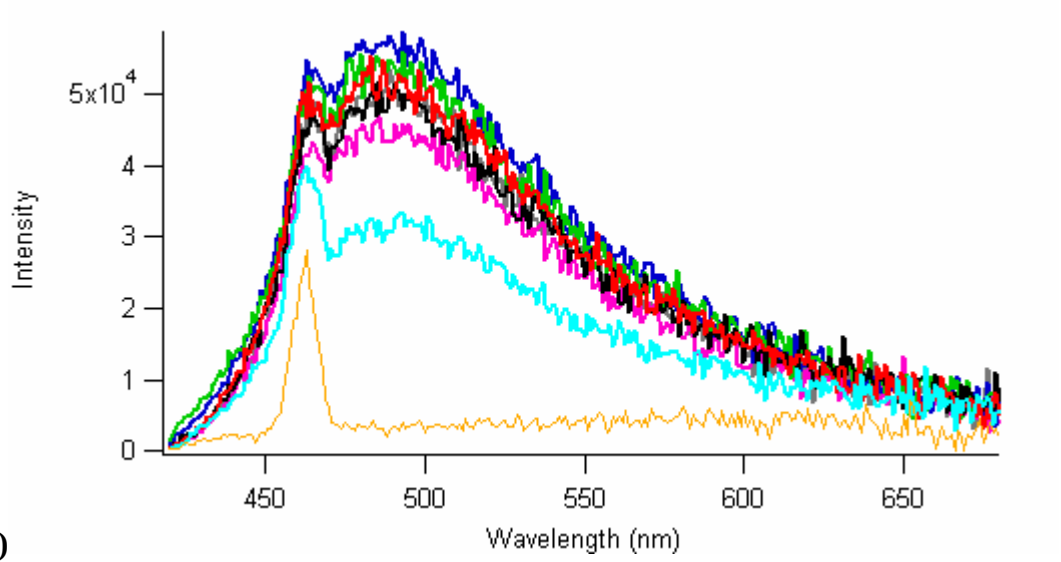

(a)

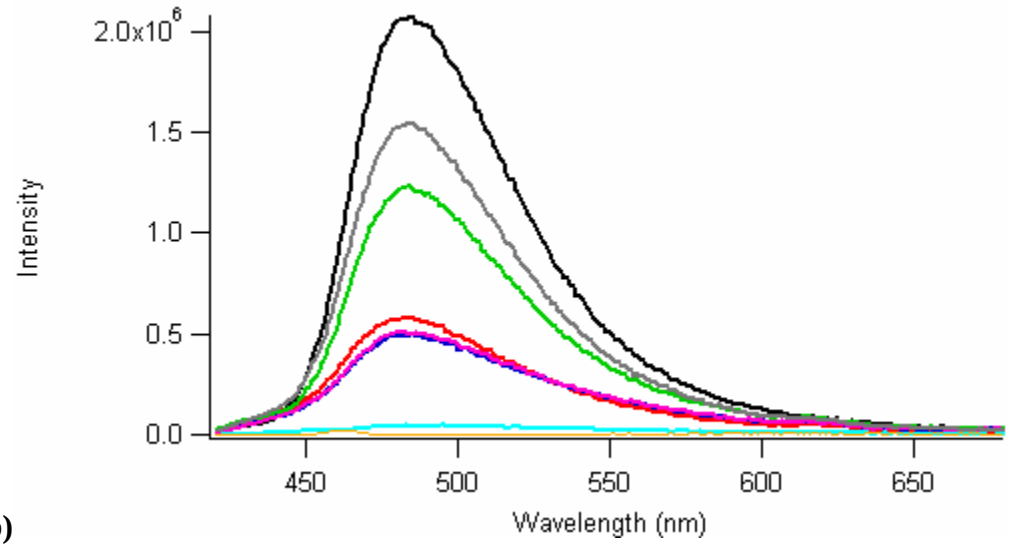

(b)

Figure 7.4. Thioflavin T fluorescence spectra of NaP_i buffer (orange), WT only (red), A30P only (black), WT + Y19/W39 (green), WT + Y19(NO_2)/W39 (blue or pink), and A30P + Y19/W39 (grey) at **(a)** Day 0 and **(b)** Day 9

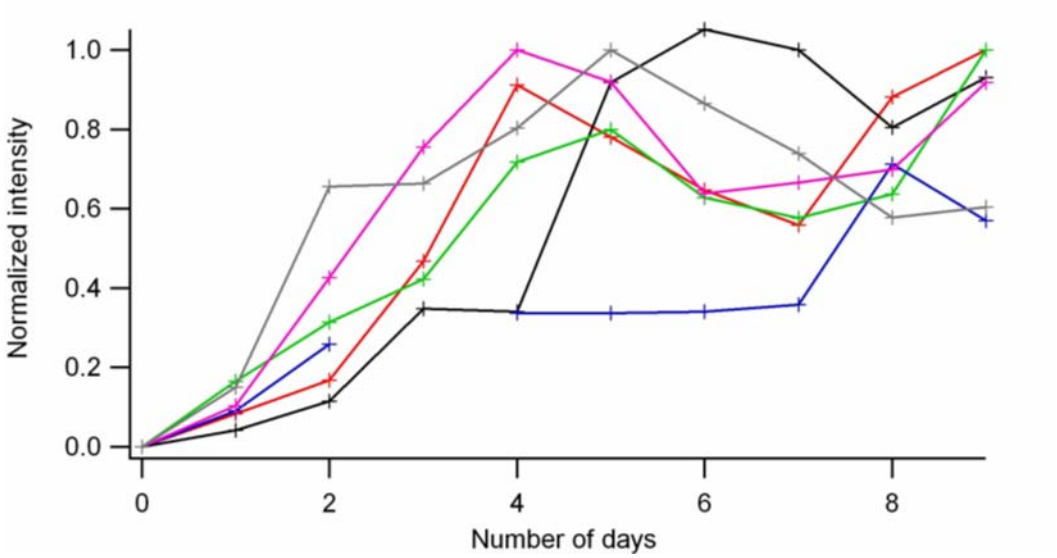

Figure 7.5. Normalized integrated intensity for the thioflavin T study for WT only (red), A30P only (black), WT + Y19/W39 (green), WT + Y19(NO_2)/W39 (blue or pink), and A30P + Y19/W39 (grey) throughout the aggregation study

Trp Steady-state Fluorescence Studies

As mentioned in previous chapters, Trp fluorescence is a powerful tool to investigate protein microenvironments.[12-15] Therefore, experimental samples were also subjected to Trp steady-state fluorescence studies to distinguish whether the W39 has become more buried as aggregation proceeds.

At the beginning of experiment, Y19/W39 samples exhibited higher fluorescence than samples containing Y19/W39(NO_2) because Trp fluorescence was quenched by the acceptor, 3-nitrotyrosine (**Figure 7.6a)**. The two samples (green and grey) containing Y19/W39 displayed comparable fluorescence, while similar emissions could be observed for samples with Y19/W39(NO_2). Even though no Trps were introduced in the WT-only and A30P-only samples, minimal fluorescence could still be observed due to minimal, though inefficient, Tyr excitation that could occur when samples were excited at 290 nm.

Figure 7.6b shows Trp fluorescence after nine days. The large increase of emission at 300 nm is mostly attributed to scattering caused by the aggregates. Trp fluorescence can be observed by the shoulder around 330 nm. Compared to the Trp emission in **Figure 7.6a**, at Day 9 we observe a higher emission, which is blue-shifted from λ_{max} = ~ 350 nm (Day 0) to ~ 330 nm (Day 9). As suggested in previous chapters, a higher fluorescence and blue-shifted λ_{max} suggest that the Trp is in a more hydrophobic environment. In this case, the Trps are now buried within the aggregates.

On the contrary, the Trp fluorescence for the supernatants (**Figure 7.6b**, dotted lines) at Day 9 are much weaker compared to the pre-centrifuged counterparts. Upon closer investigation (**Figure 7.7**), the λ_{max} (~ 340 nm) seems to be slightly blue-shifted compared to emission at Day 0. In addition, emission at ~ 450 nm can be observed,

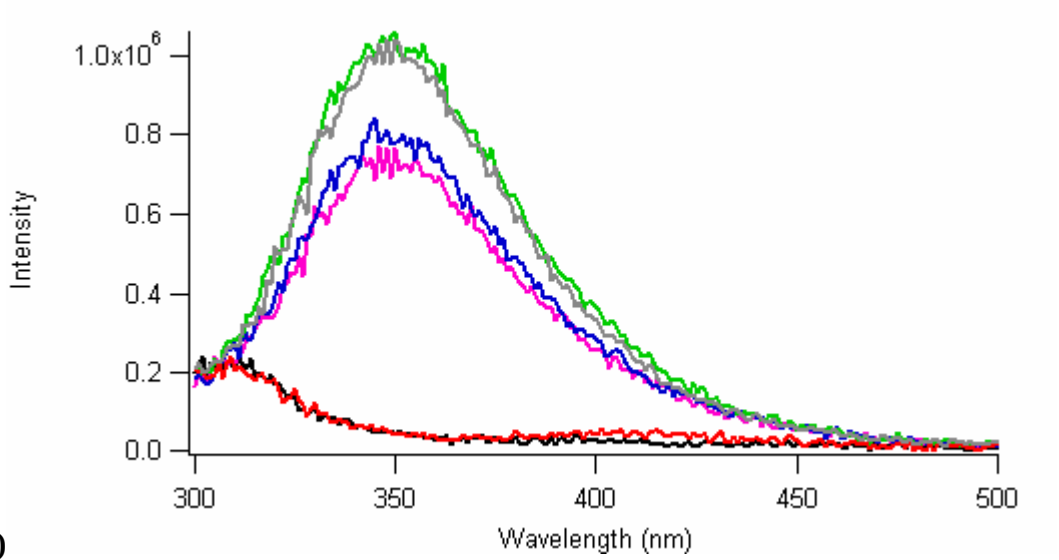

(a)

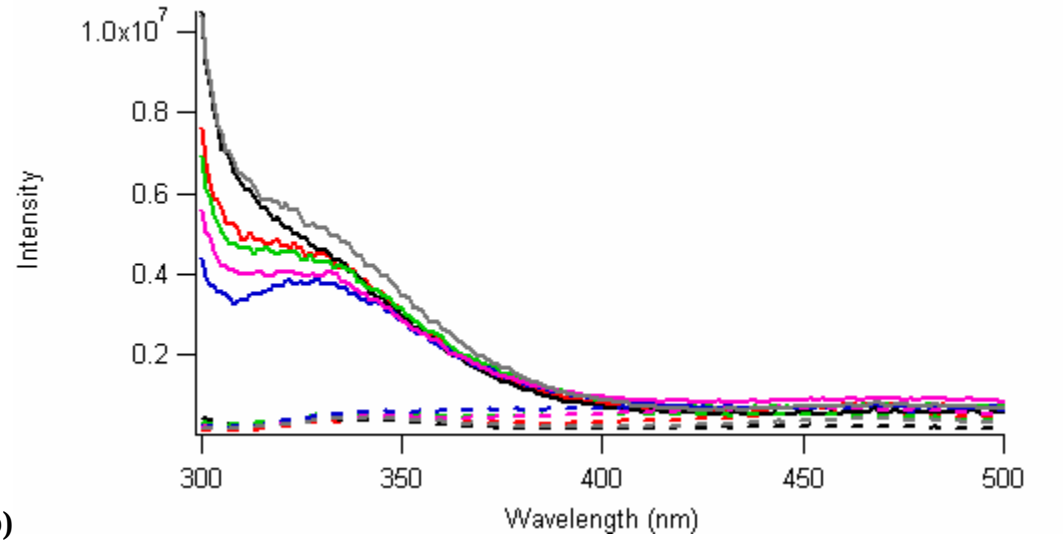

(b)

Figure 7.6. Steady-state fluorescence spectra of WT only (red), A30P only (black), WT + Y19/W39 (green), WT + Y19(NO_2)/W39 (blue or pink), and A30P + Y19/W39 (grey) at **(a)** Day 0 and **(b)** Day 9, along with spectra of their supernatants (dotted)

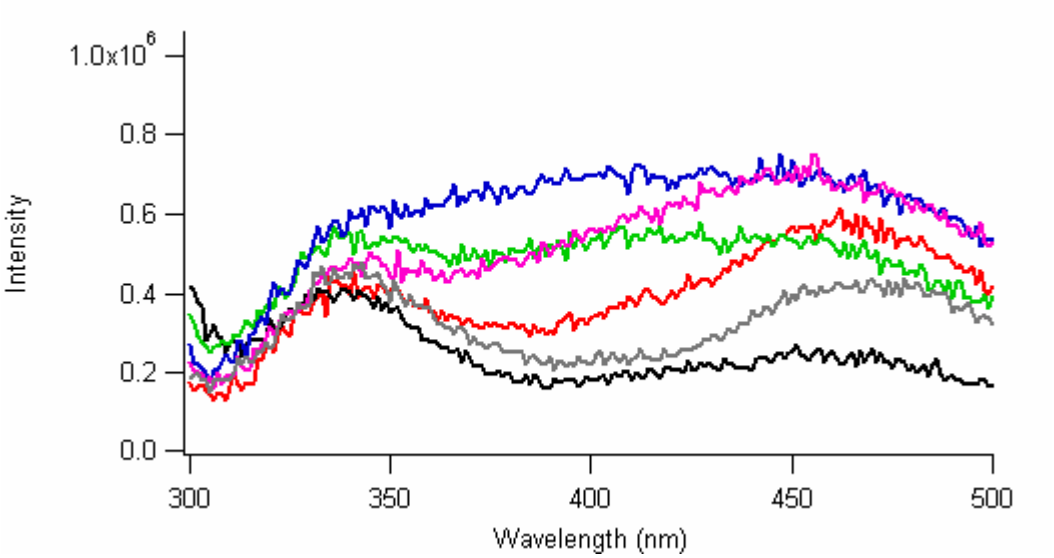

Figure 7.7. Steady-state fluorescence spectra of the supernatants for WT only (red), A30P only (black), WT + Y19/W39 (green), WT + Y19(NO_2)/W39 (blue or pink), and A30P + Y19/W39 (grey) at Day 9

suggesting the formation of a dityrosine linkage. Intermolecular tyrosine linkages may result in soluble multimers which remain in the supernatant. The presence of multimers can also bury the Trp, thus causing the blue-shift on the λ_{max}.

Circular Dichroism Experiments.

At the beginning of aggregation experiments, minimal structures were observed in the reaction mixtures (**Figure 7.8a**). After six days, **Figure 7.8b** shows that the reaction mixtures (dotted line) demonstrate a large increase of signal at ~ 218 nm, a signature peak of β-sheet formation,[16] implying aggregate formation. On the other hand, the CD signals obtained from the supernatant solutions show that the protein solutions were mostly unstructured (**Figure 7.8b**). Again, the discrepancies exhibited by similar samples show that the aggregation events studied were not reproducible.

SDS-PAGE Studies.

The reaction mixtures and their corresponding supernatants at Day 6 and Day 9 were subjected to SDS-PAGE studies (**Figure 7.9**). The monomer bands are highlighted by the arrows, showing that there were still some monomers remaining at those respective time points, with most of the monomers being consumed by Day 9. There were also more multimers shown in the SDS-PAGE from reaction mixtures on Day 9 than the corresponding SDS-PAGE from Day 6.

An interesting observation from the SDS-PAGE of the reaction mixtures from both days is that a species with a smaller molecular weight than the monomeric α-syn was present, suggesting that proteolysis may also occur during the aggregation process.

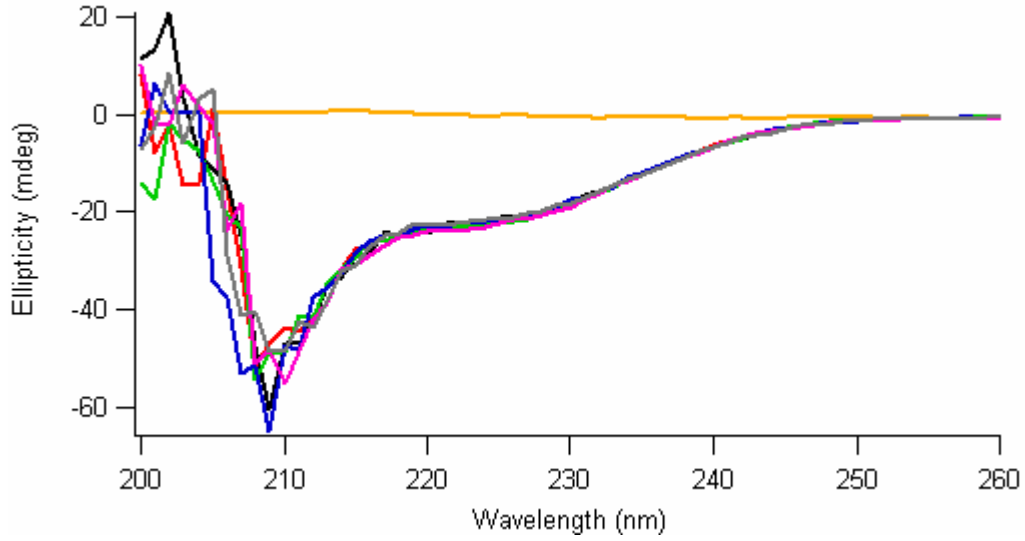

(a)

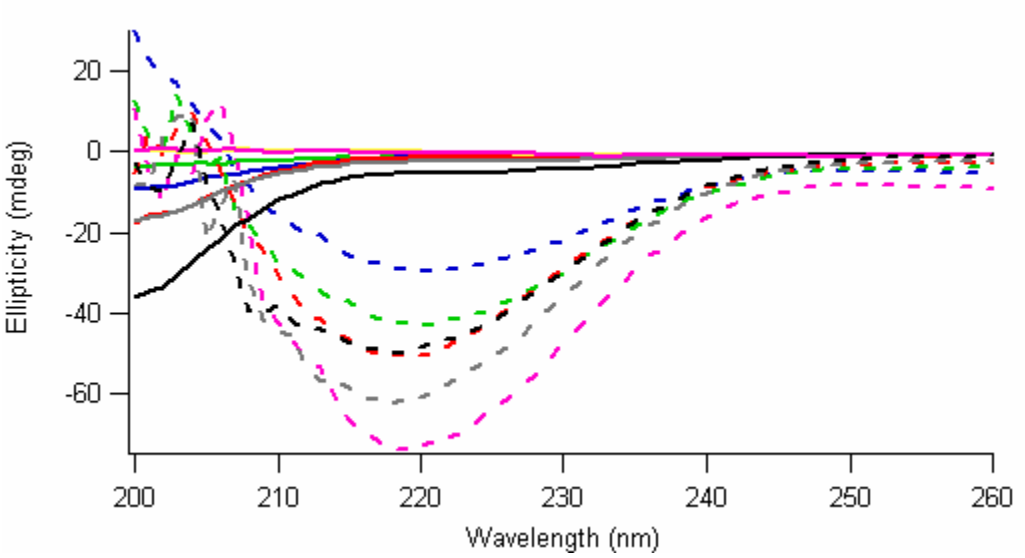

(b)

Figure 7.8. CD spectra at **(a)** Day 0 and **(b)** Day 6 of the reaction mixture (dotted) and supernatant (solid) from the following samples: NaP_i buffer (orange),WT only (red), A30P only (black), WT + Y19/W39 (green), WT + Y19(NO_2)/W39 (blue or pink), and A30P + Y19/W39 (grey)

(a)

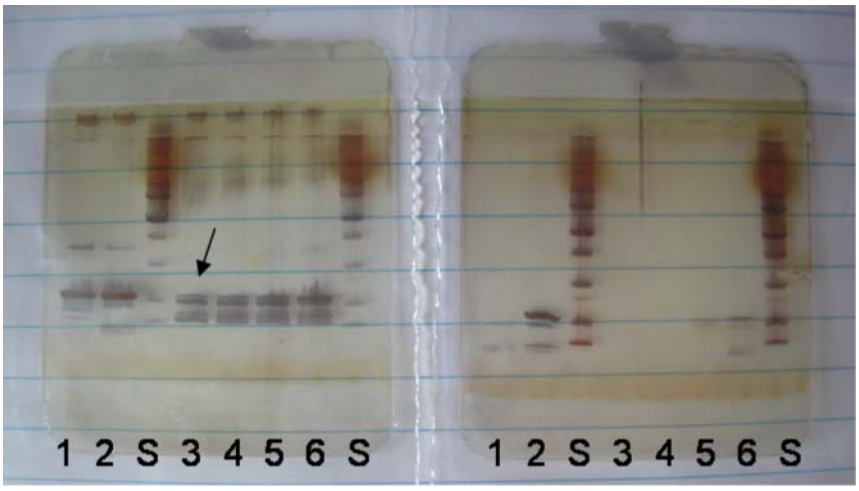

(b)

Figure 7.9. SDS-PAGE of WT only (lane #1), A30P only (lane #2), standard (lane #S), WT + Y19/W39 (lane #3), WT + Y19(NO_2)/W39 (lane #4 and #5), and A30P + Y19/W39 (lane #6) at **(a)** Day 6 and **(b)** Day 9 from reaction mixture (left) and supernatant (right). Monomeric species are indicated by arrows.

Size-exclusion Chromatography.

The aggregation mixtures from Day 6 and Day 9 were subjected to a size-exclusion column on a FPLC to separate the species in the reaction mixture according to their molecular weights. **Figure 7.10** shows these FPLC traces (red lines), along with the control (blue lines), consisting of Bovine Serum Albumin (67 kDa), Ribonuclease A (13.7 kDa), Cytochrome *c* (13.6 kDa), and Aproprotein (6.5 kDa). Since the heavier species eluted first, the peaks were assigned accordingly.

The most noticeable peak can be found after the 4th control peak, corresponding to the small aproprotein. This implies that the remaining species in the reaction mixture has a molecular weight smaller than 6.5 kDa, which is less than the 14 kDa α-syn monomer. This result further proves that proteolysis was present in the reaction mixture, giving rise to this small-molecular-weight species. This proteolysis process can be attributed to the presence of bacteria in the reaction mixture, digesting the protein during the aggregation event.

A shoulder peak corresponding to a species slightly smaller than 6.5 kDa can be observed from the reaction mixture in WT, but not in A30P. It seems that those species have been consumed in the A30P sample by this timepoint. In addition, although some of the large species can be observed in both traces, they are not dominant. Since all FPLC samples were filtered by a 220 nm filter before loading onto the size-exclusion column, it is highly likely that these high-molecular-weight species in the reaction mixture were filtered away.

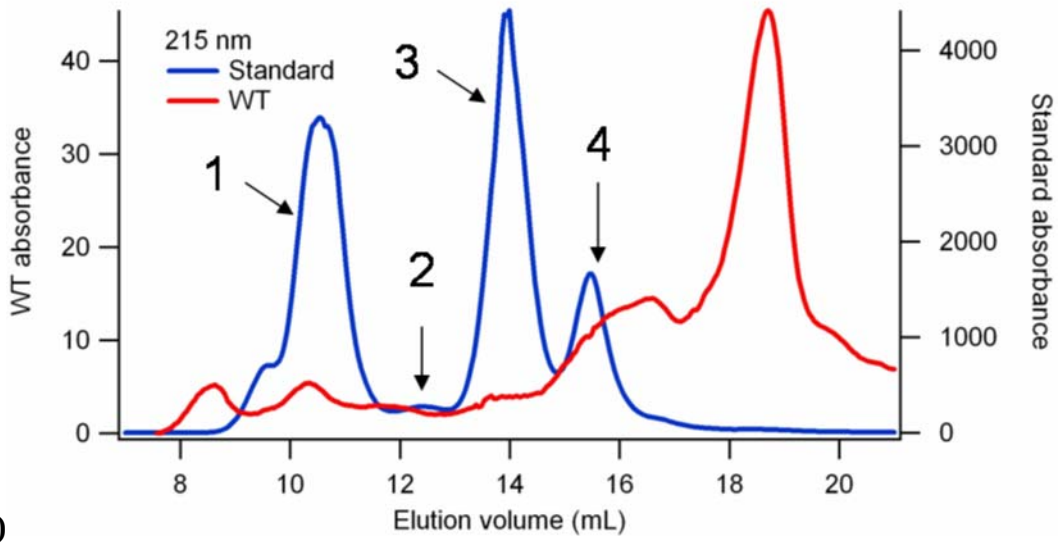

(a)

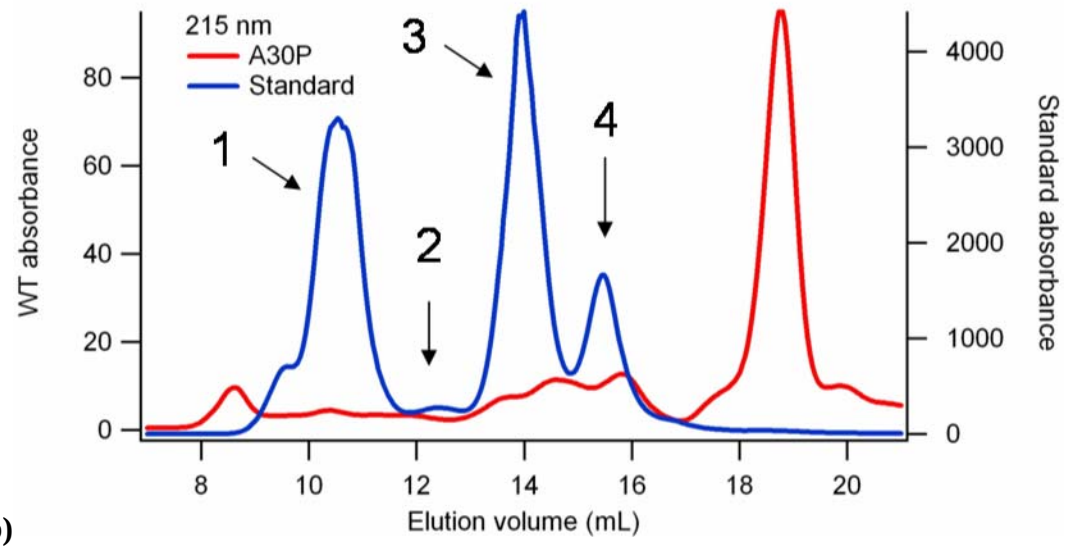

(b)

Figure 7.10. The FPLC traces of standards (blue), compared to the aggregation reaction mixture (red) from **(a)** WT only or **(b)** A30P only, using Superdex 75 10/300. The constituents of the standards are labeled by number, where 1 corresponds to Bovine Serum Albumin (67 kDa), 2 corresponds to Ribonuclease A (13.7 kDa), 3 corresponds to Cytochrome *c* (13.6 kDa), and 4 corresponds to Aproprotein (6.5 kDa).

Conclusion.

We have attempted to determine the change of intramolecular distance during the aggregation events of α-syn. However, it has been demonstrated that the aggregation process was not reproducible. Nonetheless, monitoring the aggregation of wild type and A30P α-syn protein in solution can provide some information on the formation of α-syn protofibrils. It is interesting to note that the aggregation rate for A30P mutants is faster than the wild type mutants. Also, proteolysis has been observed in the reaction mixture, possibly by the presence of bacteria, causing the irreproducible aggregation process. For future aggregation experiments, proteolysis could be prevented by introducing antibacterial agents in the aggregation mixture. Tools used in this study, such as CD, SDS-PAGE, size-exclusion columns, and ThT fluorescence studies, have been deemed appropriate for future α-syn aggregation experiments.

7.5 ACKNOWLEDGEMENTS

This project was completed in collaboration with Dr. Jennifer C. Lee.

7.6 REFERENCES

(1) Galvin, J. E.; Lee, V. M.; Schmidt, M. L.; Tu, P. H.; Iwatsubo, T.; Trojanowski *Adv. Neurol.* **1999**, *808*, 313–324.
(2) Spillantini, M. G.; Crowther, R. A.; Jakes, R.; Hasegawa, M.; Goedert, M. *Proc. Natl. Acad. Sci. U. S. A.* **1998**, *95*, 6469–6473.
(3) Spillantini, M. G.; Schmidt, M. L.; Lee, V. M. Y.; Trojanowski, J. Q.; Jakes, R.; Goedert, M. *Nature* **1997**, *388*, 839–840.
(4) Cookson, M. R. *Annu. Rev. Biochem.* **2005**, *74*, 29–52.
(5) Volles, M. J.; Lansbury, P. T. *Biochemistry* **2002**, *41*, 4595–4602.
(6) Zhu, M.; Li, J.; Fink, A. L. *J. Biol. Chem.* **2003**, *278*, 40186–40197.
(7) Kruger, R.; Kuhn, W.; Muller, T.; Woitalla, D.; Graeber, M.; Kosel, S.; Przuntek, H.; Epplen, J. T.; Schols, L.; Riess, O. *Nat. Genet.* **1998**, *18*, 106–108.

(8) Polymeropoulos, M. H.; Lavedan, C.; Leroy, E.; Ide, S. E.; Dehejia, A.; Dutra, A.; Pike, B.; Root, H.; Rubenstein, J.; Boyer, R.; Stenroos, E. S.; Chandrasekharappa, S.; Athanassiadou, A.; Papapetropoulos, T.; Johnson, W. G.; Lazzarini, A. M.; Duvoisin, R. C.; Di Iorio, G.; Golbe, L. I.; Nussbaum, R. L. *Science* **1997**, *276*, 2045–2047.
(9) LeVine, H. In *Amyloid, Prions, and Other Protein Aggregates* **1999**, *309*, 274–284.
(10) Roher, A.; Wolfe, D.; Palutke, M.; Kukuruga, D. *Proc. Natl. Acad. Sci. U. S. A.* **1986**, *83*, 2662–2666.
(11) Burns, J.; Pennock, C. A.; Stoward, P. J. *J. Pathol. Bacteriol.* **1967**, *94*, 337–.
(12) Reshetnyak, Y. K.; Koshevnik, Y.; Burstein, E. A. *Biophys. J.* **2001**, *81*, 1735–1758.
(13) Kleinschmidt, J. H.; den Blaauwen, T.; Driessen, A. J. M.; Tamm, L. K. *Biochemistry* **1999**, *38*, 5006–5016.
(14) Doring, K.; Konermann, L.; Surrey, T.; Jahnig, F. *Eur. Biophys. J.* **1995**, *23*, 423–432.
(15) Surrey, T.; Jahnig, F. *Proc. Natl. Acad. Sci. U. S. A.* **1992**, *89*, 7457–7461.
(16) Chiti, F.; Webster, P.; Taddei, N.; Clark, A.; Stefani, M.; Ramponi, G.; Dobson, C. M. *Proc. Natl. Acad. Sci. U. S. A.* **1999**, *96*, 3590–3594.